



# Timescale dependent sedimentary record during the past 130 kyr from a tropical mixed siliciclastic–carbonate shelf edge and slope: Ashmore Trough (southern Gulf of Papua)

GIANNI MALLARINO<sup>\*·1</sup> , JASON M. FRANCIS<sup>†</sup>, STEPHAN J. JORRY<sup>‡</sup>, JAMES J. DANIELL<sup>§</sup>, ANDRÉ W. DROXLER<sup>¶</sup>, GERALD R. DICKENS<sup>\*\*</sup>, LUC BEAUFORT<sup>††</sup>, SAMUEL J. BENTLEY<sup>‡‡</sup> , BRADLEY N. OPDYKE<sup>§§</sup> and LARRY C. PETERSON<sup>¶¶</sup>

<sup>\*</sup>Department of Physical and Applied Geology, Eötvös Loránd University (ELTE), Pázmány Péter sétány 1/c, Budapest, 1117, Hungary (E-mail: giannimallarino@usa.net)

<sup>†</sup>Chevron, 1500 Louisiana Street, Houston, TX 77002, USA

<sup>‡</sup>Centre de Brest, IFREMER, Géosciences Marines, BP70, Plouzané, 29280, France

<sup>§</sup>Earth and Environmental Sciences, James Cook University, Townsville, QLD 4811, Australia

<sup>¶</sup>Department of Earth, Environmental and Planetary Sciences, Rice University, 6100 Main St, Houston, Texas 77005, USA

<sup>\*\*</sup>Department of Geology, Trinity College Dublin, Dublin 02, Ireland

<sup>††</sup>Aix Marseille Univ, CNRS, IRD, INRAE, Coll. France, CEREGE, Aix-en-Provence, France

<sup>‡‡</sup>Department of Geology and Geophysics, Louisiana State University, E235 Howe Russell Geoscience Complex, Baton Rouge, Louisiana 70803, USA

<sup>§§</sup>Research School of Earth Sciences, The Australian National University, Building 142 Mills Road Acton ACT 2601, Australia

<sup>¶¶</sup>Rosenstiel School of Marine and Atmospheric Science, University of Miami, 4600 Rickenbacker Causeway, Miami, FL 33149, USA

Associate Editor – Jody Webster

## ABSTRACT

In tropical and sub-tropical mixed siliciclastic–carbonate depositional systems, fluvial input and *in situ* neritic carbonate interact over space and time. Despite being the subject of many studies, controls on partitioning of mixed sediments remains controversial. Mixed sedimentary records, from Ashmore Trough shelf edge and slopes (southern Gulf of Papua), are coupled with global sea-level curves and anchored to Marine Isotope Stage stratigraphy to constrain models of sediment accumulation at two different timescales for the past 130 kyr: (i) 100 kyr scale for last glacial cycle; and (ii) millennial scale for last deglaciation. During the last glacial cycle, carbonate production and accumulation were primarily controlled by sea-level fluctuations. Export of neritic carbonate to the slopes was initiated during re-flooding of previously exposed reefs and continued during Marine Isotope Stage 5e and 1 interglacial sea-level highs. Siliciclastic fluxes to the slope were controlled by interplay of sea level, shelf physiography and oceanic currents. Heterogeneous accumulation of siliciclastic mud on the slope, took place during Marine Isotope Stage 5d to Marine Isotope Stage 3 sea-level fall. Siliciclastics reached adjacent depocentres during Marine Isotope Stage 2. Coralgall reef and oolitic–skeletal sand resumed at the shelf edge during the subsequent stepwise sea-level rise of the last deglaciation. Contemporaneous, abrupt

<sup>1</sup>Present address: MOL Group, E&P Subsurface and Field Development, Budapest, Hungary

siliciclastic input from increased precipitation and fluvial discharge illustrates that climate controlled deglacial sedimentation. Siliciclastic input persisted until *ca* 8.5 ka. Carbonate accumulation waned at the shelf edge after *ca* 14 ka, whereas it increased on the slopes since *ca* 11.5 ka, when previously exposed reef and bank tops were re-flooded. When comparing the last sea-level cycle sedimentation patterns of the southern Gulf of Papua with other coeval mixed systems, sea level and shelf physiography emerge as primary controls on deposition at the 100 kyr scale. At the millennial scale, siliciclastic input was also controlled by climate change during the unstable atmospheric and oceanic conditions of the last deglaciation.

**Keywords** Gulf of Papua, high-Mg calcite ooids, large benthic foraminifera, last deglaciation, last sea-level cycle, mass accumulation rates, Mystery Interval, mixed siliciclastic–carbonate system.

## INTRODUCTION

In tropical and subtropical mixed siliciclastic–carbonate depositional systems, terrigenous riverine sediments can enter the marine environments and accumulate in juxtaposition with neritic carbonate production. In these mixed depositional settings, a combination of physical, chemical and biological processes control the siliciclastic–carbonate co-existence. Such a combination makes mixed system particularly sensitive to physical, chemical and environmental changes. Analyses of lateral juxtaposition of modern mixed systems allow assessing and understanding current sedimentary processes, such as reef growth, riverine input, sediment reworking, bypass and accumulation, and the (semi) quantification of the different physical, chemical and biological parameters involved in their co-habitation (Brodie & Furnas, 1996; Testa & Bosence, 1999; Dunbar *et al.*, 2000; Francis *et al.*, 2007; Ryan-Mishkin *et al.*, 2009; Webster *et al.*, 2018; Le Roy *et al.*, 2019). On the other hand, the vertical stacking of mixed sediment has recorded how these different parameters have varied through time. Outstanding examples of modern mixed systems include, to cite only a few, the Great Barrier Reef (GBR, Maxwell & Swinchart, 1970; Dunbar & Dickens, 2003; Francis *et al.*, 2007; Hinestrosa *et al.*, 2016), the New Caledonia Barrier Reef (Le Roy *et al.*, 2008, 2019) and the Belize Barrier Reef (Esler *et al.*, 1998; Ferro *et al.*, 1999; Gischler *et al.*, 2010); a few examples among many from the geological record include the Carboniferous of New Mexico, USA (Wilson, 1967), the Permian of West Texas and New Mexico, USA (Silver & Todd, 1969; Borer & Harris, 1991), the Jurassic of Mississippi, USA (Shew, 1991), and the Upper

Jurassic–Lower Cretaceous of Argentina (Zeller *et al.*, 2015).

For these mixed systems in the distant past, relative sea-level fluctuations have long been considered as the main control on partitioning of siliciclastic and carbonate sediments, particularly on rimmed shelves and adjacent basins during icehouse climate intervals (Wilson, 1967; Handford & Loucks, 1993; Kerans & Tinker, 1999). However, ancient records are characterized by low stratigraphic resolution and often their contemporaneous sea-level curves are derived from their own sediment accumulation patterns and, therefore, are not independently constrained. Such limitations can conceal the true origin of depositional controls. For example, the relative importance of sea-level fluctuations, shelf physiography and climate change on sediment distribution in the ancient record is difficult to quantify. In contrast, the influence of sea-level fluctuations in mixed systems has been clearly documented in the late Quaternary, and in particular during the last glacial cycle or the past 130 kyr (Ferro *et al.*, 1999; Jorry *et al.*, 2008, 2010; Gischler *et al.*, 2010; D'Agostini *et al.*, 2015; Accordi & Carbone, 2016). These relatively recent mixed systems offer the opportunity to investigate the variations of the siliciclastic–carbonate sediment juxtaposition and vertical stacking within the framework of an independently reconstructed sea-level curve. Moreover, analyses of relatively recent mixed systems should allow a test of how the interpretation of observed mixed sedimentary patterns and variability was affected at different time-scales: from a full 100 kyr long late Quaternary glacial cycle with sea-level fluctuation amplitude of 100 m or more to millennial-long intervals, characterized by rapid rates of sea-level

rise (in the order of metres per century) and extreme climate changes.

The Gulf of Papua (GoP), a tropical siliciclastic–carbonate system since the late Miocene (Pigram *et al.*, 1989; Tcherepanov *et al.*, 2008, 2010), provides a prime location to analyze a mixed system at different timescales of observation. From late Pliocene to Late Pleistocene, sustained siliciclastic input allowed the shelf edge to migrate >100 km seaward (Tcherepanov *et al.*, 2010). In spite of the high flux of siliciclastics, corallgal edifices developed on top of the prograding shelf edge. Larger build ups with flat tops developed during the Pliocene episodes of sea-level rise, whereas smaller, lenticular corallgal edifices grew during the Pleistocene (Fig. 1A to C). The latter represented short-lived carbonate sedimentation that took place during temporary re-flooding of the shelf margin (Tcherepanov *et al.*, 2008; Fig. 1D and E).

The sedimentary record of the last sea-level cycle (i.e. 100 kyr scale), cored on the slope of the southern GoP at 657 m of water depth in Ashmore Trough (core MD05-49) is consistent with the above depositional patterns observed on seismic profiles (Fig. 2; Jorry *et al.*, 2010). Carbonates (mostly reef-derived aragonite and high-Mg calcite) dominated during the penultimate and last deglacial sea-level rise intervals [Marine Isotope Stage (MIS) 6-5 and 2-1 transitions] and highstands (MIS 5e and MIS 1). In contrast, siliciclastics prevailed during the initial leg of the MIS 5d to MIS 4 sea-level fall, and bypassed into the adjacent depocentre (Pandora Trough) during the MIS 3 to MIS 2 late sea-level fall. These transitions from glacial to interglacial

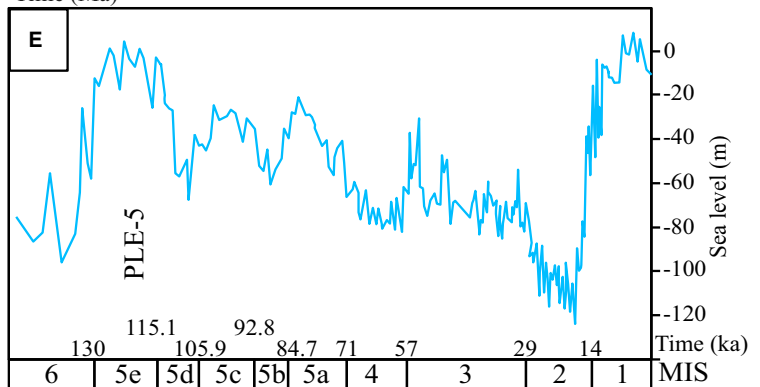
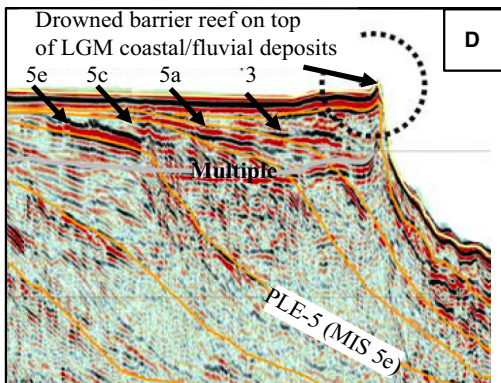
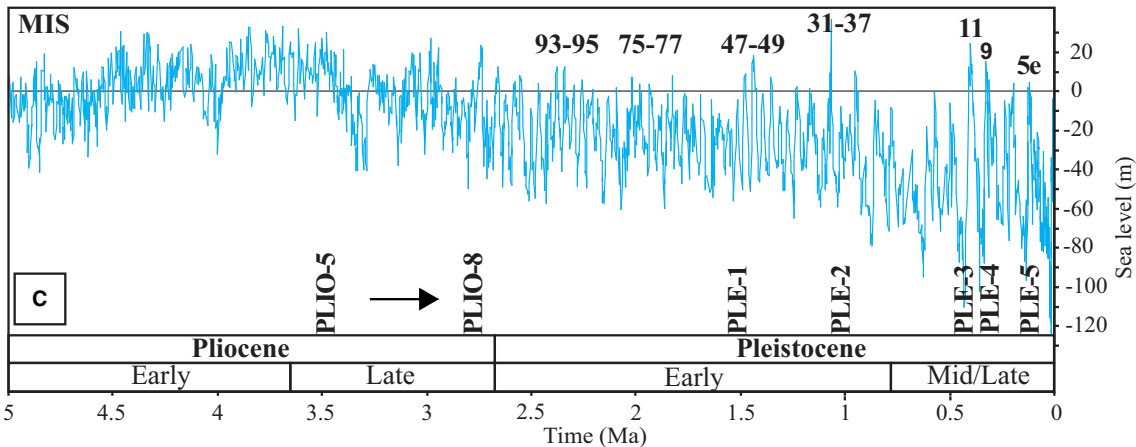
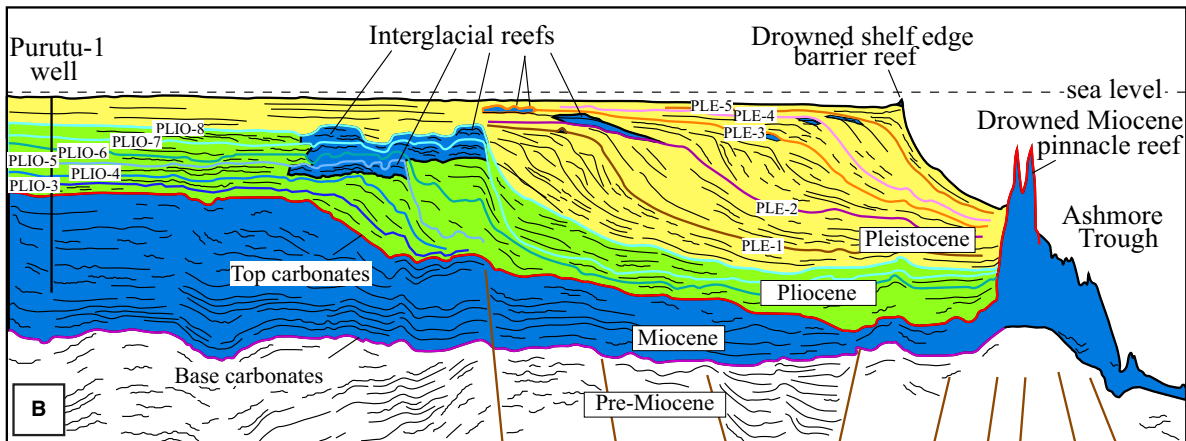
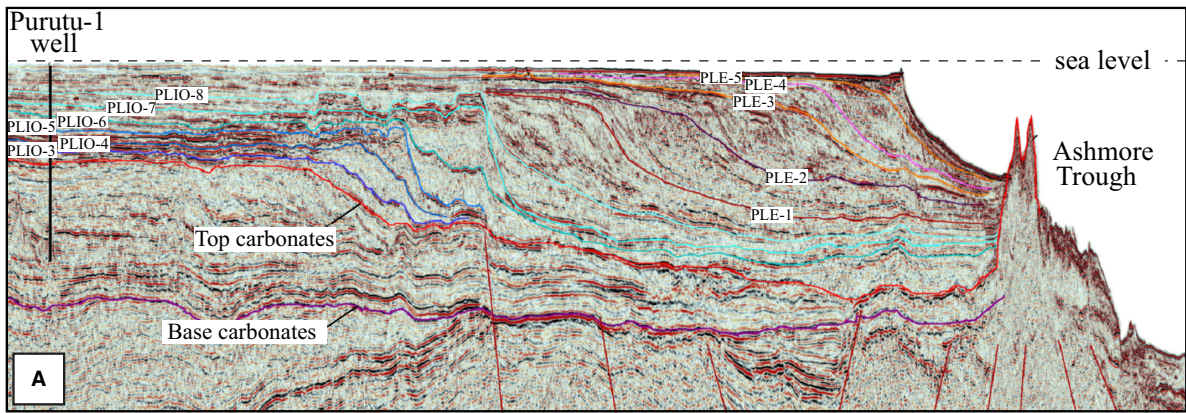
(i.e. deglaciations) are characterized by shifts in siliciclastic and carbonate dominated sedimentation. The last-glacial cycle sedimentary record of the Jorry *et al.* (2010) study reveals that sea-level change is the main process controlling the partitioning of the two sediment sources. However, given the short 12 to 14 kyr long deglacial intervals, a high-resolution scale of observation (hundreds to thousands of years) is required to fully capture the complex vertical stacking of mixed sediment during this interval of dramatic sea-level and climatic transition.

The last deglaciation, initiated at the end of Last Glacial Maximum (LGM) at about 20 ka, is ideally suited for a high-resolution investigation because sea-level rise is best constrained. It is well-established that, during the last deglaciation, sea level did not rise smoothly but rather in a stepwise manner, with intervals of rapid sea-level rise (i.e. meltwater pulses) alternating with periods of slow rise and even standstill (Liu & Milliman, 2004; Lambeck *et al.*, 2014). From a climate point of view, the last deglaciation was characterized by disruption of global patterns of ocean and atmospheric circulation contemporaneous with the collapse of the large Northern Hemisphere ice sheets (Denton *et al.*, 2010; Clark *et al.*, 2012). As a consequence, repeated north/south shifts of the intertropical convergence zone (ITCZ) resulted in alternating wet/dry periods across the equator (Denton *et al.*, 2010).

In summary, despite the numerous studies on ancient and modern mixed systems, the relative importance of sea-level fluctuations, shelf physiography and climate change on temporal and

---

**Fig. 1.** Oil and Gas industry seismic profile across the southern Gulf of Papua (GoP) illustrating its Neogene–Quaternary sedimentary evolution along with global sea-level curves. (A) Seismic profile across the southern GoP showing prograding mixed siliciclastic–carbonate late Pliocene–Pleistocene sequences overlying Miocene carbonate sequences (see Fig. 3A for seismic profile trace). During the late Pliocene–Late Pleistocene interval, the shelf edge prograded >100 km due to high siliciclastic discharge (green and yellow). In spite of the persistent terrigenous flux, shelf-edge reefs and carbonates (blue) developed during the Mid Pliocene Warm Period (MPWP; McManus *et al.*, 1999; Draut *et al.*, 2003) (horizons PLIO-5 to PLIO-8) and Pleistocene super interglacials and interglacials (MIS 47 to 49, 31 to 37, 11, and MIS 11, 9, 5 and 1, respectively) (horizons PLE-1 to PLE-5), during times of relative sea-level rise and re-flooding of the shelf (modified from Tcherepanov *et al.*, 2010). (B) Interpreted seismic profile. (C) Neogene–Quaternary global mean sea-level curve based on Pacific benthic foraminiferal  $\delta^{18}\text{O}$  and Mg/Ca records showing sea level during deposition of main seismic horizons of (A) and (B). MIS = Marine Isotope Stage (modified from Miller *et al.*, 2020). (D) Close-up of (A) showing seismic facies and geometry of the prograding shelf margin since the penultimate interglacial (i.e. MIS 5). Shelf edge seismic facies consist of lenticular high-amplitude reflections interpreted as short-lived carbonate build ups deposited during sea-level rise and temporary flooding of the shelf edge. LGM = Last Glacial Maximum (modified from Tcherepanov *et al.*, 2008). (E) Late Quaternary global mean sea-level curve based on Pacific benthic foraminiferal  $\delta^{18}\text{O}$  and Mg/Ca records showing last sea-level cycle and corresponding MIS (modified from Miller *et al.*, 2020).



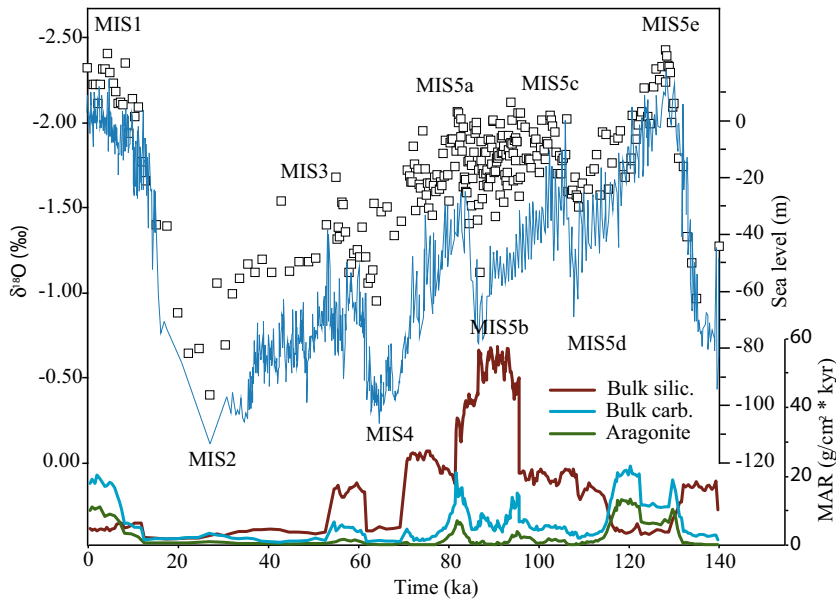


**Fig. 2.** Composite plot showing changes in composition and oxygen isotope data from core MD05-49 during the last sea-level cycle. Bottom curves are bulk siliciclastic (brown), bulk carbonate (blue) and aragonite (green) mass accumulation rates (MARs). Top curve is relative sea level from Rohling *et al.* (2009). Squares are oxygen isotope data from the core (from Jorjy *et al.*, 2010).

spatial sediment distribution remains controversial. Furthermore, how the interpretation of observed sedimentary patterns is affected at different timescales of investigation stays untested. In order to address the above points, this study focuses on several piston cores recovered along the shelf edge and upper slope of Ashmore Trough in the southern GoP (Fig. 3). The sedimentary record of the last sea-level cycle is investigated at the 100 kyr scale as well as the millennial scale during the last deglaciation. Seismic, stratigraphic, sedimentological and geochemical data are integrated to reconstruct the depositional history since the past 130 kyr. Finally, the last sea-level cycle sedimentary record of Ashmore Trough is compared to other coeval mixed systems (for example, Great Barrier Reef, New Caledonia Barrier Reef and Belize Barrier Reef). This comparison highlights similarities and differences, and allows identifying first-order depositional controls, other than sea level, in tropical and subtropical mixed siliciclastic-carbonate systems.

## GULF OF PAPUA MORPHOLOGICAL AND GEOLOGICAL SETTINGS

### Gulf of Papua modern morphologies

The Gulf of Papua lies between Papua New Guinea (PNG), north-east Australia, and the Coral

Sea. It includes shelf and slope environments as well as adjacent deep basins oriented either north-east or south-east, such as Ashmore/Pandora troughs and Moresby Trough, respectively (Fig. 3A). The width and structure of the GoP shelf varies considerably, from about 150 km across in the south and south-west to <25 km in the east and north-east (Fig. 3A). Based on geomorphic elements, the shelf can be divided into three main areas: (i) a broad south-west area with barrier reefs and patch reefs south of latitude 9°20', that represents the northernmost terminus of the GBR (Harris *et al.*, 1996); (ii) an even broader central area hosting, in water depths less than 50 m, deltas and pro-deltas of several rivers including the Fly, Bamu, Turama, Kikori and Purari rivers. Here, the outer shelf, ranging in water depths between 50 m and *ca* 125 m, is mostly covered by thin Holocene sediment accumulation and devoid of outer-shelf carbonate mounds (Harris *et al.*, 1996); (iii) a narrow north-east area, fed by minor rivers and flanked with drowned shelf-edge reefs south of latitudes 8°20' (Droxler & Jorjy, 2013; Harper, 2014). Several large offshore atolls occur in the central portion of the gulf (Fig. 2A), notably Ashmore Reef (AR), Booth Reef (BR), Portlock Reef (PR) and Eastern Fields Reef (EFR) (Francis *et al.*, 2008; Tcherepanov *et al.*, 2008). Portlock Reef (PR) has been incorporated into the GoP shelf edge by prograding siliciclastic clinofolds (Tcherepanov *et al.*, 2010).

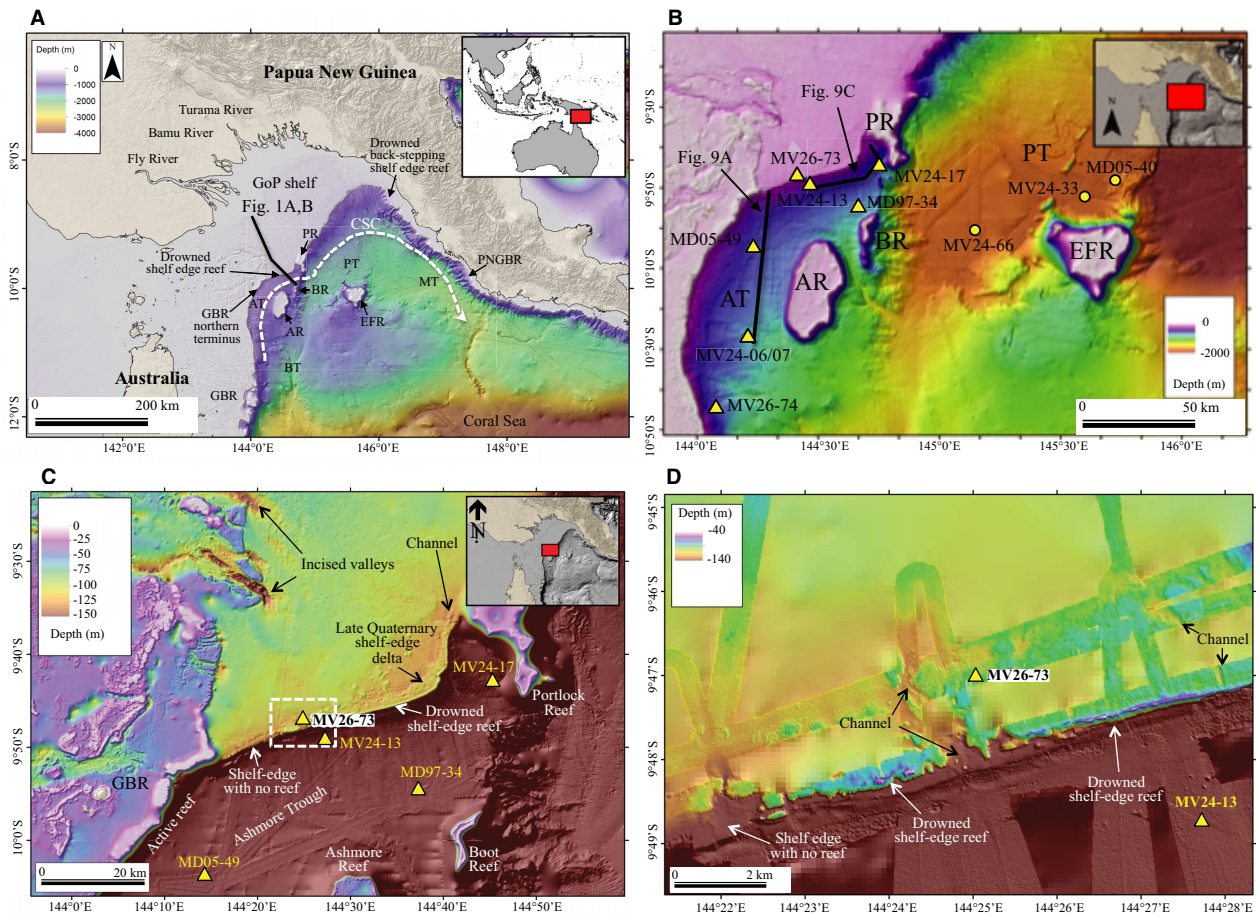


**Fig. 3.** (A) Elevation map and bathymetry of the Gulf of Papua (GoP) showing the main physiographic and oceanographic elements. The present-day shelf is a mixed siliciclastic–carbonate environment. Siliciclastic sediment is delivered in the broad central and northern shelf by Papua New Guinea rivers, whereas carbonate sedimentation takes place mostly on the southern shelf, at the northern terminus of the Great Barrier Reef (GBR), as well as on off-shore atolls. An active barrier reef is also present on the narrow eastern GoP shelf (PNGBR). Late Quaternary drowned barrier reefs occur in southern GoP (Droxler & Jorry, 2013) as well as in its north-eastern sector (Harper, 2014). AR = Ashmore Reef; AT = Ashmore Trough; BR = Boot Reef; BT = Bligh Trough; EFR = Eastern Field Reef; GBR = Great Barrier Reef; MT = Moresby Trough; PNGBR = Papua New Guinea Barrier reef; PR = Portlock Reef; PT = Portlock Trough; CSC = Coral Sea Current. (B) Bathymetry map of the southern GoP showing the location of Ashmore Trough cores analyzed in this study (triangles) as well as Portlock Trough referenced cores (circles). (C) Bathymetry map of the southern GoP, including the northern terminus of the GBR, showing details of the outer shelf/shelf edge geomorphic elements including delta complex and drowned shelf-edge barrier reef. (D) Close-up of the shelf margin area around core MV26-73 [white-dashed rectangle in (C)] showing segments of the drowned barrier reef, shelf margin with no drowned reef, and channels perpendicular to the shelf edge.

**Cenozoic and Quaternary evolution of the Gulf of Papua continental shelf**

In the northern GoP, the south-east Papuan Peninsula and its shelf and upper slopes consist of the south-east termination of the Papuan Fold and Thrust Belt (PFTB), including its Papuan Foreland Basin created by the Oligocene collision of the Pacific island arcs with the Australian Plate (van Ufford & Cloos, 2005). The

PFTB late Oligocene – Neogene foreland basin is represented by the Aure Trough (a relict trench in the northern GoP) and modern Moresby Trough (van Ufford & Cloos, 2005; Cloos *et al.*, 2005).

On the other hand, the overall GoP tectonic configuration consists of several north-east trending structural ridges and troughs, formed during the late Cretaceous and Palaeocene

opening of the Coral Sea (Davies *et al.*, 1989; Pigram *et al.*, 1989; Tcherepanov *et al.*, 2008). The Cenozoic GoP neritic carbonate system, mostly deeply buried under the modern siliciclastic shelf, is represented by one large extensive rimmed carbonate shelf (Borabi Platform), and several buried platforms drowned from the early Miocene to early Pliocene. In addition to the buried platforms are unburied still active today isolated carbonate platforms, such as Ashmore, Boot, Portlock and Eastern Fields Reefs, that were initially established in the Eocene on top of the north-east trending structural ridges (Davies *et al.*, 1989; Tcherepanov *et al.*, 2008, 2010).

Plio-Quaternary mostly siliciclastic successions, up to 3 to 4 km thick, have infilled the troughs and buried the intervening drowned carbonate platforms established on the ridge crest through south-eastward prograding siliciclastic sequences (Davies *et al.*, 1989; Pigram *et al.*, 1989; Tcherepanov *et al.*, 2008, 2010; Droxler & Jorry, 2013). The burial of the Cenozoic GoP carbonate system by siliciclastic sediment was initiated during the late Miocene–early Pliocene and linked to the erosion of the Central Range Orogeny. However, the most significant largest siliciclastic influx was triggered by the renewed uplift of the PFTB during the early part of the late Pliocene. It took only two million years at most for the GoP shelf edge to prograde south-eastward as much as 150 km, forming in this short period of time more than 80% of the modern shelf (Tcherepanov *et al.*, 2010). This high siliciclastic influx was certainly also enhanced by the Mid Pliocene Warm Period (MPWP; McManus *et al.*, 1999; Draut *et al.*, 2003) and intensified East Asian monsoon at 3.6–2.9 Ma (Tcherepanov *et al.*, 2010).

In spite of this late Pliocene huge flux of siliciclastics fed by the rejuvenation of the Papuan orogeny, strengthening of monsoon and overall falling of sea level, neritic carbonates still thrived during periods of sea-level rise and highstand (Fig. 1A and B). The late Pliocene prograding/aggrading sequences, including outer shelf – shelf edge environments (PLIO-4 to PLIO-8, Fig. 1A and B), are characterized, in particular in the south-west part of the study area, by high-amplitude reflections and mounded seismic facies. Such seismic facies are more abundant in the youngest PLIO-6 to PLIO-8 sequences where a series of flat-topped banks, 5 to 10 km in size, are observed. The high-amplitude, mounded seismic facies are interpreted to

represent transgressive and early highstand outer shelf and shelf-edge carbonate reefs (Tcherepanov *et al.*, 2010).

Importantly, despite the structural complexity of the region, the GoP is in the late Quaternary a tectonically quiescent area with no significant historical earthquakes and no faults that reach the sea floor (Bird, 2003; Tcherepanov *et al.*, 2010; Baldwin *et al.*, 2012).

## Late Quaternary to modern evolution

### *Gulf of Papua continental shelf*

The GoP receives from the high mountains of PNG massive amounts of siliciclastic sediments (*ca* 150 to 200 Mt year<sup>-1</sup>; Milliman, 1995; Slingerland *et al.*, 2008a). Sediment distribution on the shelf is governed by a combination of tidal, wind, oceanic and thermohaline currents (Harris *et al.*, 1990; Wolanski & Alongi, 1995; Walsh *et al.*, 2004; Ogston *et al.*, 2008). Coastal currents are bidirectional and seasonal with south-west direction during monsoon season and north-east direction during trade wind season (Wolanski *et al.*, 1995; Slingerland *et al.*, 2008b). Tidal currents are across-shore and are considered to be responsible for sediment resuspension and seaward transport by means of mudflow (Harris *et al.*, 1996; Walsh *et al.*, 2004; Ogston *et al.*, 2008; Slingerland *et al.*, 2008a). Overprinted on these seasonal currents is a clockwise gyre influenced by the off shelf Coral Sea Current (CSC, Fig. 3A; Andrews & Clegg, 1989) that produces a net sediment transport from the central shelf to the east (Wolanski *et al.*, 1995; Harris *et al.*, 1996; Slingerland *et al.*, 2008a).

Shallow seismic profiling of the shelf shows that the uppermost 100 m of sediment consists of two stacked, primarily siliciclastic, clinoforms. The lower one, extending to the outer shelf, was built mostly during the Late Pleistocene. The upper one, restricted to the inner and mid shelf, has been built since the Holocene as result of sediment transport by gravity flows and suspension (Harris *et al.*, 1996; Walsh *et al.*, 2004; Slingerland *et al.*, 2008a; Wei *et al.*, 2019).

Surficial sediment composition on the shelf reflects the interaction of river discharge, carbonate reefs, and tidal and coastal currents (Harris *et al.*, 1996; Francis *et al.*, 2008). Siliciclastic sedimentation is dominant within 10 to 20 km from the river deltas. Siliciclastics transit, rather sharply, into mostly carbonate sediment veneer towards the outer shelf and its margin in the

central area of the shelf as well to the south-west, towards the GBR northern termination (Harris *et al.*, 1996). In the narrow north-eastern shelf, siliciclastics extend to the shelf edge (Howell *et al.*, 2014). In the broad central and south-western shelf areas, *Halimeda* bioherms and biostromes, both living and Holocene in age, are observed at water depth of up to 100 m (Harris *et al.*, 1996). In the southern GoP another locus of carbonate sedimentation is the northern termination of the GBR consisting of ribbon, deltaic and dissected reefs (Fig. 3B and C; Veron, 1978; Hopley, 2006).

### Gulf of Papua shelf edge

Shelf edge water depths across the central GoP generally fall between 120 m and 130 metres below present sea level (mbpsl) (Francis *et al.*, 2008). On the other hand, in the south-western GoP, the modern outer shelf margin depths range from 60 to 130 mbpsl (Fig. 3C; Daniell, 2008; Francis *et al.*, 2008). This wider depth range can be explained by the occurrence of a narrow (<1 km wide), shelf-parallel ridge with an overall length of about 50 km (Fig. 3B to D; Harris *et al.*, 2005; Droxler *et al.*, 2006; Daniell, 2008; Francis *et al.*, 2008). The height of this ridge ranges from 30 to 60 m above the surrounding sea floor, such that its top can approach 60 to 70 mbpsl (Fig. 3D). This ridge has been interpreted as a coralgal barrier reef that presumably grew on top of a LGM siliciclastic beach-barrier complex during the MWP-1A, and subsequently drowned during MWP-1B (Droxler *et al.*, 2006; Francis *et al.*, 2008; Droxler & Jorry, 2013). Other geomorphological elements in the south-western GoP shelf edge include incised valleys and a large shelf-edge delta complex. Where no barrier reef is present, the shelf edge bathymetry falls in a narrow range from 120 to 130 mbpsl (Fig. 3C and D). In the north-eastern GoP, drowned shelf-margin edifices are interpreted as deglacial backstepping coralgal reefs with tops dating from *ca* 19 ka to recent, and a few pinnacles that seem to be active at present-day (Fig. 3A; Droxler & Jorry, 2013; Harper, 2014).

### Slope and adjacent basin

Off the shelf, and at present-day, both siliciclastic and neritic carbonate sediments accumulate in four main intraslope basins (Fig. 3A): Bligh Trough (BT), Ashmore Trough (AT), Pandora Trough (PT) and Moresby Trough (MT). The

GoP region remains sparsely sampled but, in several studies, sediment fluxes to slopes have been documented partly by coupling shallow seismic and piston cores (Jorry *et al.*, 2008; Muhammad *et al.*, 2008; Howell *et al.*, 2014; Septama *et al.*, 2016; Septama & Bentley, 2017; Wei & Driscoll, 2020). Glacial siliciclastic and interglacial carbonate components have had variable accumulation across the Australia–PNG slopes and adjacent troughs over time. In the south, offshore of the northern GBR, siliciclastic turbidites occurred before *ca* 31 ka, paused during the LGM, and briefly resumed during the last deglaciation (*ca* 8 to 11 ka). Differently, carbonate turbidites initiated since 11 ka (Webster *et al.*, 2012). In the central GoP Pandora Trough, siliciclastic turbidites were abundant during the LGM and decreased during the subsequent early sea-level rise, in particular during the Bølling–Allerød (B–A) interval (Jorry *et al.*, 2008). Siliciclastics briefly re-occurred during the Younger Dryas (YD) and then disappeared, being replaced by calciturbidites from 11 ka (Jorry *et al.*, 2008). Accumulation of bank-derived fine aragonite and high-Mg calcite typically occurred during interglacials such MIS 5e, MIS 5c, MIS 5a and MIS 1, clearly initiated during MWP-1B at 11.5 ka (Jorry *et al.*, 2010). In contrast, in the eastern GoP Moresby Trough, siliciclastic turbidites were deposited since the past 40 ka (Septama & Bentley, 2017).

## LATE QUATERNARY SEA-LEVEL AND CLIMATE CHANGE

### Sea level

Two sea-level curves were used in this study: (i) Lambeck *et al.* (2002) for the last glacial cycle; and (ii) Lambeck *et al.* (2014) for the millennial scale sea-level reconstruction of the last deglaciation (Fig. 4A and B). The last glacial cycle curve, correlated to marine oxygen isotope stages (MIS), is based mostly on coral reef core data from Huon Peninsula (Papua New Guinea) and supplemented with sediment core data from Bonaparte Gulf (Australia). During the last interglacial MIS 5e, sea level peaked a few metres higher than present level. This sea-level high was followed by a large oscillation, up to 60 m of magnitude, during sub-stages 5d to 5a and resulted in relative sea level *ca* 30 m lower than today by the end of MIS 5a (Fig. 4A). Sea level continued falling during MIS 4 when it reached about



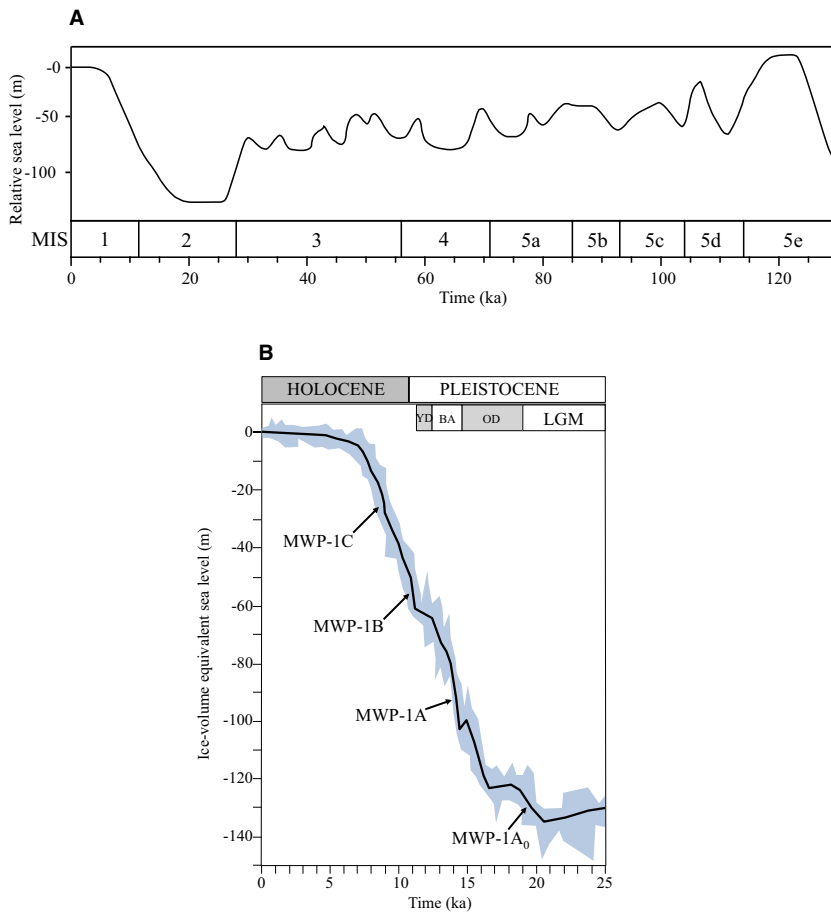


**Fig. 4.** Sea-level curves used in this study. (A) Relative sea-level curve for the last glacial cycle with marine isotope oxygen stages and substages (MIS 1 to 5e). Sea-level estimates, error bars are not included, are based on coral reef data points from Huon Peninsula (Papua New Guinea) and sediment core data Bonaparte Gulf (Australia) (modified from Lambeck *et al.*, 2002). (B) Ice-volume equivalent sea-level curve for the last deglaciation with meltwater pulses (MWPs) and main climate events. Blue envelope represents individual data point sea-level estimates (nearly 1000 data points) with  $2\sigma$  error. Black line is an objective estimate of the same dataset based on Markov chain Monte Carlo approach. LGM = Last Glacial Maximum; OD = Oldest Dryas, BA = Bølling–Allerød; YD = Younger Dryas (modified from Lambeck *et al.*, 2014).

60 mbpsl. During the following MIS 3, sea level fluctuated at smaller magnitude of 20 to 30 m and reached about 70 mbpsl by the end of MIS 3 (Fig. 4A). Sea level continued falling during MIS 2 when it reached its glacial minimum at about 120 to 130 mbpsl around 20 ka (Fig. 4A).

The last deglacial sea-level curve of Lambeck *et al.* (2014) is based on global datasets from far-field locations in tectonically stable areas (Fig. 4 B). This is likely to average out undetected tectonic components, as well as crustal rebound and subsidence due to ice decay (i.e. glacial isostatic adjustment – GIA – Peltier & Andrews, 1976; Nakada & Lambeck, 1987; Mitrovica & Milne, 2002). Following LGM, from about 20 to 18 ka, sea level rose rapidly by about 10 m (i.e. MWP-1A<sub>0</sub> also referred to 19-kyr MWP; Clark *et al.*, 2004).

The first meltwater pulse was followed by an interval of stationary sea level from *ca* 18 to 16.5 ka (Fig. 4B). Sea level resumed rising at rapid rates from *ca* 16.5 to 15 ka, when it rose by about 25 m (Fig. 4B). This rise was followed

by a very short-lived period of near constant sea level (Fig. 4B). These last three legs of sea-level change occurred mostly during the Oldest Dryas stadial (OD; Clark *et al.*, 2012). The major pulse in sea-level rise during the last deglaciation MWP-1A, started no earlier than 14.65 ka and ended before 14.3 ka, making it coeval with the Bølling warming (Bard *et al.*, 1996; Deschamps *et al.*, 2012) (Fig. 4B). Based on this Tahiti data set, sea level most probably rose between 14 m and 18 m during MWP-1A, implying that the rate of eustatic sea-level rise exceeded 4 m per century. Then, sea level continued rising, although at slower rates, until about 12.5 ka when it reached *ca* 70 mbpsl (Abdul *et al.*, 2016). Chronologically, this interval corresponds to the Bølling–Allerød (B-A), during which lower amplitude MWPs, in the order of a few metres, are also suggested based on small coral reef terraces offshore the south Texas shelf (Khanna *et al.*, 2017). Sea-level rise significantly slowed from *ca* 12.5 to 11.5 ka during the YD to reach 60 mbpsl (Fig. 4B). The YD ended

abruptly by MWP-1B, an interval spanning from 11.45 to 11.1 ka, contemporaneous with North Hemisphere insolation maximum and characterized by a  $14 \pm 2$  m jump in sea level corresponding to rates of sea-level rise of 4 m per century (Abdul *et al.*, 2016). Sea level rose steadily until the 8.2 ka cold event during which sea level was estimated to be at *ca* 20 mbpsl (Fig. 4B). The last meltwater pulse, MWP-1C, occurred from 8.2 to 7.6 ka characterized by a sea level jump of about 10 m (Blanchon & Shaw, 1995; Blanchon *et al.*, 2002) (Fig. 4B).

### Climate change

Present-day climate in the GoP is influenced by seasonal monsoon–trade winds and interannual El Niño–La Niña fluctuations. Whereas seasonal variations influence shelf oceanic circulation (Wolanski *et al.*, 1995), El Niño–La Niña fluctuations are considered to be mostly responsible for long-term sediment discharge variations (Dietrich *et al.*, 1999; Ogston *et al.*, 2008). During El Niño conditions, reduced precipitation and reduced fluvial run off create a negative perturbation to the relatively constant sediment discharge (Dietrich *et al.*, 1999; Ogston *et al.*, 2008).

Climate fluctuations at the millennial scale characterize the transition from glacial to interglacial periods (i.e. glacial termination). These fluctuations are due to major reorganization of global atmospheric and oceanic circulation patterns (Denton *et al.*, 2010).

Climate reconstruction in the GoP region since the LGM, shows that warming began by 18 to 17 ka (Turney *et al.*, 2006; Reeves *et al.*, 2013) with possible millennial-scale hydrological cycles recorded both on land (north-east Australia, Muller *et al.*, 2008;) and offshore (Coral Sea; Shiau *et al.*, 2011). These cycles are linked to the ITCZ latitudinal displacement (Denniston *et al.*, 2013). North/south shifts of the ITCZ are interpreted to result from a chain of global climate events, in turn initiated from changes in Northern Hemisphere insolation (Denton *et al.*, 2010; Clark *et al.*, 2012; McGee *et al.*, 2014). The most prominent southward shift of the ITCZ, occurred from 17.5 to 14.5 ka and brought warmer and wetter conditions in the Australian–Indonesian region (Ayliffe *et al.*, 2013; Denniston *et al.*, 2013). This time interval, also referred to as Mystery Interval (MI; Denton *et al.*, 2006), was characterized by apparent contradictory climate events between the Northern

Hemisphere (cooling) and Southern Hemisphere (warming) which could be explained by inter-hemispheric teleconnections (Sirocko *et al.*, 1996; Denton *et al.*, 2006; Denton *et al.*, 2010; Zhang *et al.*, 2014).

In south-east Asia, the warm and wet MI was followed by a relatively drier period that occurred from *ca* 15 to 12.9 ka. This drier period, corresponding to the Antarctic Cold Reversal/Bølling–Allerød (ACR/B-A), is in turn followed by another wet period from 12.9 to 11.5 ka including the YD (Ayliffe *et al.*, 2013; Denniston *et al.*, 2013). Warmer and wetter conditions predominantly continued after the YD due to strengthening of the Indo-Australian summer monsoon (IASM) which peaked at around 8.5 ka (Sirocko *et al.*, 1996; Denniston *et al.*, 2013; Kuhnt *et al.*, 2015; Ishiwa *et al.*, 2019). A drier period was established between *ca* 8 ka and 5 ka, and it was associated with a northward displacement of the ITCZ (Kuhnt *et al.*, 2015; Ishiwa *et al.*, 2019). Since then, the ITCZ shifted back southward coupled with re-intensification of the IASM (Sirocko *et al.*, 1996; Kuhnt *et al.*, 2015; Ishiwa *et al.*, 2019). Furthermore, since the early Holocene monsoon variability has been documented also at the centennial to decadal timescale (Dykovski *et al.*, 2005; Chen *et al.*, 2015). This high-frequency variability suggests controls other than solar variability such as changes in atmospheric and oceanic circulation (i.e. El Niño–Southern Oscillation; Dykovski *et al.*, 2005).

## MATERIAL AND METHODS

### PANASH and PECTEN cruises

Two research cruises, PANASH and PECTEN, provided the multi-beam bathymetry data, 3.5 kHz seismic data and the cores used in this study. The PANASH cruise was conducted on *R/V Melville* in March and April 2004, as part of the NSF MARGINS ‘Source-to-Sink’ programme aiming to quantitatively study sedimentation in the GoP. The PECTEN cruise was conducted on *R/V Marion Dufresne* in June and July 2005, as part of an IMAGES program. Seven piston cores collected during the PANASH and PECTEN cruises are included in this study. Cores were retrieved across the southern GoP shelf edge and slope (i.e. Ashmore Trough), at water depths ranging from 113 to 775 m and spanned in length from 8.5 to 36.6 m (Table 1; Fig. 3B).

**Table 1.** Location, water depth, core length and laboratory data type from cores used in this study. Data references are the following: no superscript number = this study; 1 = de Garidel-Thoron *et al.* (2004); 2 = Carson *et al.* (2008); 3 = Jorry *et al.* (2010) (NAT = northern Ashmore Trough; SAT = southern Ashmore Trough).

Core	Location	Latitude and Longitude	Water depth (m)	Core length (m)	Laboratory data type and reference
MV26-73	NAT-Shelf	9.783°S 144.417°E	113	8.50	Grain size, carbonate content, mineralogy, microfauna abundance, petrography, radiocarbon dating, MARs
MV24-13	NAT-Slope	9.812°S 144.462°E	376	14.78	Stable oxygen isotopes, carbonate content, mineralogy, grain size, radiocarbon dating, MARs
MV24-17	NAT-Slope	9.744°S 144.744°E	682	12.21	Carbonate content, mineralogy, grain size, radiocarbon dating, MARs
MD97-34	NAT-Slope	9.907°S 144.661°E	760	26.90	Stable oxygen isotopes <sup>1</sup> , carbonate content, mineralogy, grain size, radiocarbon dating <sup>1</sup> , MARs
MD05-49	SAT-Slope	10.068°S 144.230°E	657	36.59	Stable oxygen isotopes <sup>2</sup> , carbonate content, mineralogy, grain size, radiocarbon dating <sup>2</sup> , aragonite MAR <sup>3</sup> , other MARs
MV24-06/07	SAT-Slope	10.440°S 144.205°E	775	13.80	Stable oxygen isotopes <sup>2</sup> , carbonate content, mineralogy, grain size, radiocarbon dating <sup>2</sup> , MARs <sup>2</sup>
MD26-74	SAT-Slope	10.733°S 144.079°E	684	11.34	Stable oxygen isotopes <sup>2</sup> , carbonate content, mineralogy, grain size, radiocarbon dating <sup>2</sup> , MARs <sup>2</sup>

### Multi-beam data

Bathymetric data for the study area were sourced from both high-resolution multibeam sonar surveys and a regional compilation of bathymetric data. Multibeam bathymetry data were acquired by the *R/V Melville* and *R/V Marion Dufresne*. The *R/V Melville* data were acquired sporadically during March and April 2004 using the vessel's 12kHz Sea Beam 2000 multibeam echosounder (L-3 Communications ELAC Nautik, Kiel, Germany). The *R/V Marion Dufresne* data were acquired during June 2005 using a Thomson Marconi TSM 5265 multibeam sonar (Thales Underwater Systems, Weybridge, UK). These data were processed and combined within Caris HIPS/SIPS to produce a 20 m resolution bathymetry raster. A regional bathymetric data compilation was sourced from Daniell (2008). This regional bathymetric dataset incorporated data from multiple sources including: multibeam sonar, single beam data, bathymetry derived from Landsat imagery and digitized nautical charts. Interpolation was used to fill gaps between bathymetry soundings and the resolution of the raster dataset was approximately 110 m. For display purposes, the higher-resolution multibeam bathymetry raster is overlain on the lower-resolution regional raster dataset.

### Shallow seismic profiling

The *R/V Melville* echosounder data were acquired using a Knudsen Engineering Limited 3.5 kHz system (KNUDSEN, Perth, ON, Canada), whereas the *R/V Marion Dufresne* was equipped with a SeaFalcon SBP 120 (Thales Underwater Systems). Data were used to image shallow sediment nature and accumulation geometry, in addition to selecting core locations.

### Shipboard core analyses

After core retrieval, shipboard measurements consisted of bulk density and magnetic susceptibility using a GeoTek Multi Sensor Core Logger (MSCL; Geotek Limited, Daventry, UK). Bulk density was calculated from the attenuation of gamma rays emitted from a 10 milli-Curie <sup>137</sup>Cs source through the sediment core. GeoTek MSCL-derived bulk density units are g cm<sup>-3</sup> and referred to as gamma-ray density (GRD) to separate them from traditional wet and dry bulk density measurements (Weber *et al.*, 1997). Magnetic susceptibility (MS) was measured using a Bartington MS2C Loop Sensor attached to the MSCL (Bartington Instruments Limited, Witney, UK). The MS values were corrected with respect to density and units are reported in 10<sup>-8</sup> m<sup>3</sup> kg<sup>-1</sup> (Thompson & Oldfield, 1986). Both MS and GRD

were measured on the MSCL at 1 cm intervals. After the measurements, cores were logged with focus on sediment colour, sedimentary structures, grain size, grain composition and fossils. This preliminary core description was later integrated with laboratory analyses.

### Laboratory core analyses

#### *Shelf core (MV26-73)*

In core MV26-73, thirty-five samples of about 20 g each were taken at approximately 20 cm depth intervals. After oven drying, samples were weighed and split into subsamples for compositional, textural and palaeontological analyses, as well as age dating.

#### *Slope cores (MV24-13, MV24-17, MD97-34, MD05-49, MV24-06/07 and MV26-74)*

Samples of approximately 10 g were taken from each core at 10 cm depth intervals. Samples were first freeze-dried to remove pore water. Small subsamples of the dried bulk sediment were then powdered with mortar and pestle, and put aside for carbonate and mineralogical analyses. The remaining samples were weighed, soaked overnight in a hydrogen peroxide solution, and sonicated to disaggregate grains. The disaggregated samples were then wet sieved to separate coarse (>63  $\mu\text{m}$ ) from fine (<63  $\mu\text{m}$ ) components. The coarse size fractions were dried overnight in an oven at *ca* 60°C and then weighed. The masses were subtracted from those of bulk samples to determine the percentage of coarse and fine components. The coarse fractions were then put aside to be further sieved, examined and sorted for stable oxygen isotope and radiocarbon analyses. The fine size fractions were allowed to settle out of suspension in a large beaker before being oven dried at *ca* 60°C. They were then powdered with mortar and pestle, and reserved for carbonate and mineralogical analyses.

#### *Carbonate content*

Bulk samples of about 2 to 3 g were analyzed with the standard carbonate bomb technique by Müller & Gastner (1971). Powdered sediment was placed into a glass bell jar with a vial containing 10 ml of 2.3N HCl. The top of the bell jar was connected to a burette filled with water and graduated in 0.1 ml increments. With the bell jar sealed, samples and acid were reacted to produce CO<sub>2</sub>, which was measured by water displacement. Carbonate content was calculated

from the volume of CO<sub>2</sub> produced using a standard curve generated by measuring and reacting different masses of laboratory-grade calcium carbonate. Replicate analyses of every tenth sample indicate a precision within 2%.

#### *Mass accumulation rate calculations*

Carbonate and siliciclastic mass accumulation rates (MAR<sub>carb</sub> and MAR<sub>silic</sub>, respectively) were calculated according to:

$$\text{MAR}_{\text{carb}} = (\text{carbonate } \%) * \text{LSR} * \rho_{\text{db}}$$

$$\text{MAR}_{\text{silic}} = (100 - \text{carbonate } \%) * \text{LSR} * \rho_{\text{db}}$$

where carbonate % is carbonate content measured by carbonate bomb, LSR is linear sedimentation rate, and  $\rho_{\text{db}}$  is dry bulk density. The LSR was determined by dividing a thickness of sediment by the time to accumulate this thickness. The dry-bulk density was calculated according to:

$$\rho_{\text{db}} = \rho_{\text{bulk}} - (\Phi_{\text{frac}} * 1.025)$$

where  $\rho_{\text{bulk}}$  is the bulk density of the sediment measured by the GeoTek MSCL (i.e. GRD),  $\Phi_{\text{frac}}$  is the fractional porosity of the sediment also measured by the MSCL, and 1.025 g cm<sup>-3</sup> is the average density of seawater.

#### *Grain size*

Bulk samples were wet sieved with a 2 mm sieve. The >2 mm component was weighed and used for grain identification. About 5 to 10 g of the <2 mm component was used for grain-size analysis. Grain size was measured on both bulk sediment and siliciclastic-only after acid removal of carbonate sediment. The distribution of different sizes was measured by analyzing light scatter patterns using a Malvern Mastersizer 2000 instrument (Malvern Panalytical, Malvern, UK) housed at the Department of Earth, Environmental and Planetary Science, Rice University.

#### *X-ray diffraction*

Part of the <2 mm bulk fraction was further wet sieved with a 63  $\mu\text{m}$  sieve. The <63  $\mu\text{m}$  fraction was examined by X-ray diffraction (XRD) analysis for mineralogy. Samples were ground by hand with an agate mortar and pestle. Ground samples, depending on their amount, were either packed with a spatula on an aluminum sample holder or dispersed in a methanol solution and pipetted onto a glass slide. Analyses were run on a Rigaku D/Max Ultima II machine (Rigaku, Tokyo, Japan) housed at the

Department of Earth, Environmental and Planetary Science, Rice University. Each sample was scanned twice at a fast speed of  $2^\circ \text{ min}^{-1}$  from  $2^\circ$  to  $100^\circ 2\theta$  and a low speed of  $0.25^\circ \text{ min}^{-1}$  from  $25^\circ$  to  $31^\circ 2\theta$ , the latter for an optimal resolution of carbonate phases.

#### *Microscopy (core MV26-73 only)*

The  $>63 \mu\text{m}$  sediment component was used for grain identification using reflected light microscopy and for foraminifera point counting analyses. From each sample a minimum amount of 300 specimens were picked, identified and percentage abundances were determined for palaeoenvironmental interpretations.

In addition, selected samples of the  $>63 \mu\text{m}$  component were used for petrographic analysis. Petrography was conducted on standard  $30 \mu\text{m}$  thick thin sections with a transmitted-light microscope. Unconsolidated samples were impregnated with epoxy prior to thin section preparation.

#### *Radiocarbon age dating*

*Shelf-edge core (MV26-73).* Six samples of *Halimeda* flakes, collected at various core depths, were used for accelerator mass spectrometry (AMS) radiocarbon analyses (Table 2). *Halimeda* flakes were chosen because they are present throughout the whole core, thus assuring consistent results. Samples of about 10 mg were rinsed and sonicated in distilled water and dried at  $60^\circ\text{C}$ . Then, they were dissolved in 103% orthophosphoric acid and the  $\text{CO}_2$  gas was collected under vacuum. The  $\text{CO}_2$  was converted to graphite by reaction with hydrogen over an iron catalyst at  $600^\circ\text{C}$ . The AMS analyses were performed at the Research School of Earth Science, The Australian National University. The AMS dates were corrected using the reservoir age for Heron Island, southern GBR (latitude  $23^\circ\text{S}$ , longitude  $152^\circ\text{E}$ ) of  $344 \pm 14$  year (Druffel & Griffin, 1999). Radiocarbon ages were calibrated using the Calib 4.3, Marine 98 database (Stuiver *et al.*, 1998).

*Slope cores (MV24-13, MV24-17).* Accelerator mass spectrometry (AMS) radiocarbon analyses were performed on 11 samples selected from two cores (MV24-13 and MV24-17), and used in conjunction with 28 additional published radiocarbon dates from five cores (MV24-06, MV24-07, MV26-74 and MD05-49, Carson *et al.*, 2008; MD97-34, de Garidel-Thoron *et al.*, 2004) (Table 2). Approximately 8 to 12 mg of mixed planktonic foraminifera (*Globigerinoides ruber*

and *Globigerinoides sacculifer*, ca 500 tests) were picked from the  $>150 \mu\text{m}$  size fraction using a binocular microscope. Specimens with obvious dissolution effects and secondary calcification were rejected. Analyses were performed at the University of California, Irvine Keck AMS facility. Ages are reported as conventional  $^{14}\text{C}$  years before present as well as corrected calendar years. Corrected ages were determined by using the Fairbanks *et al.* (2005) calibration program and CALIB 5.0.2 marine reservoir correction database (Stuiver *et al.*, 1998).

#### *Stable oxygen isotopes*

*Slope cores (MV24-13).* Stable oxygen isotopes were measured in core MV24-13 and integrated with oxygen isotope curves of the other five slope cores previously published (MV24-06, MV24-07, MV26-74 and MD05-49, Carson *et al.*, 2008; MD97-34, de Garidel-Thoron *et al.*, 2004). Samples consisted of six to eight specimens of *G. ruber* (white) (*G. sacculifer* without the large chamber for core MD05-49). Samples were picked from the 250 to  $300 \mu\text{m}$  size fraction and were analyzed at depth intervals ranging from 5 to 10 cm. Specimens with obvious indications of dissolution or secondary calcification were rejected, although preservation was generally good in each core. Stable oxygen isotope analyses were performed at the University of California, Davis (UCD), using a GV Instruments Optima mass spectrometer (Micromass Communications Inc., Charlotte, NC, USA). Isotope values are reported in delta notation relative to V-PDB (Vienna Pee Dee Belemnite) and have an analytical precision of  $\pm 0.05\text{‰}$ .

## RESULTS

In the following section, first are presented data from the six slope cores spanning the last sea-level cycle (i.e. MV26-74, MV24-06/07, MD05-49, MD97-34, MV24-13 and MV24-17). Next is the sedimentary record of the last deglaciation at the shelf edge (i.e. core MV26-73) along with slope core MARS from the same time interval.

The different segments of the last glacial/interglacial sea-level curve and corresponding MIS (Fig. 4A) are referred to as the following: penultimate interglacial maximum sea-level high (MIS 5e), early sea-level fall (MIS 5d to 5a), late sea-level fall (MIS 4 and 3), LGM sea-level low (MIS 2), last deglaciation (MIS 2 to 1 transition) and current interglacial sea-level high (MIS 1).

**Table 2.** Conventional and calibrated radiocarbon ages from cores used in this study.

Core	Sample depth	<sup>14</sup> C Age (years BP)	Calibrated <sup>14</sup> C Age (calendar years BP)	Reference	
MV26-73	0–20 cm	10 140 ± 194	10 970 ± 362	This study	
MV26-73	35 cm	10 386 ± 195	11 250 ± 418		
MV26-73	70 cm	11 682 ± 201	13 150 ± 207		
MV26-73	222 cm	14 044 ± 218	16 270 ± 335		
MV26-73	621 cm	15 274 ± 242	17 680 ± 371		
MV26-73	843 cm	14 718 ± 226	17 040 ± 347		
MV24-13	5–7 cm	2115 ± 20	1683 ± 32	This study	
MV24-13	78–80 cm	7570 ± 20	8016 ± 15		
MV24-13	279–281 cm	9630 ± 30	10 484 ± 48		
MV24-13	389–391 cm	10 780 ± 30	12 398 ± 95		
MV24-13	470–472 cm	13 600 ± 45	15 772 ± 124		
MV24-13	730–732 cm	15 400 ± 60	18 390 ± 159		
MV24-13	1248–1252 cm	29 170 ± 250	33 629 ± 512		
MV24-17	80–82 cm	9930 ± 30	10 929 ± 107	This study	
MV24-17	320–322 cm	13 050 ± 40	14 800 ± 89		
MV24-17	600–602 cm	24 710 ± 180	29 141 ± 238		
MV24-17	974–976 cm	29 000 ± 400	34 047 ± 441		
MD97-34	0 cm	780 ± 60	490 ± 51	de Garidel-Thoron <i>et al.</i> (2004)	
MD97-34	9 cm	1220 ± 60	785 ± 71		
MD97-34	96 cm	3880 ± 60	3817 ± 82		
MD97-34	130 cm	5050 ± 70	5445 ± 96		
MD97-34	176 cm	7630 ± 70	8090 ± 81		
MD97-34	210 cm	8040 ± 80	8475 ± 75		
MD97-34	303 cm	10 510 ± 90	11 832 ± 194		
MD97-34	344 cm	12 320 ± 90	13 869 ± 120		
MD97-34	368 cm	14 010 ± 110	16 366 ± 194		
MD97-34	468 cm	22 880 ± 190	27 021 ± 217		
MD97-34	502 cm	27 850 ± 310	32 328 ± 261		
MD97-34	601 cm	30 090 ± 340	34 876 ± 361		
MD97-34	720 cm	31 390 ± 370	35 993 ± 442		
MD05-49	10 cm	1685 ± 15	1283 ± 7		Carson <i>et al.</i> (2008)
MD05-49	140 cm	7930 ± 25	8392 ± 13		
MD05-49	200 cm	10 980 ± 45	12 902 ± 93		
MD05-49	260 cm	23 080 ± 120	27 232 ± 151		
MD05-49	330 cm	34 090 ± 470	38 752 ± 791		
MV24-06	10–12 cm	1680 ± 25	1278 ± 20	Carson <i>et al.</i> (2008)	
MV24-06	80–82 cm	9265 ± 20	10 080 ± 89		
MV24-07	10–12 cm	11 295 ± 25	12 865 ± 78	Carson <i>et al.</i> (2008)	
MV24-07	50–52 cm	26 710 ± 140	21 412 ± 32		
MV24-07	120–122 cm	39 300 ± 360	43 291 ± 445		
MV26-74	10–12 cm	2215 ± 20	1819 ± 31	Carson <i>et al.</i> (2008)	
MV26-74	100–102 cm	8095 ± 25	8534 ± 33		
MV26-74	150–152 cm	9825 ± 25	10 719 ± 36		
MV26-74	165–167 cm	11 005 ± 25	12 632 ± 35		
MV26-74	235–237 cm	37 420 ± 270	42 001 ± 175		

### Last sea-level cycle sedimentary record: slope cores

#### Chronostratigraphy

Core chronostratigraphy was established through integration of radiocarbon dating and high-

resolution planktonic oxygen isotope stratigraphy on five out of the six slope cores (Fig. 5). Distinct peaks and troughs in the foraminiferal  $\delta^{18}\text{O}$  records, correlated to and dated with the LR04 stacked benthic oxygen isotopic record of Lisiecki

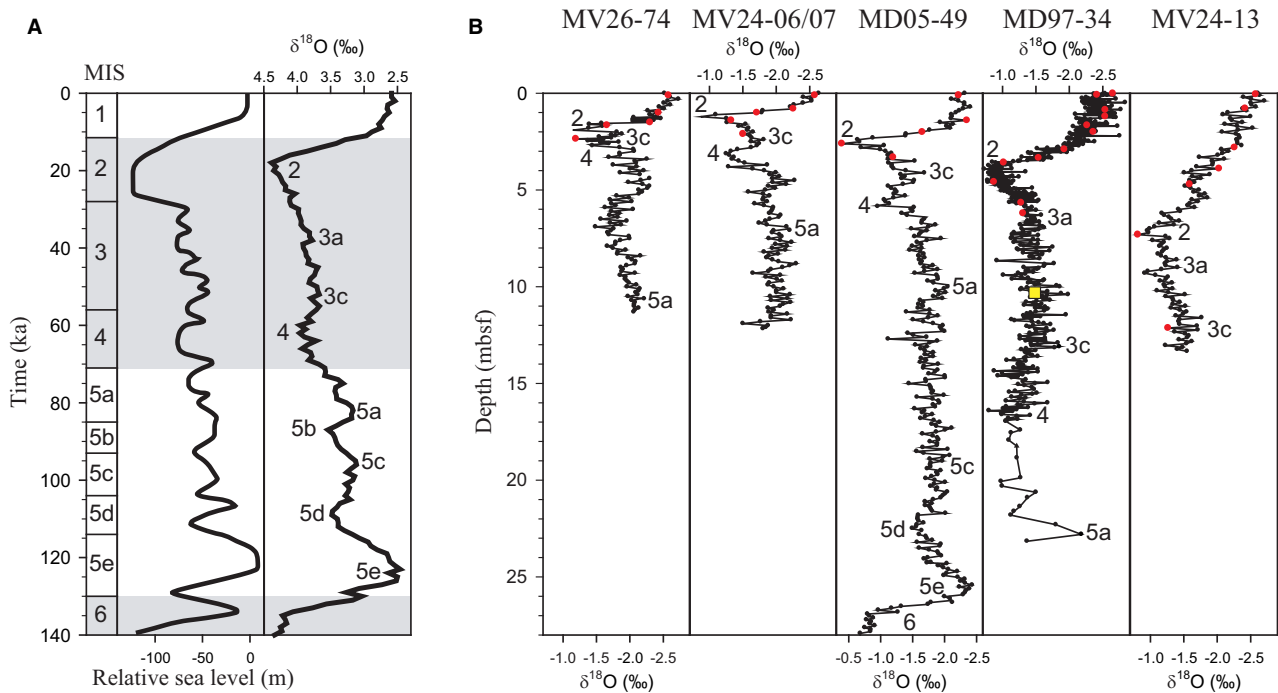


**Fig. 5.** Chronostratigraphy of Ashmore Trough cores. (A) Relative sea-level curve for the last glacial cycle (left; modified from Lambeck *et al.*, 2002) and stacked benthic foraminiferal oxygen isotope curve (right, modified from Lisiecki & Raymo, 2005) with MIS stages and substages (Railsback *et al.*, 2015). The grey shading in MIS 2, 3, 4 and 6, indicates glacial periods, while the non-shaded intervals, MIS 1 and 5, indicate interglacial periods. (B) Stable oxygen isotope data and MIS stages from Ashmore Trough cores. Marine isotope stages were correlated to the Lisiecki & Raymo (2005) curve. Oxygen isotope data points are depicted as black circles. Depths that also contain radiocarbon dates are marked with red circles. The location of the Laschamp Excursion, identified by Blanchet *et al.* (2006), is marked by a yellow square on core MD97-34.

& Raymo (2005), demonstrate that core MD05-49 covers the longest time interval up, to 140 ka (Fig. 5). Moreover, in core MD05-2949, the last occurrence of pink-pigmented *G. ruber* clearly indicates the transition between MIS 6 and MIS 5 (Thompson *et al.*, 1979; Jorry *et al.*, 2010).

Overall, light oxygen isotope values mark interglacial intervals, with the most depleted values occurring in MIS 5e and MIS 1, during which sea level was at its maximum (Fig. 5). Heavy oxygen isotope values mark the glacial intervals, with the most enriched values occurring in MIS 6 and MIS 2 when sea level reached its minimum (Fig. 5). Thirty-nine corrected radiocarbon ages (Table 2) anchor the age model. Additionally, the Laschamp geomagnetic excursion was identified in MD97-34 (Blanchet *et al.*, 2006; Leduc *et al.*, 2006) and was also used as age datum (41 ka at 10.3 m) in this core.

#### Overall sediment composition and grain size

Sediment in Ashmore Trough slope cores consists of two dominant components: carbonate

and siliciclastic material. Siliciclastic contents are reciprocal of carbonate contents and, therefore, were quantified as:  $100 - \text{CaCO}_3 \%$ . Carbonate sediment is made of biogenic material shed from surrounding carbonate platforms and tests of pelagic organisms settled through the water column, resulting in a mixture of aragonite, high-Mg calcite (HMC) and low-Mg calcite (LMC). Siliciclastic sediment was delivered to the GoP shelf edge by PNG rivers. It consists of quartz with lesser amounts of plagioclase feldspar, illite, muscovite, chlorite, kaolinite and smectite.

Grain size is unevenly distributed, ranging from clay to sand-sized particles. Coarse-size fraction,  $>63 \mu\text{m}$ , is generally  $<20\%$  (Fig. 6) and it is dominated by pelagic carbonate particles, primarily planktonic foraminifera (LMC) and pteropods (aragonite). Benthic constituents are minimal (for example, benthic foraminifera, ostracods, echinoderm fragments and sponge spicules). Coarse fraction  $>20\%$  occurs in southern Ashmore Trough cores during minimum sea

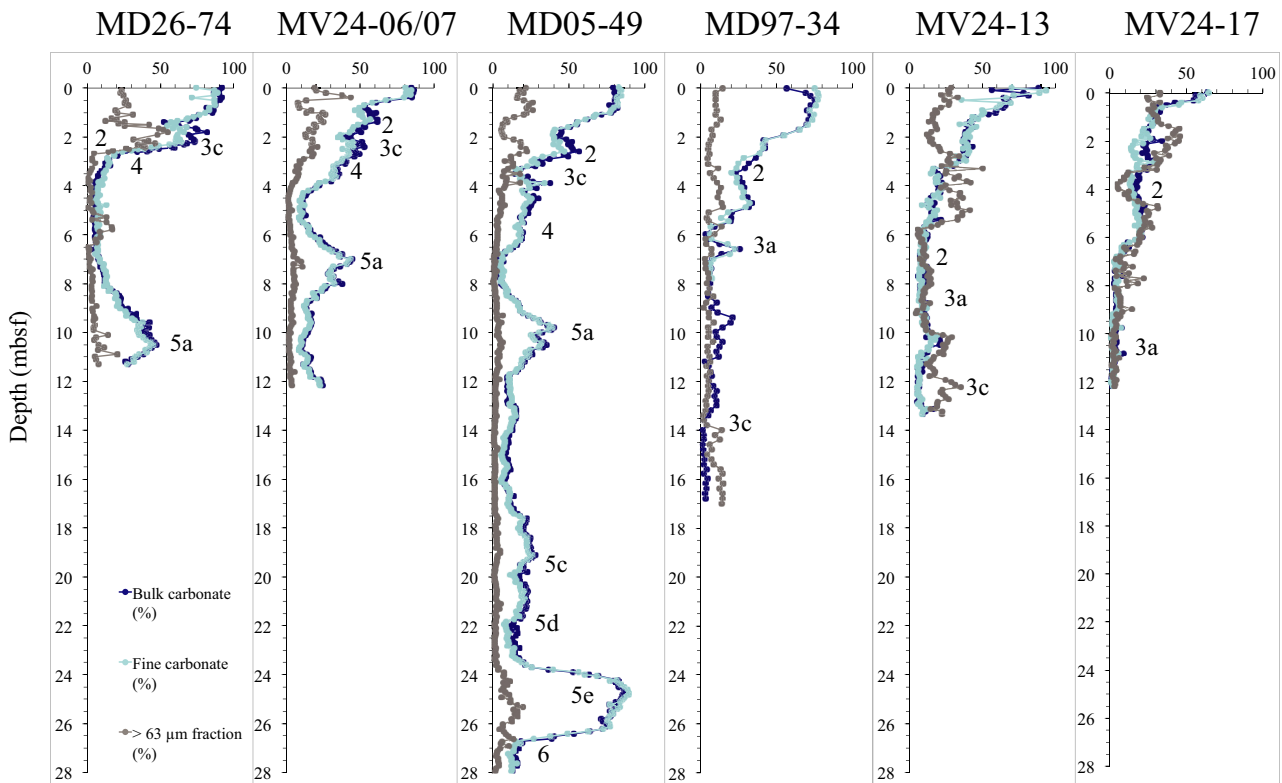


**Fig. 6.** Bulk carbonate content, fine (<63  $\mu\text{m}$ ) carbonate content, and coarse (>63  $\mu\text{m}$ ) bulk size fraction from Ashmore Trough cores. Numbers represent marine isotope stages and substages depth-correlated to Fig. 4. Peaks of the bulk coarse fraction co-varying with bulk carbonate content indicate intervals with coarse carbonate sediment such as planktonic foraminifera (for example, cores MD26-74 and MD05-49). Peaks of the bulk coarse fraction crossing over bulk carbonate content indicate intervals with siliciclastic sand (for example, base of core MD97-34, cores MV24-13 and MV24-17).

level (MIS 2) and last deglacial early sea-level rise (MIS 2 to 1 transition) (Fig. 6). In such intervals the coarse fraction co-varies with bulk carbonate content indicating dominant carbonate mineralogy (Fig. 6). Intervals with coarse fraction spanning from 20 to 50% and crossing over the bulk carbonate curve, occurs in the northern Ashmore Trough (cores MV24-13 and MV24-17) during late sea-level fall (MIS 3) and last deglacial early sea-level rise (MIS 2 to 1 transition) (Fig. 6). These intervals correspond to deposition of silty/sandy siliciclastic turbidites.

Fine-size fraction, <63  $\mu\text{m}$ , dominates in all cores (Fig. 6). Carbonate fine fraction >50% occurs during interglacial sea-level maximum (MIS 5e and MIS 1), and between 20% and 50% during the smaller amplitude sea-level rise of MIS 5 sub-stages (i.e. 5c and 5a). Fine carbonate consists of bank-derived (i.e. neritic) aragonite, HMC and coccoliths (LMC).

#### *Siliciclastic/carbonate content and mass accumulation rates*

Siliciclastic sediment across Ashmore Trough is highly variable (Fig. 7). In southern Ashmore Trough (i.e. cores MD26-74, MV24-06/07, MD05-2949), siliciclastic MARs were highest (ca 20 to 60  $\text{g cm}^{-2}\text{kyr}$ ) during early sea-level fall (MIS 5d to 5a), and lowest (<5  $\text{g cm}^{-2}\text{kyr}$ ) during late fall and LGM sea-level low (MIS 4, 3 and 2). In northern Ashmore Trough (i.e. cores MV97-34, MV24-13 and MV24-17, although with a more limited record span to 60 or 40 ka), siliciclastic MARs were highest (ca 20 to 100  $\text{g cm}^{-2}\text{kyr}$ ) through late sea-level fall (MIS 4 and 3), lessen during LGM sea-level low (MIS 2) and resumed to pre-LGM levels during last deglacial sea-level rise (MIS 2 to MIS 1 transition) (Fig. 7).

Carbonate sediment is mostly fine material thus resulting in similar bulk and fine carbonate



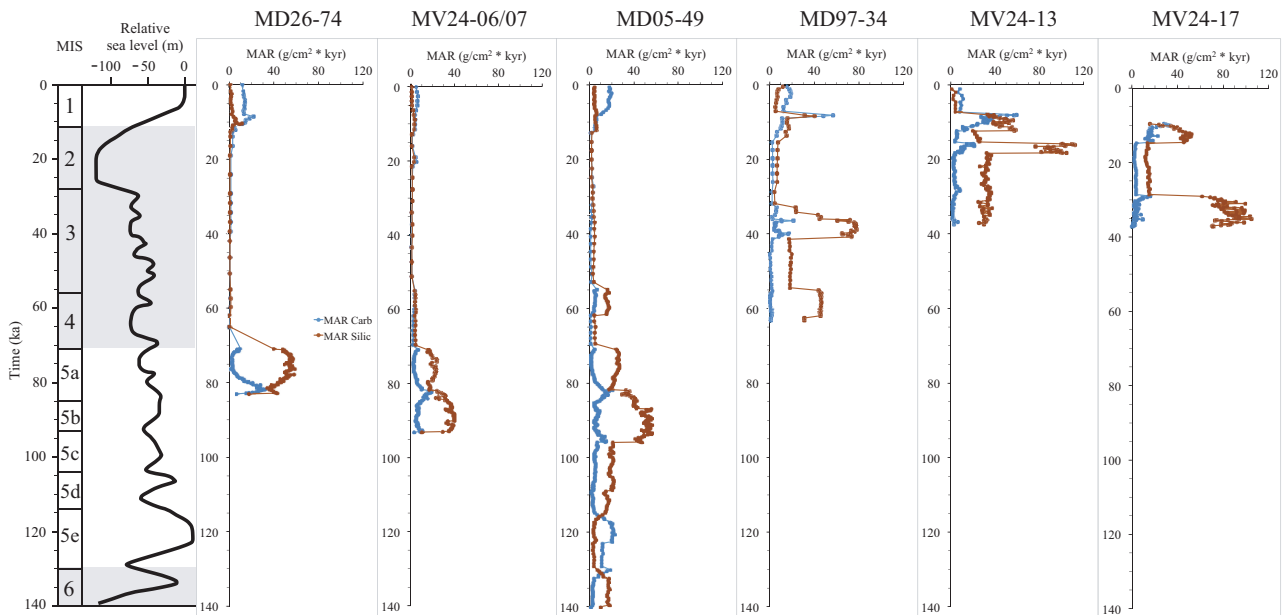


**Fig. 7.** Bulk siliciclastic and carbonate mass accumulation rates ( $MAR_{\text{silic}}$  and  $MAR_{\text{carb}}$ , respectively) from Ashmore Trough slope cores correlated to the last glacial cycle relative sea-level curve and marine isotope stage (MIS). Only core MD05-49 in southern Ashmore Trough recovered sediments from the penultimate interglacial substages MIS 5e to 5c.

contents (Fig. 6). Carbonate content is extremely variable across the cores ranging between *ca* 1% and 92% (Fig. 6). The highest carbonate MARs (up to  $60 \text{ g cm}^{-2}\text{kyr}$ ) occurred during penultimate and current interglacial sea-level high (MIS 5e and MIS 1) (Fig. 7). Relatively high values occurred during small amplitude sea-level rise of early sea-level fall (MIS 5c and MIS 5a) (Fig. 7).

#### *Carbonate mineralogy and mass accumulation rates*

Aragonite usually dominates the fine-fraction carbonate mineralogy ranging from values of *ca* 1 to 60% of total fine fraction sediment. Maximum aragonite MARs (up to *ca*  $35 \text{ g cm}^{-2}\text{kyr}$ ) typically occurred during penultimate and current interglacial sea-level high (MIS 5e and MIS 1; Fig. 8). During the deglacial transition, the first occurrence of fine aragonite is in most of the cores dated at 11.5 to 11.0 ka (Fig. 8). Relatively high values occurred during small amplitude sea-level rise (i.e. MIS 5c and MIS 5a) of longer-term fall. Aragonite MAR peaks also correlate to negative excursions in the oxygen isotope record. The lowest aragonite MARs ( $<5 \text{ g cm}^{-2}\text{kyr}$ ) occurred during late sea-level fall and LGM sea-level low (MIS 4, 3 and 2). The HMC and LMC content ranges from 1 to

22% and 3 to 20%, respectively. The HMC and LMC MARs generally co-vary with aragonite MARs, however the former have lower maximum values up to  $15 \text{ g cm}^{-2}\text{kyr}$  (Fig. 8). The LMC accumulation rates episodically exceeded aragonite accumulation rates during low amplitude sea-level fall of the longer-term fall (MIS 5b, MIS 4 and MIS 3) (Fig. 8). LMC MARs higher than HMC MARs occur during substage MIS 5b sea-level fall (i.e. cores MV24-06/07 and MD05-49; Fig. 8).

#### *Shallow seismic*

The 3.5 kHz data provide an important tool for correlating between cores and across Ashmore Trough as well as revealing sediment package geometry. Southern Ashmore Trough contains several seismic reflections that are regionally correlative (Fig. 9A).

Such reflections correspond to acoustic impedance contrasts expected to be controlled by a combination of sediment composition, grain size, compaction and early cementation (Slowey *et al.*, 1989; Breitzke, 2000). Two-way travel time to depth conversion was based on P-wave velocity of  $1500 \text{ m s}^{-1}$ , typical of near sea floor unconsolidated hemipelagic mud (Breitzke, 2000). Seismic to core tie shows that there is a good

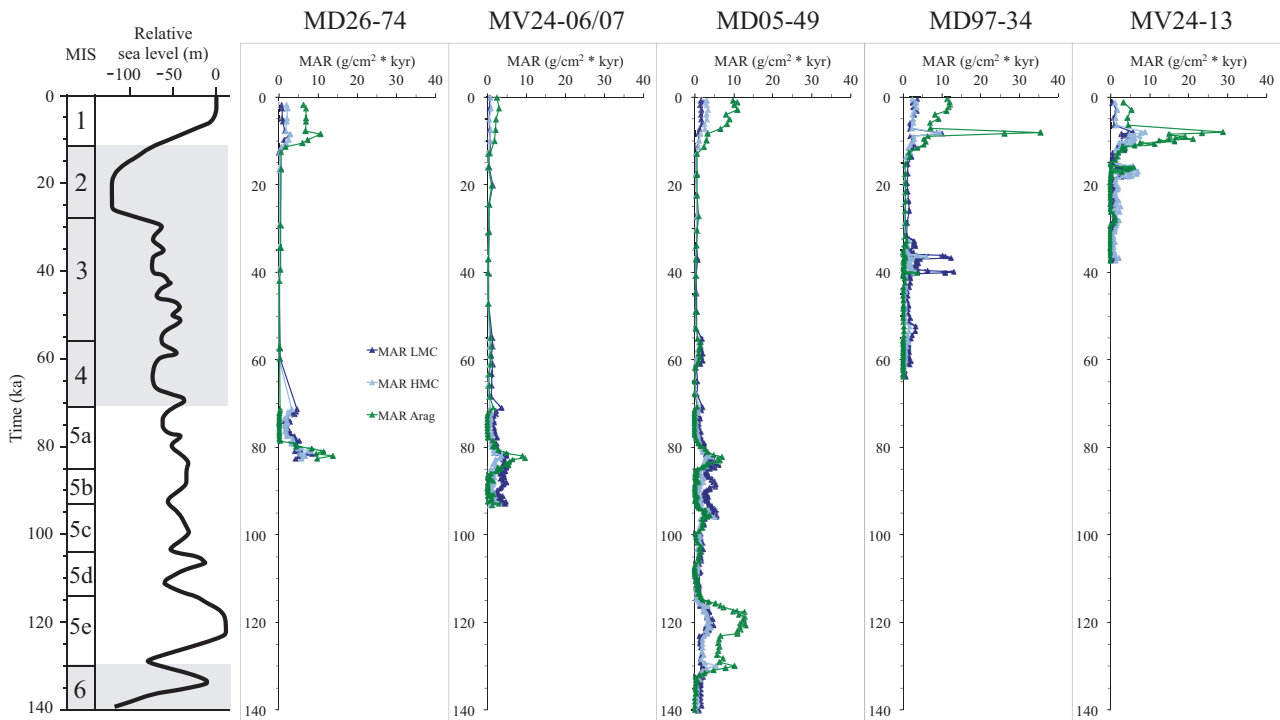


**Fig. 8.** Carbonate mineral mass accumulation rates (MAR) from Ashmore Trough slope cores correlated to the last glacial cycle relative sea-level curve and marine isotope stage (MIS) ( $MAR_{arag}$  = aragonite;  $MAR_{HMC}$  = high-Mg calcite;  $MAR_{LMC}$  = low-Mg calcite). Only core MD05-49 in southern Ashmore Trough recovered sediments from the penultimate interglacial substages MIS 5e to 5c.

correspondence between acoustic impedance contrast and major changes in sediment composition. For example, in core MD05-49, a high amplitude reflection at *ca* 27 metres below sea floor (mbsf) corresponds to the bottom of a carbonate mud interval dated at *ca* 130 ka (i.e. MIS 6 to MIS 5e transition; Fig. 9B). Other moderate to high-amplitude reflections occur at 23 mbsf and 7 mbsf and, based on core to seismic tie, they can be dated at 115 ka and 70 ka, respectively (Fig. 9 B). These major compositional changes are expected to be synchronous and, therefore, approximate time lines. This is confirmed by the compositional change at 70 ka recorded across the southern Ashmore Trough in cores MV24-06/07, MV24-74 and MD05-49 (Figs 7 and 8).

Using the 115 ka, 70 ka and sea floor reflection, two sedimentary units are mapped across southern Ashmore Trough (Fig. 9A). The lower unit (between the 115 ka and 70 ka reflections) shows semi-transparent homogeneous seismic facies ranging in thickness from 18 to 50 m, and thinning towards the south and downslope. In a few locations internal reflections can be identified. The upper unit (between the 70 ka and sea floor

reflections) is a high-amplitude, homogeneous seismic facies ranging in thickness from 2 to 12 m.

In northern Ashmore Trough seismic reflections show limited lateral continuity because often they are juxtaposed to chaotic/transparent seismic facies. One such facies is located on the lower slope just north-east of MD05-49 where it truncates adjacent reflections (Fig. 9A). This seismic interval is part of a sedimentary body that displays positive relief on the sea floor. Chaotic/transparent facies are interpreted as mass transport deposits.

Lastly, a southward thinning transparent seismic wedge covers much of the northern slope (Fig. 9C). This unit, penetrated in cores MV24-13 and MV24-17, is thickest in north-east Ashmore Trough, south-east of Portlock Reef, where it contains few internal reflections.

### Last deglacial sedimentary record: shelf-edge core and slope cores

#### *Shelf edge sea-floor bathymetry*

The two most prominent geomorphic elements on Ashmore Trough shelf edge are the delta

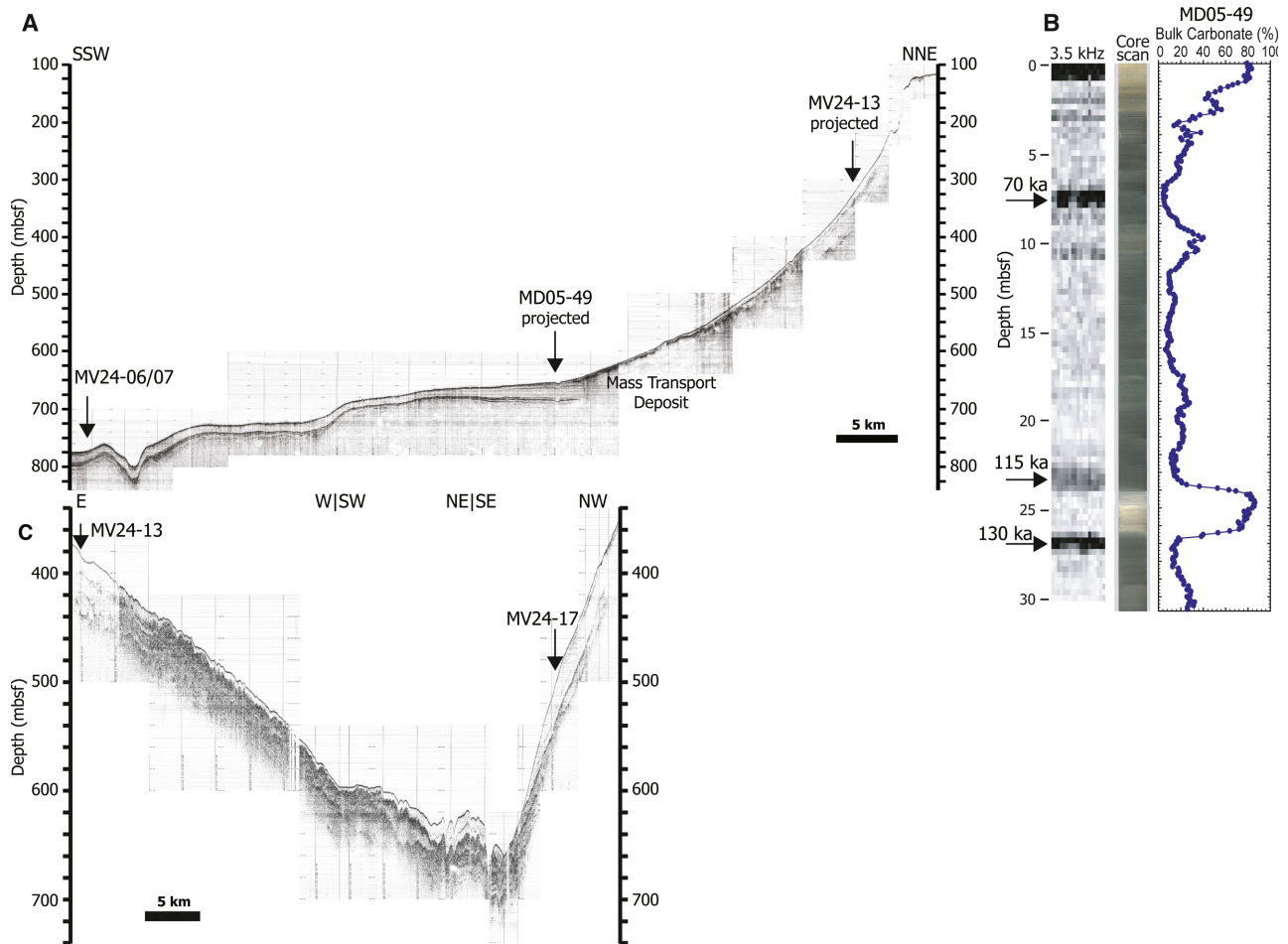


**Fig. 9.** Shallow 3.5 kHz seismic profiles, including intersected and nearby projected cores, and seismic to core correlation. (A) Seismic profile across southern Ashmore Trough (AT; see Fig. 3B for seismic profile trace). A sediment wedge is present in the northern sector of the profile (with projected core MV24-13), which is truncated by chaotic and transparent seismic facies interpreted as a mass transport deposit. The southern sectors of the profile, between core MD05-49 and MV24-06/07, show a sediment interval characterized by seismic facies with alternating high amplitude and transparent reflections. Notice the sediment interval thinning southward. (B) Seismic to core correlation for core MD05-49. From left to right are: slice of 3.5 kHz seismic, core scan, and bulk carbonate content. Black arrows point to main reflections dated at 130, 115 and 70 ka on the base of seismic to core tie. Such reflections show a good correspondence with major compositional changes. (C) Shallow 3.5 kHz seismic profile parallel and across northern AT slope with intersected cores (see map in Fig. 3B for trace of the profile). Notice the sediment wedge in the northern leg of the profile, which runs perpendicular to the slope.

complex to the north and the drowned barrier reef (Fig. 3C).

Core MV26-73 is located about 2 km landward of the modern shelf edge at a water depth of 113 m (Fig. 3D). In this portion of the shelf edge, the top of the drowned barrier reef is as shallow as *ca* 60 to 70 mbsf (Fig. 3D). Moreover, the drowned reef is segmented due to the presence of channels running approximately perpendicular to the shelf edge (Fig. 3D).

#### *Shelf-edge core stratigraphy and composition*

The 8.5 m long MV26-73 core contains major variations in sediment composition (Figs 10 and 11). These differences can be divided into five stratigraphic units based on sedimentology, mineralogy and faunal composition. For convenience, these units are labelled 'A' to 'E' from bottom to top. Chronostratigraphy of core MV26-73 is based on six radiocarbon ages (Table 2) showing that sediment accumulated from *ca* 17 to 11 ka.

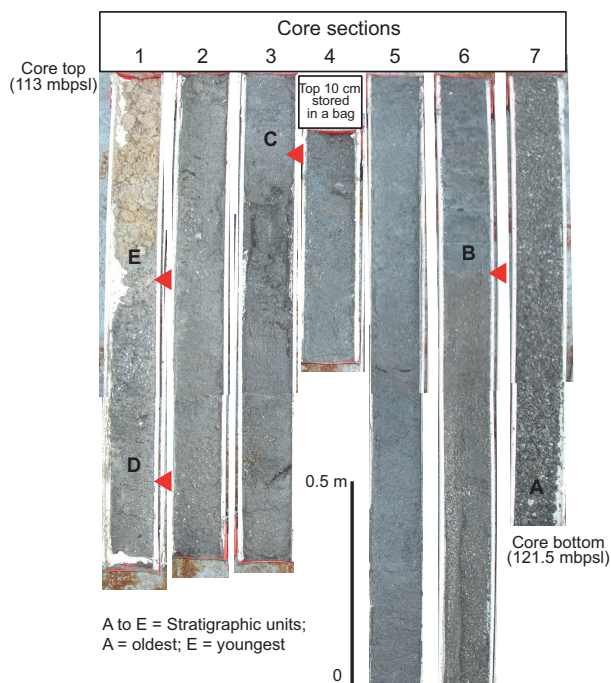


**Fig. 10.** Core MV26-73 photograph with stratigraphic units A to E. The core shows an overall fining-upward succession. Composition of units A, D and E is predominantly carbonate whereas units B and C are siliciclastic. Unit E is weakly cemented and appears as rubble. Red triangles mark unit boundaries.

**Unit A.** The lowermost Unit A, from 8.5 to 6.5 mbsf, is a fining-upward carbonate sandy gravel (Figs 10 and 11). Carbonate content is >80%, MS is below 20 SI, and GRD is *ca*  $2.1 \text{ g cm}^{-3}$ . Siliciclastic grains are a minor constituent and the <2 mm siliciclastic fraction ranges from fine sand to silt. XRD analysis of the bulk fine fraction (<63  $\mu\text{m}$ ) shows that it is mainly composed of quartz and calcite with virtually no clay minerals (Fig. 12A). The bottom of Unit A is dated at  $17.040 \pm 0.347 \text{ ka}$  (Fig. 11).

The gravel fraction, more abundant in the lower half of the unit, consists of carbonate bioclasts such as molluscs, *Halimeda*, echinoderms, coral and bryozoan fragments, as well as larger benthic foraminifer tests. Molluscs include gastropods and disarticulated bivalves such as *Barbatia* sp., *Prothotaca* sp., *Cyclinella* sp., *Colisella* sp., *Conus* sp. and *Cypraea* sp. Across the entire unit, benthic foraminiferal fauna is dominated by Calcarinidae (for example, *Calcarina gaudichaudii*, *Calcarina defrancii* and *Neorotalia calcar*; Fig. 11). The remainder of the fauna consists of Amphisteginidae (for example, *Amphistegina lobifera* and *Amphistegina lessonii*),

Soritidae (for example, *Marginopora* sp., *Amphisorus* sp. and *Parasorites* sp.), Elphiidae and Miliolidae (Fig. 11).

Sand-sized grains consist of ooids, subangular and rounded quartz grains, and smaller bioclasts. Ooid sizes range between 0.2 mm and 1.0 mm. Petrographic analysis shows that the cortex thickness is generally much thinner than the diameter of the nucleus and, therefore, they can be classified as superficial ooids (*sensu* Carozzi, 1957; Fig. 13A). The crystal arrangement of the cortex is radial and microboring is common (Fig. 13B). Only a few ooids show a fully micritized cortex. Nuclei mainly consist of bioclasts (for example, red algae and benthic foraminifera) and quartz grains (Fig. 13A and B). X-ray diffraction analysis of pulverized ooids shows that HMC is the dominant mineralogy (Fig. 12B).

**Unit B.** Unit B, the thickest of all units, spans from 6.5 to 2.8 mbsf, and consists mostly of bioturbated quartz-skeletal medium-fine sand (Figs 10 and 11). Carbonate content is mostly below 25%, with the exception of a bed at about 3.9 mbsf where it increases above 80% due to abundant coated grains (Fig. 11). Magnetic susceptibility is the highest recorded in the core and it peaks at 120 SI near the base of the unit, whereas GRD is lower than the underlying Unit A with values approximately at  $2 \text{ g cm}^{-3}$  (Fig. 11). Grain-size distribution of the <2 mm siliciclastic fraction is coarsening-upward (Fig. 11). The XRD and petrographic analyses show greater detrital quartz and clay content compared to the underlying Unit A (Figs 12C and 13C). Clay minerals consist of chlorite and illite (Fig. 12C). From 5.8 mbsf and upward, detrital wood debris is present whereas ooids decrease (Fig. 11). Bioclasts >2 mm in size are minor and consist of gastropods, *Halimeda*, echinoderms and bryozoans. The foraminiferal content is very similar to Unit A, with Calcarinidae representing the predominant genus (foraminiferal relative abundance >80%; Fig. 11). The carbonate bed at about 3.9 mbsf corresponds to a return of abundant ooids and coated grains (Figs 11 and 13D). In this bed, other grains are peloids, larger benthic foraminifera, *Halimeda*, echinoderm spines, coral fragments, bryozoans and rare detrital quartz. A  $^{14}\text{C}$  date at the base of the unit shows an age of  $17.680 \pm 0.371 \text{ ka}$ , slightly older than the underlying date (Fig. 11).

**Unit C.** This unit, spanning from 2.8 to 1.0 mbsf, records some major compositional changes,

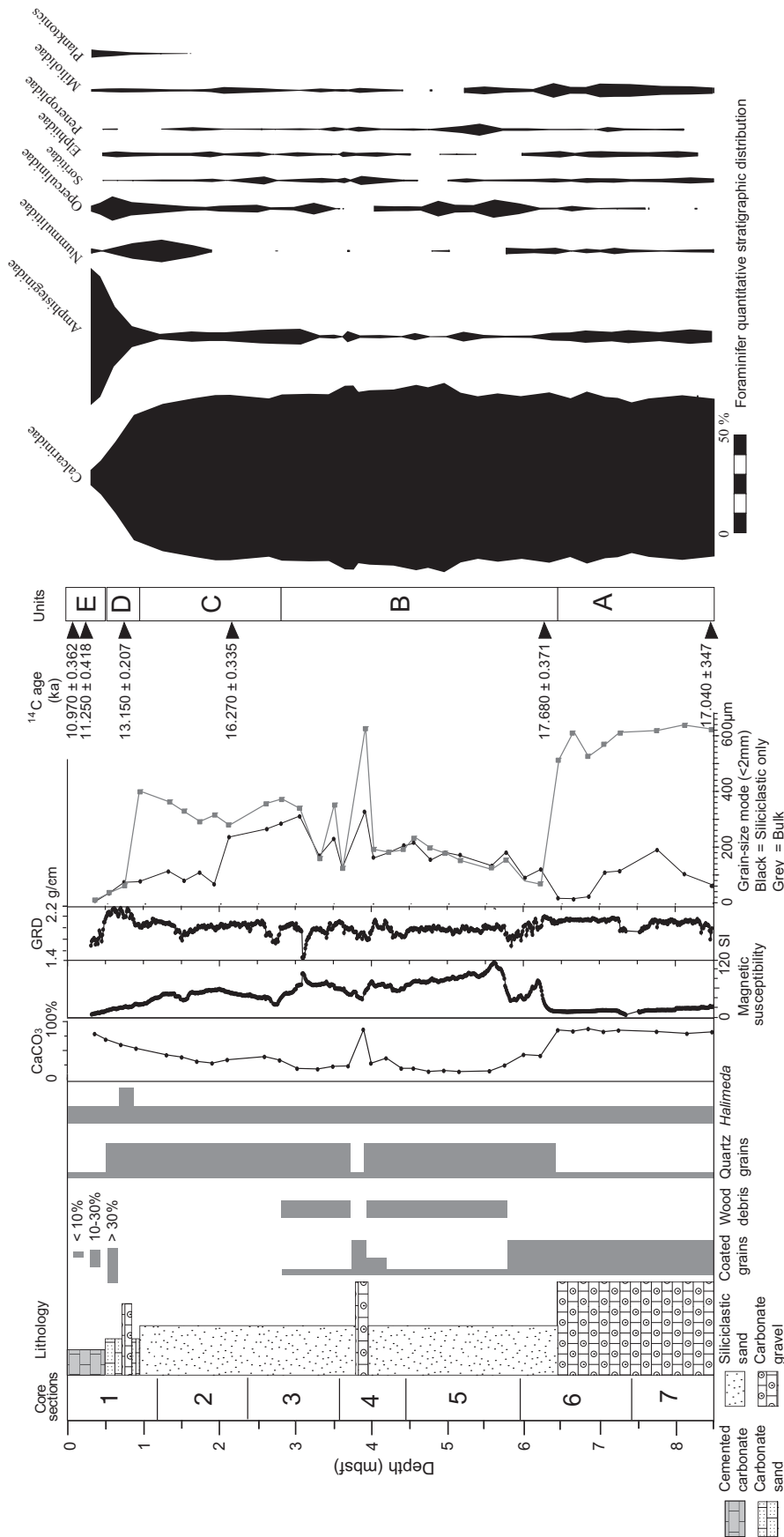


**Fig. 11.** Core MV26-73 lithology, texture, stratigraphy, age and quantitative vertical distribution of foraminifera. Distribution of coated grains, wood debris, quartz and *Halimeda* are semi-quantitative, based on visual comparison charts (Flügel, 1982), and derived from reflected light microscopy analysis. Magnetic susceptibility and gamma-ray derived bulk density (GRD) were measured at 1 cm intervals. Carbonate content is from bulk samples. Grain size was measured on <2 mm sediment fraction on both bulk and siliclastic only sediment (grey and black curves respectively). The AMS radiocarbon ages were measured on selected *Halimeda* flakes from six different intervals. Quantitative stratigraphic distribution of foraminiferal assemblage is based on point-counting analysis of 35 samples with approximately 20 cm spacing. From each sample a minimum amount of 300 specimens were identified. Overall, Calamidae is the dominant group in units A to C whereas Amphisteginidae is dominant from middle of Unit D to the top (i.e. Unit E).

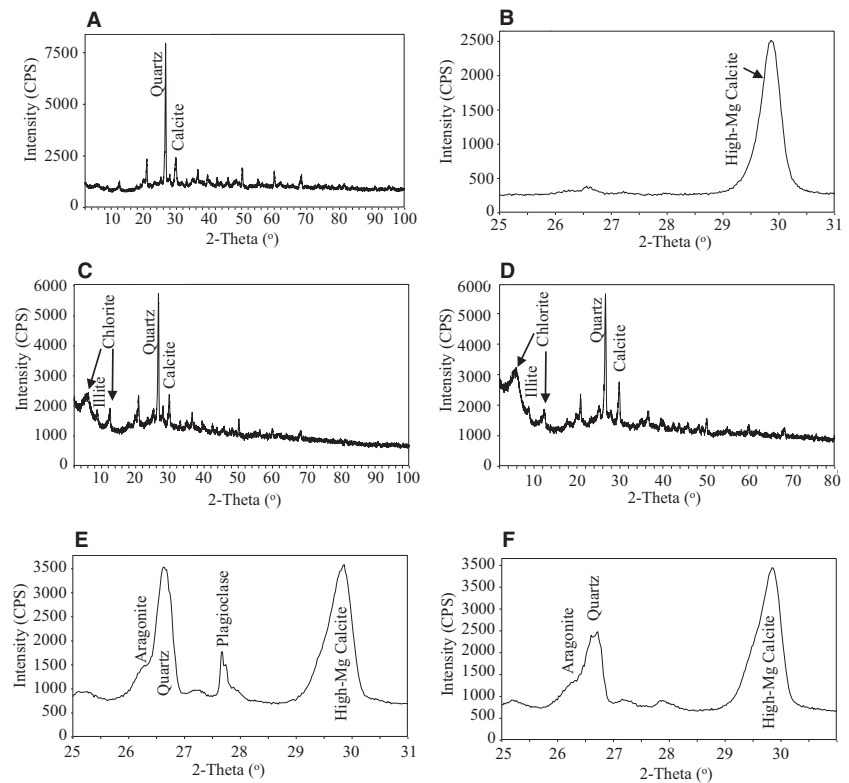


**Fig. 12.** X-ray diffractograms of select samples: (A), (C) and (D) are scans at a fast speed of  $2^{\circ} \text{ min}^{-1}$  from  $2^{\circ}$  to  $100^{\circ} 2\theta$ ; (B), (E) and (F) are scans at a low speed  $0.25^{\circ} \text{ min}^{-1}$  from  $25^{\circ}$  to  $31^{\circ} 2\theta$  for an optimal resolution of the carbonate phases. (A) Unit A, 8.1 mbsf; (B) ooid mixture from units A and B; (C) Unit B, 5.6 mbsf; (D) Unit C, 1.9 mbsf; (E) Unit D, 0.52 mbsf; (F) Unit E, 0.38 mbsf.

such as the absence of ooids and wood debris, and the first appearance of planktonic foraminifera at 1.7 mbsf (Fig. 11). It consists of bioturbated quartz-skeletal fine sand with carbonate content increasing upward from about 30 to 50% (Figs 10 and 11). Magnetic susceptibility increases from 40 SI at the base of the Unit, to *ca* 60 SI at 2 mbsf and it decreases back to 40 SI towards the top of the unit (Fig. 11). Gamma-ray density (GRD) is *ca*  $2 \text{ g cm}^{-3}$  and increases to  $2.2 \text{ g cm}^{-3}$  in the topmost 50 cm of the unit (Fig. 11). Grain-size distribution of the siliciclastic-only fractions ( $<2 \text{ mm}$ ) is fining-upward (Fig. 11). The grain size of the bulk fraction ( $<2 \text{ mm}$ ) shows a similar trend up to 2.1 mbsf, followed by an opposite coarsening upward trend to the top of the unit (Fig. 11). Bioclasts  $>2 \text{ mm}$  consist mainly of *Halimeda*, articulated bivalves, gastropods, echinoderms and bryozoans. XRD analyses of the  $<63 \mu\text{m}$  fraction shows quartz, calcite and clays (for example, chlorite and illite) as the main minerals (Fig. 12D). The benthic foraminiferal fauna is still dominated by Calcarinidae with a relative abundance  $>75\%$  (Fig. 11). A  $^{14}\text{C}$  date in the lower part of the unit indicates an age of  $16.270 \pm 0.335 \text{ ka}$  (Fig. 11).

**Unit D.** This unit spans from 1.0 to 0.5 mbsf and it consists of bioturbated carbonate

bioclastic medium to fine sand with subordinate quartz grains (Figs 10 and 11). Carbonate content increases steadily upward from 50 to 70%, along with GRD values up to  $2.4 \text{ g cm}^{-3}$ . Conversely, magnetic susceptibility decreases from 40 to 20 SI (Fig. 11). Bioclasts mainly consist of *Halimeda*, bivalves, gastropods, echinoderms and bryozoans. A 20 cm thick bed, made mostly of *Halimeda* flakes, is present at 0.75 mbsf. XRD analyses of the  $<63 \mu\text{m}$  bulk fraction show that quartz and high-Mg calcite are the dominant mineralogies (Fig. 12E), with HMC becoming relatively more abundant at the top of the unit. Unit D is characterized by a major change in the benthic foraminiferal fauna. Towards its top, *Amphisteginidae* (for example, *Amphistegina radiata*, *Amphistegina bicirculata* and *Amphistegina papillosa*) replace Calcarinidae as the predominant group (Fig. 11). Relative abundance of planktonic foraminifera is greater than in the underlying Unit C (Fig. 11). The age of Unit D is constrained by a  $^{14}\text{C}$  date at 0.7 mbsf of  $13.150 \pm 0.207 \text{ ka}$  (Fig. 11).

**Unit E.** The uppermost Unit E is 0.5 m thick and consists of weakly cemented carbonate with colour transitioning upward from light grey to light brown (Figs 10 and 11). Its rubbly texture did not permit core measurements such as

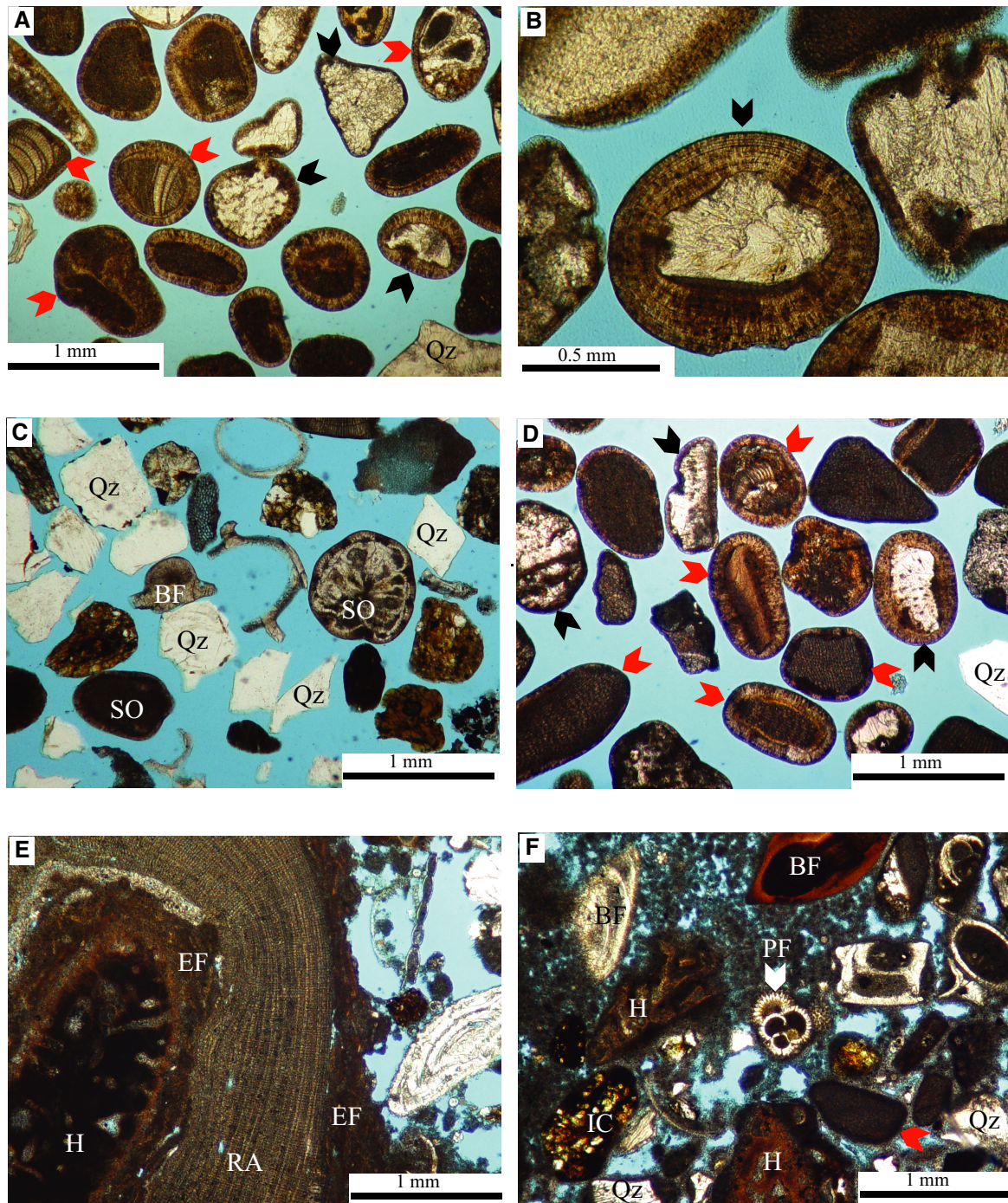


**Fig. 13.** Transmitted-light photomicrographs of selected samples (blue background is epoxy): (A) Unit A ooids. Notice the thin cortex of the majority of the ooids (i.e. superficial ooids). Nuclei mainly consist of quartz (black arrows) and bioclaster (red arrows). Uncoated quartz grains (Qz) are also present. (B) Close-up of an ooid (black arrow) with quartz nucleus and radial cortex. Dark brown patches in the cortex represent micro-borings. (C) Unit B silt/sand fraction with abundant angular quartz grains (Qz), subordinate superficial ooids (SO) and benthic foraminifera (BF). (D) Ooid-rich bed within Unit B. Similar to the underlying Unit A, ooids are mostly superficial with nuclei consisting of quartz (black arrows) and bioclaster (red arrows). Uncoated quartz grains (Qz) are also present. (E) Unit E with *Halimeda* flake (H) coated by multiple layers of encrusting foraminifera (EF) and red algae (RA). (F) Unit E microfacies consists of grainstone with benthic and planktonic foraminifera (BF and PF, respectively), *Halimeda* fragments (H), quartz grains (Qz) and intraclasts (IC). Most grains are coated with an isopachous rim of bladed calcite cement (red arrow).

magnetic susceptibility and bulk density. For the same reason, washing and sieving was only possible from the base of the unit up to 0.35 mbsf. XRD analysis of the <63  $\mu\text{m}$  fraction near its base shows a strong high-Mg calcite peak with a less pronounced quartz peak (Fig. 12F). Microfacies consist mainly of bioclastic packstone–grainstone with *Halimeda*, molluscs, bryozoans, echinoderms, red algae, encrusting foraminifera (*Gypsina* sp.), amphisteginids and planktonic foraminifera (Fig. 13E and F). Non-carbonate grains are quartz, feldspar and rare glauconite. Carbonate cements exhibit two morphologies: micropeloidal with clotted texture; and schalenodric (Fig. 13F). Relative abundance of foraminifera at the base of Unit E (up to 0.35 mbsf), shows that Amphisteginidae (for example, *Amphistegina bicirculata* and *Amphistegina papillosa*) remains the predominant group (*ca* 70%) (Fig. 11). In the same interval, mineralogy of the fine fraction consists mainly of HMC with subordinate quartz and aragonite (Fig. 12F).  $^{14}\text{C}$  dates indicate ages of  $11.250 \pm 0.418$  and  $10.970 \pm 0.362$  ka at the bottom and top of the unit, respectively (Fig. 11).

#### Mass accumulation rates

**Shelf core.** Highest bulk carbonate and siliciclastic MARs, up to  $1200 \text{ g cm}^{-2}\text{kyr}$ , occurred at core MV26-73 location from *ca* 17 ka until *ca* 16.2 ka and correspond to deposition of units A and B (Fig. 14A). However, the above value should be considered an approximation because the bottom of Unit A was not recovered in the core and relatively few radiocarbon ages constrain these two units, which together represent 65% of the entire core thickness. Both MARs decreased afterwards during deposition of units C to E; but while siliciclastic MARs steadily declined down to  $<10 \text{ g cm}^{-2}\text{kyr}$  near 11 ka, carbonate MARs remained more constant spanning from *ca* 20 and  $50 \text{ g cm}^{-2}\text{kyr}$  (Fig. 14A).

**Slope cores.** In southern Ashmore Trough siliciclastic and bulk carbonate MARs were low ( $<10 \text{ g cm}^{-2}\text{kyr}$ ) through the LGM and initial part of the last deglaciation (Fig. 14A). In northern Ashmore Trough, during LGM, bulk carbonate MARs were also low,  $<10 \text{ g cm}^{-2}\text{kyr}$ , whereas siliciclastic MARs were higher, up to  $40 \text{ g cm}^{-2}\text{kyr}$  (Fig. 14A). Siliciclastic MARs in core MV24-13 (downdip of MV26-73) abruptly increased at *ca* 18 ka up to  $100 \text{ g cm}^{-2}\text{kyr}$ , and remained as such until *ca* 15 ka (Fig. 14A). During the same interval, bulk carbonate MARs

increased up to  $20 \text{ g cm}^{-2}\text{kyr}$  (Fig. 14A) with relatively higher rates of HMC and LMC and lower aragonite (Fig. 14B). From 15 ka to 11 ka, siliciclastic MARs continued heterogeneously along Ashmore Trough slope: low values,  $<10 \text{ g cm}^{-2}\text{kyr}$ , in the southern area (i.e. MD26-74, MV24-06/07 and MD05-49) and moderate to high values up to  $50 \text{ g cm}^{-2}\text{kyr}$  in the northern area (i.e. MD97-34, MV24-13 and MV24-17). During this time interval bulk carbonate MARs remained generally low with the exception of core MV24-17 where rates were up to  $20 \text{ g cm}^{-2}\text{kyr}$ . Since *ca* 11.0 – 11.5 ka, bulk carbonate MARs increased across the entire Ashmore Trough with aragonite being the most abundant carbonate mineralogy (Fig. 14A and B). In northern Ashmore Trough, aragonite MARs peaked at *ca* 8 ka (Fig. 14B). In southern Ashmore Trough, siliciclastic MARs remained low from 11 ka to recent, whereas in northern Ashmore Trough they peaked at *ca* 8.5 ka, in turn followed by low rates similar to the southern sector (Fig. 14A).

## DISCUSSION

Sediment composition and partitioning in the southern Gulf of Papua (GoP) can be interpreted relative to an independently reconstructed sea-level curve during the last glacial cycle. In addition to the 100 kyr scale of investigation, higher resolution observation, at millennial scale, was carried out to determine what controlled sedimentation during the climatically unstable, high-amplitude sea-level fluctuations, glacial (LGM) to interglacial (Holocene) transition.

Initially, the mixed siliciclastic–carbonate accumulation along the upper and lower slope of the southern GoP (i.e. Ashmore Trough) will be interpreted within the framework of five intervals of the last interglacial/glacial sea-level cycle and corresponding MIS described earlier. Then, the sedimentary evolution of the outer shelf will be analyzed at millennial scale during the last deglaciation and, subsequently, it will be integrated in a shelf-edge/slope contemporaneous sedimentation conceptual model.

### Sedimentation in the Ashmore Trough during the last sea-level cycle

#### *Penultimate interglacial maximum sea-level high (MIS 5e, ca 130 to 115 ka)*

The sediment composition of MD05-49, coupled with 3.5 kHz imaging, shows that carbonate input



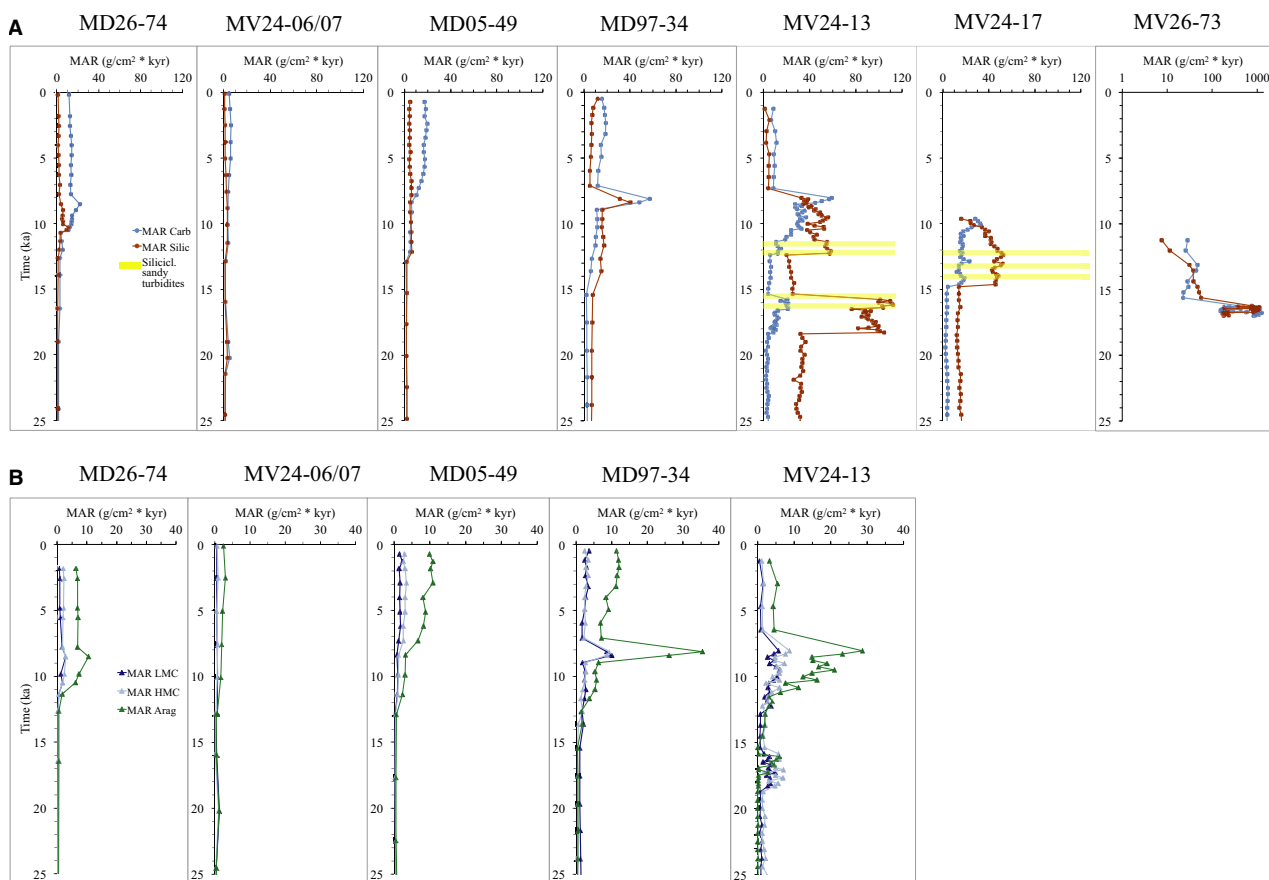


**Fig. 14.** Mass accumulation rates during the last deglaciation (including LGM at *ca* 20 ka) from shelf edge and slope cores along Ashmore Trough. (A) Bulk siliciclastic and carbonate mass accumulation rates,  $MAR_{\text{silic}}$  and  $MAR_{\text{carb}}$ , respectively. MAR values in shelf-edge core MV26-73 are in logarithmic scale. Notice the heterogeneous, both in time and space, distribution of siliciclastic sediment along the slope. (B) Carbonate mineral mass accumulation rates (MAR) from Ashmore Trough slope cores (five out of six) during the last deglaciation ( $MAR_{\text{arag}}$  = aragonite;  $MAR_{\text{HMC}}$  = high-Mg calcite;  $MAR_{\text{LMC}}$  = low-Mg calcite). On the slope, aragonite accumulation rates increased since *ca* 11.0–11.5 ka.

dominated (up to 90%) Ashmore Trough deposition during the penultimate interglacial maximum sea level (i.e. MIS 5e; Fig. 15A). At that time, sea level was up to 5 to 6 m higher than today (Fig. 4A), keeping the top of the Great Barrier Reef (GBR), Ashmore, Boot and Portlock reefs submerged and within the photic zone. Fine aragonite and HMC dominated the carbonate sediment composition. This mineralogy indicates export of neritic carbonate from the surrounding reef and bank tops towards the slopes of Ashmore Trough, in accordance with the highstand-shedding model for carbonate systems (Schlager *et al.*, 1994; Jorjy *et al.*, 2010). Pelagic carbonate zooplankton and phytoplankton provided a LMC component in the periplatform ooze settling to the sea floor (Fig. 8). High sea level also

submerged the broad southern GoP shelf, positioning the mouth of major rivers (for example, the palaeo-Fly River) much further landward and (*ca* 200 km) far away from the Ashmore Trough upper slope. As a result, very little siliciclastic material accumulated in Ashmore Trough. Siliciclastic sediment was likely stored on the inner shelf as a series of prograding clinofolds, similar to the inner shelf today (Harris *et al.*, 1993; Walsh *et al.*, 2004; Slingerland *et al.*, 2008a).

#### *Early sea-level fall (MIS 5d to 5a, ca 115 to 70 ka)*

Early sea-level fall was characterized by maximum siliciclastic mud input (Fig. 15B), and only short, punctuated intervals characterized by increased carbonate input (sub-interglacials MIS

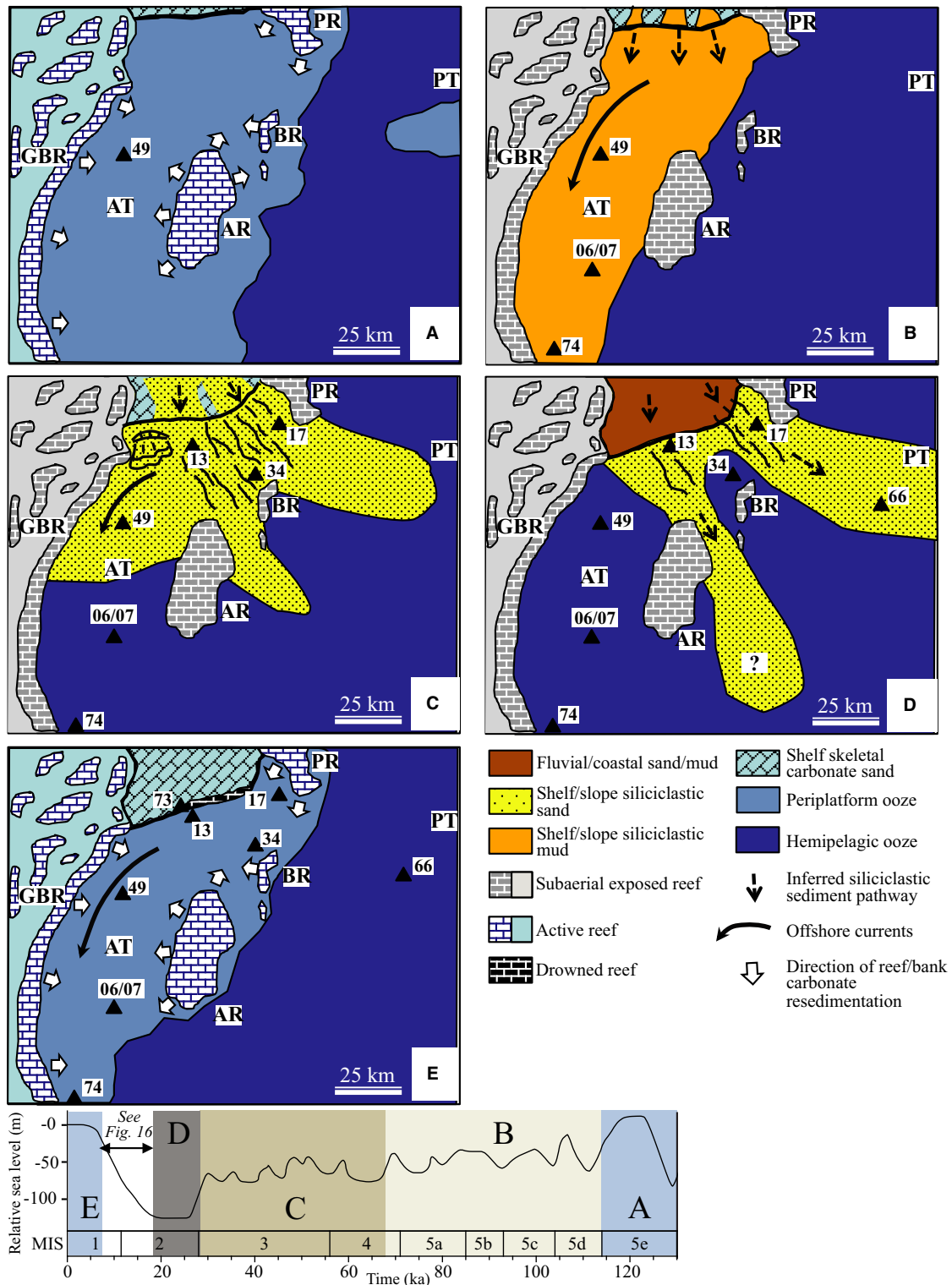


**Fig. 15.** Cartoons illustrating the reconstructed depositional history along Ashmore Trough during the last glacial cycle (100 kyr scale). Time intervals correspond to marine isotope stages/substages and each interval displays cores with coeval sedimentary record. (A) Penultimate interglacial maximum sea-level high: MIS 5e, ca 130 to 115 ka. (B) Early sea-level fall: MIS 5d to 5a, ca 115 to 70 ka. (C) Late sea-level fall: MIS 4 and MIS 3, ca 70 to 30 ka. (D) LGM sea-level low: MIS 2, ca 30 to 19 ka. (E) Current interglacial sea-level high: MIS 1, ca 7 ka to present. Last deglacial interval, ca 19 to 7 ka, is described at the millennial scale in Fig. 16 (AR = Ashmore Reef; AT = Ashmore Trough; BR = Boot Reef; GBR = Great Barrier Reef; PR = Portlock Reef; PT = Pandora Trough).

5c and MIS 5a; Fig. 6). During MIS 5d to 5a, sea level oscillated between 20 and 60 mbpsl (Fig. 4A; Lambeck & Chappell, 2001; Lambeck *et al.*, 2002). Because of the sea-level oscillations (some reaching *ca* 20 to 40 m of magnitude in <10 kyr), the carbonate platforms went through several periods of exposure and re-flooding. During the short re-flooding events, neritic carbonate material (aragonite and HMC) was exported to the basin (Jorry *et al.*, 2010). Pelagic carbonate (LMC) remained as minor background sediment because particulates reached the sea floor by settling through the water column. During this time of overall sea-level fall, unconsolidated siliciclastic mud, stored on the inner shelf during MIS 5e, was systematically exposed, reworked, transported as suspended material across the narrowed shelf, and ultimately delivered to the Ashmore Trough upper slope (Fig. 15B). Sediment was remobilized in response to the drop in base level. Moreover, the overall lowering of sea level by as much as 60 m likely strengthened the tidal currents enough to keep the fine siliciclastics in suspension within the water column (Harris *et al.*, 2005). Sands were not found in Ashmore Trough during the early sea-level fall, implying that river mouths were not yet at the shelf-edge, but had only partially migrated across the previous highstand shelf (Slingerland *et al.*, 2008a; Wei & Driscoll, 2020).

The early-fall siliciclastic muddy package is well imaged in 3.5 kHz seismic profiles as a wedge thick transparent unit in southern Ashmore Trough. Its thickness decreases both southward and downslope. The overall wedge geometry of this unit is easily explained by the major northern source for the muddy siliciclastic sediment. Subglacial 5d and 5b sediments, cored along the western slope of Ashmore Trough (MV26-74, MV24-06/07 and MD05-49) (Fig. 7), consist of almost exclusively siliciclastic mud.

The north-easterly Coral Sea Current (CSC) characterizes present-day oceanic circulation in the GoP. This main current generates a counter-clockwise rotating eddy at the shelf break with prevailing south-westward currents with speed up to  $0.3 \text{ m s}^{-1}$  (Wolanski *et al.*, 1995). If such a circulation pattern was present also during the last early sea-level fall, it is conceivable that south-westerly currents transported muddy siliciclastic sediment from the northern Ashmore Trough shelf edge in a south-westerly direction along the upper slopes of Ashmore Trough. Mud was likely originated from reworking of the partially exposed shelf.

#### *Late sea-level fall (MIS 4 and MIS 3, ca 70 to 30 ka)*

Late sea-level fall (MIS 4 and 3) is characterized by low carbonate accumulation rates and significant variability in siliciclastic accumulation across Ashmore Trough (Fig. 15C). A *ca* 35 m step in the overall sea-level fall observed at *ca* 70 ka (Figs 4A and 15C; Lambeck & Chappell, 2001; Lambeck *et al.*, 2002) likely controls the major change in sediment accumulation across Ashmore Trough. From 70 ka until 30 ka (MIS 3), sea level fluctuated between 50 and 80 mbpsl (Fig. 4A). During this time interval, the neritic carbonate producing regions remained completely exposed, essentially cutting off neritic carbonate supply to Ashmore Trough (Jorry *et al.*, 2010). As during early sea-level fall, minor amounts of pelagic carbonate still accumulated in Ashmore Trough at this time. At *ca* 70 ka, siliciclastic input, transport, distribution and accumulation also changed dramatically on the slopes of Ashmore Trough. Very high siliciclastic input is documented in northern Ashmore Trough, while siliciclastic input was cut off in southern Ashmore Trough (Fig. 15C). During this time, gravity flow sandy deposits appear in northern Ashmore Trough (i.e. bottom of core MD97-34; Figs 6 and 7) and a large MTD is imaged in the seismic data cross-cutting the early sea-level fall unit (Fig. 9 A). Presumably, the *ca* 35 m fall in sea level at *ca* 70 ka allowed river deltas to approach the northern shelf edge, facilitating sand and mud transport directly to the proximal upper slope, possibly funnelled through valleys incised during MIS 4 sea-level low. Similarly, in the central sector of the GoP shelf during MIS 4 and MIS 3, siliciclastic sediment reached Pandora Trough aided by offshore-incised valleys (Wei & Driscoll, 2020).

Sediment delivery to the upper slope allowed the shelf edge in the northern Ashmore Trough to prograde basinward and to infill the northern end of the trough (Fig. 1C).

#### *Last glacial maximum sea-level low (MIS 2, ca 30 to 19 ka)*

The LGM sea-level low was characterized by reduced sedimentation rates and minimal carbonate and siliciclastic input in Ashmore Trough (Fig. 15D). The last major pre-LGM sea level drop (*ca* 45 m) occurred at *ca* 30 ka (Fig. 4A; Lambeck & Chappell, 2001; Lambeck *et al.*, 2002), dropping sea level to 130 to 120 mbpsl. Carbonate platforms remained exposed, limiting input of neritic carbonate sediment. Input of pelagic carbonates continued to be constant minor background

sedimentation. By this time, the shelf edge reached its present-day location, likely built by prograding deltas. Multi-beam data of the modern shelf-edge bathymetry indicate a broad protruding bulge on the northernmost shelf-edge portion of Ashmore Trough (Fig. 4A; Francis *et al.*, 2008). The shape and depth (*ca* 110 to 120 m bpsl) of the bulge, and presence of well-developed submarine gullies originating from its apex, suggest a more than 50 km wide delta, formed when sea level was at its lowest and large masses of fluvial sediment extended to the shelf-edge (Francis *et al.*, 2008).

During the LGM sea-level low, a marked decrease in siliciclastic accumulation is observed on the northern Ashmore Trough slope (Figs 7 and 15D). This change is attributed to the transport of siliciclastic sediment directly to Pandora Trough, bypassing much of northern Ashmore Trough (Jorry *et al.*, 2008). Sediment was transported from the LGM shelf edge through deeply incised channels, gullies and canyons incising the shelf edge, slope and sea floor passages between Boot and Portlock reefs, and leading to Pandora Trough and possibly Bligh Trough as well (Fig. 15D).

The 45 m sea-level drop at *ca* 30 ka, likely led to increased incision at the mouth of the shelf-edge delta and the development of one or several south-east trending gullies that funnelled sediment directly towards Pandora Trough. A focused sediment dispersal system on the shelf edge, therefore, could have re-directed sediment gravity flows into Pandora Trough, precluding them from deposition in Ashmore Trough. The basin physiography, particularly the proximity of the shelf-edge delta to a potential pathway out of the basin, plays an important role in this process, facilitating sediment bypass as shown in the upper slope of the northern Gulf of Mexico (Pirmez *et al.*, 2012). The LGM sandy and muddy siliciclastic turbidites in cores MV25-33, MV26-66 and MD05-40 confirm that gravity flow deposits accumulated in central Pandora Trough at this time (Jorry *et al.*, 2008). In addition, siliciclastic turbidites also reached Pandora Trough through conduits north of Portlock Reef (Septama & Bentley, 2017; Wei & Driscoll, 2020).

#### *Last deglaciation (MIS 2 to 1 transition; ca 19 to 7 ka)*

During the last deglaciation, rates of siliciclastic and carbonate sediment accumulation in Ashmore Trough varied in space and time (Fig. 7). Following LGM, sea level rose in stepped fashion

with periods of accelerated rates (i.e. meltwater pulses) alternating with periods of lower rates or even standstill (Fig. 4B; Lambeck *et al.*, 2014).

Controls on sedimentation during the last deglaciation, a time period of pronounced and rapid atmospheric and oceanographic changes, are illustrated below, in the *Shelf edge evolution during the last deglaciation* section. In this section, sedimentary records of the shelf edge and slope cores are integrated at the millennial scale.

#### *Current interglacial sea-level high (late MIS 1, 7 ka to present)*

Sea level rose to its present level at *ca* 7 to 6 ka and remained relatively constant in the last 6 ka (Fig. 4B). This interval was characterized by moderate to high carbonate input and minimal siliciclastic input (Figs 7 and 15E). Reef and carbonate platform tops remained within the photic zone and continued to produce neritic carbonate, specifically fine aragonite and HMC, which was either exported to the Ashmore Trough slopes or accumulated within lagoons in atolls with aggrading rims (Fig. 8; Jorry *et al.*, 2008). Pelagic carbonate tests (LMC) continued to settle through the water column and accumulate on the sea floor as minor background sediment (Fig. 8). Very little siliciclastic sediment had been deposited in Ashmore Trough over the last 7 ka (Fig. 7). Most of this material has been sequestered on the central GoP inner shelf, while some has been re-routed by shelf currents to the narrow north-eastern GoP shelf and delivered to the northern slope of the Pandora and Moresby troughs (Walsh & Nittrouer, 2003; Muhammad *et al.*, 2008; Septama *et al.*, 2016; Wei & Driscoll, 2020).

#### **Shelf edge evolution during the last deglaciation**

The sedimentary record of core MV26-73, uniquely located on the modern shelf edge, starts at about 17 ka during a near constant sea-level interval that followed the first meltwater pulse MWP-1A<sub>0</sub> at *ca* 19 ka (Fig. 4B). At *ca* 17 ka global mean sea level was *ca* 120 to 110 m bpsl. By this time, post-LGM warming was underway, as shown by sea surface temperature from the Coral Sea (Tachikawa *et al.*, 2009; Reeves *et al.*, 2013).

#### *Unit A*

Unit A consists of a 2 m thick carbonate sandy gravel with abundant ooids and skeletal grains.

The base of Unit A lies at a present-day depth of *ca* 122 m, including 113 m of water depth and 8.5 m of core thickness. A palaeo-water depth up to 7 m is estimated at time of deposition based on sea level as shallow as 115 mbpsl at *ca* 17 ka (Fig. 4B). No compaction is assumed to have affected the sediments due to their coarse grain size, and tectonic subsidence in the southern GoP can be considered negligible (Bird, 2003).

The ooids present in this unit are <1 mm in size, are composed of HMC, and show a radial crystal arrangement as well as a thin cortex. Generally, modern ooids are made of aragonite with tangentially oriented crystals, a cortex at least as thick as the nucleus diameter, and form in normal marine agitated shallow waters (<5 m) (Simone, 1981, and references therein). However, HMC ooids with a radial crystal arrangement are much less common and present-day accumulations are found in few locations such as Texas (i.e. Baffin Bay; Land *et al.*, 1979), the Arabian Gulf (Aqrabi & Sadooni, 1987) and Cook Islands (Rankey & Reeder, 2009).

The enigmatic formation of these ooids is interpreted to be controlled, at least in part, by calcium carbonate saturation levels slightly below those necessary for aragonite precipitation (Opdyke & Wilkinson, 1990; Rankey & Reeder, 2009). From a hydrodynamic point of view, superficial ooids are interpreted to form in lower energy environments (for example, protected lagoons), are significantly smaller than their maximum 2 mm size, and are associated with non-coated grains (Carozzi, 1957).

Modern ooids, in the northern Persian Gulf near the Iraq–Kuwait border, form in a mixed siliciclastic–carbonate proximal lagoon 5 to 10 m deep and located on the western edge of Shatt El Arab estuary (confluence of Tigris, Euphrates and Karun rivers; Aqrabi & Sadooni, 1987). Tide excursion in this part of the gulf is *ca* 3 m with current velocity in excess of 50 cm s<sup>-1</sup> (Riegl *et al.*, 2010). Ooids are found along an east–west belt that stretches eastward of the lagoon at maximum water depth of 20 m. Their size ranges from 0.15 to 0.5 mm (Aqrabi & Sadooni, 1987). The smaller examples are found in the shelter inner part of the lagoon and are characterized by a thin radial cortex made of high-Mg calcite. The larger ones occur in small tidal shoals in more agitated waters and show a mixed radial/concentric cortex made of high-Mg calcite and aragonite, respectively (Aqrabi &

Sadooni, 1987). Nuclei are either bioclasts or quartz grains. By analogy, Unit A is interpreted to be deposited in a subtidal environment (<7 m water depth) of a tidally-influenced lagoon partially protected by an incipient barrier reef (see below). In such lagoons, water agitation and calcium carbonate saturation level met the peculiar conditions favourable for the formation of radial, HMC ooids. Tidal range on the present-day GoP shelf is up to 3.3 m with measured maximum current speeds up to 80 cm s<sup>-1</sup> (Ogston *et al.*, 2008).

Similar HMC ooids were described in the central GBR (i.e. Capricorn Channel) from a present-day water depth of about 120 m and dated at 16.8 ka (Marshall & Davies, 1975; Yokoyama *et al.*, 2006). The GBR and GoP ooids indicate that during the early deglaciation, in this region, carbonate seawater saturation levels were consistently favourable for the formation of HMC ooids.

Throughout Unit A the benthic foraminiferal assemblage is dominated by Calcarinidae (for example, *Calcarina defranci* and *Calcarina gaudichaudii*). At present day, calcarinids are one of the main sources of carbonate sand in Indo–West-Pacific reef deposits (Yamano *et al.*, 2000; Renema, 2010). Their habitat generally spans from reef flat to reef edge and they are found in high abundance along with macroalgae (Hoenecker *et al.*, 1999; Renema, 2010; Dawson *et al.*, 2014). Tests of calcarinids can be reworked and accumulate in adjacent environments (Dawson *et al.*, 2014). Therefore, the abundance of calcarinids in Unit A can be related to the proximity of a coralgal reef, more specifically the southern termination of the GoP transgressive shelf-edge barrier reef described by Droxler *et al.* (2006). Based on the foraminiferal assemblage of core MV26-73, it is inferred that the reef was already active around 17 ka and possibly even earlier (19 or 21 ka). Shelf-edge coralgal edifices bearing an age of 19 ka, were documented in the north-eastern portion of the GoP as part of a transgressive backstepping reef system (Droxler & Jorry, 2013; Harper, 2014). Similarly, in the northern GBR transgressive reefs started to grow from 21 ka on top of older reef edifices exposed during LGM sea-level lowstand (Webster *et al.*, 2018).

#### Unit B

A radiocarbon date at the base of Unit B shows an age of 17.68 ka. This date is older than the 17.04 ka age date of the underlying Unit A, thus

pointing to sediment reworking. The overlying Unit C bears an age date of 16.27 ka (Fig. 11). Taking into account radiocarbon dating analytical error (*ca* 0.3 kyr), the age of Unit B can be constrained to 17.3 to 16.5 ka. During this short-time interval, global mean sea level remained constant (Fig. 4B). Compositionally, Unit B is characterized by an abrupt increase in terrigenous content including quartz, clay (i.e. illite and chlorite) and wood debris (Fig. 11). Modern Fly River sediments consist of silt and clay with subordinate fine-grained quartz-rich sand (Harris *et al.*, 1996). Clay mineralogy is dominantly made of illite, smectite and chlorite, with different proportions along the river bed reflecting the two main tributaries: the Upper Fly River and the Strickland River (Bolton *et al.*, 2008). Abundant wood fragments are found in interdistributary island deposits of its tide-dominated delta (Harris *et al.*, 1996). Unit B sediment composition shows affinity with sediment composition from Fly River discharge. However, the location of the palaeo-Fly River delta during LGM, and the following deglaciation, remain unresolved with some authors positioning it south of Portlock Reef (Harris *et al.*, 1996) and others positioning it north of the reef (Wei & Driscoll, 2020). Results from this study are consistent with a palaeo-Fly river delta position south of Portlock Reef, so that its discharge could have been in part re-directed south-westward by outer shelf currents.

High siliciclastic MAR of Unit B (Fig. 14A) could reflect near-constant sea level (Fig. 4B), and reduction of accommodation space during deposition of this unit. These rates are the same order of magnitude of MARs recorded in the muddy core MV-41 at the north-east GOP shelf edge during the YD when, similarly, sea-level rise markedly slowed (Fig. 4B; Howell *et al.*, 2014). However, controlling factors other than base level could also be considered. Deep-water core from Coral Sea (Shiau *et al.*, 2011) and speleothem record from Indonesia (Ayliffe *et al.*, 2013) indicate increased precipitation and siliciclastic run off starting at *ca* 17 ka in the south-east Asia region. A change to wetter conditions compared to the drier LGM climate is related to the southern migration of the ITCZ (Shiau *et al.*, 2011; Ayliffe *et al.*, 2013). The southern migration of the ITCZ is one of the dramatic changes in atmospheric and oceanic circulation that characterized the 'Mystery Interval' (Denton *et al.*, 2006), a time interval spanning from *ca* 17.5 to 14.5 ka. Underlying causes of such abrupt mode switches, corresponding to the last termination,

could have been massive ice melting in the Northern Hemisphere, reduction of Atlantic water masses overturning, and rising CO<sub>2</sub> atmospheric concentration in the Southern Hemisphere (Denton *et al.*, 2006; Clark *et al.*, 2012). In summary, the large and abrupt siliciclastic input to Unit B could represent the sedimentary record of major climatic change events that took place at the onset of the last termination in the Southern Hemisphere, during a period of near-constant sea level. Unit B was deposited in a lagoonal environment similar to underlying Unit A. The coarsening upward trend of the <2 mm fraction (Fig. 11) may suggest a short-lived (i.e. centennial scale) regression of the coastline.

#### Unit C

The age of Unit C is constrained by the 16.27 ka radiocarbon date measured in the lower part of the unit and the 13.15 ka date from the overlying Unit D (Fig. 11). Because the MWP-1A is recorded in the overlying Unit D (see below), the age of Unit C can be assigned to *ca* 16.5 to 15.0 ka. During its deposition, sea level resumed rising reaching about 100 mbpsl (Fig. 4B; Clark *et al.*, 2012). The main compositional characteristics of this unit are the lack of coated grains and wood debris, and the first appearance of planktonic foraminifera. Quartz sand is dominant, grain size of the siliciclastic fraction shows a fining-upward trend, and carbonate content gradually increases upward (Fig. 11). Both siliciclastic and carbonate MARs are much lower than those of units A and B (Fig. 14A). The above observations are consistent with sea-level rise, backstepping of the coastline, and an overall deeper depositional environment compared to the underlying Unit B. Unit C, therefore, is interpreted to represent deepening of the lagoon with water depth of about 20 to 30 m. Yet, the abundant calcarinids indicate that the shelf margin corallgal reef kept up with sea-level rise during this time interval.

#### Unit D

A radiocarbon date of 13.15 ka was measured in the middle of Unit D (Fig. 11). Based on this date and the radiocarbon dates from both the underlying Unit C and overlying Unit E (Fig. 11), Unit D is assigned an age spanning from *ca* 15.0 to 12.5 ka. During this time interval, encompassing MWP-1A and the B–A, sea level rose from *ca* 100 to 65 mbpsl (Fig. 4B). These sea level figures allow estimating a palaeo-water depth of about 60 m during

deposition of Unit D. This unit is much thinner than the underlying units, it is fining upward, and its carbonate content gradually increases towards the top (Fig. 11). Siliciclastic accumulation rates decrease steadily upward whereas carbonate MARs remain constant (Fig. 14A). These sedimentological trends are consistent with rapid rates of sea-level rise and associated reduced sedimentation rates. The benthic faunal assemblage records a major change within Unit D: a relative increase of Amphisteginidae (for example, *A. radiata*, *A. papillosa* and *A. bicirculata*) is paralleled by a relative decrease of Calcarinidae, and amphisteginids become the predominant benthic foraminiferal group at the top of the unit (Fig. 11). Ecological studies of large benthic foraminifera in reef environments show a water depth control on their distribution. Whereas calcarinids can withstand high energy and inhabit the reef top, amphisteginids are abundant on the slope starting at water depth of 40 m and deeper (Hohennegger *et al.*, 1999; Renema, 2006). Moreover, in Unit D the planktonic foraminiferal content increases compared to the underlying Unit C (Fig. 11). Overall, the sedimentological and palaeontological trends recorded in this unit are interpreted to reflect the accelerated sea-level rise that occurred during MWP-1A and then the rise during B–A. Unit D deposition took place in a mid-outer shelf environment, and the abrupt reduction of calcarinids is interpreted to reflect the incipient drowning of the southern termination of the GoP shelf-edge barrier reef. This initial stage of the partial reef demise was likely triggered by the accelerated sea-level rise rates of MWP-1A, in turn followed by punctuated sea-level rise during B–A, at centennial scale, as observed in backstepping terraces in shelf-edge corallgal banks offshore Corpus Christi (Texas, USA) (Khanna *et al.*, 2017).

#### Unit E

The age of the uppermost Unit E is constrained by two radiocarbon dates, 11.25 ka and 10.97 ka, measured near the middle and top, respectively (Fig. 11). Based on these dates, as well as the age of the underlying Unit D, Unit E age spans from *ca* 12.5 to 11 ka. During this time, sea level initially rises at slow rates (i.e. YD interval), followed by another episode of accelerated rates, MWP-1B (Fig. 4B). By 11 ka, sea level had reached about 50 mbpsl suggesting a palaeo-water depth of about 70 m during the deposition

of Unit E. Similar to Unit D, the thin Unit E reflects reduced rates of sediment accumulation. In the lower half of the unit, the foraminiferal assemblage is dominated by *Amphistegina* spp. similar to the top of the underlying Unit D (Fig. 11). Planktonic foraminifera are relatively more abundant, thus supporting further deepening of the outer shelf (Fig. 11). Microfacies consists of skeletal grainstone/packstone with lithoclasts, intraclasts, detrital quartz, and encrusting biotas such as red algae and foraminifera (Fig. 13E and F). In modern reef environments, associations of red algae and encrusting foraminifera are described at depths >40 m (Rasser & Piller, 1997). The lack of sediment younger than 11 ka in core MV26-73 points to bottom currents sweeping the sea floor that prevented, at least at this location, further sediment accumulation. At the same time, such currents favoured seawater circulation through sediments, thus promoting early marine cementation (James & Choquette, 1990). The isopachous bladed cement of Unit E is consistent with early marine cementation (Fig. 13F). Present-day south-westward currents at the shelf break, and down to a depth of 60 m, show speeds of 0.1 to 0.3 m s<sup>-1</sup> (Wolanski *et al.*, 1995). It is inferred that such currents were also active during the last deglaciation. Finally, the shallowest present-day depths of the shelf-edge barrier reef crest at *ca* 60 mbpsl (Fig. 4B) suggest that its ultimate drowning occurred during MWP-1B. This depth of *ca* 60 mbpsl, falls within the 57.5–61.8 mbpsl depth range in which the crests of the majority of corallgal reefs along the South Texas shelf edge occur (Khanna *et al.*, 2017). Similarly to the southern GoP reefs, their drowning was most likely triggered by the high rates of sea-level rise during MWP-1B (Khanna *et al.*, 2017).

#### Shelf margin to slope sedimentation during the last deglaciation in Ashmore Trough (southern Gulf of Papua)

Integrating the sedimentary record of core MV26-73 with downslope cores MV26-74, MV24-06/07, MV24-13, MV24-17, MD05-49 and MD97-34 allowed the reconstruction of the main sedimentation patterns along the shelf margin—upper slope of the Ashmore Trough from *ca* 17 to 11 ka. Below is the interpreted depositional history during time intervals corresponding to stratigraphic Unit A to E as described in core MV26-73.

*Approximately 17.0 to 16.5 ka (Units A and B; Fig. 16A)*

In the southern GoP during LGM sea-level low, when global sea level dropped to about 130 to 125 mbpsl (Fig. 4B), the coastline reached the shelf edge (Francis *et al.*, 2008; Droxler & Jorry, 2013). During the early stage of the following sea-level rise, global sea level rose at fairly rapid rates corresponding to MWP-1A<sub>0</sub> at 19 ka (Fig. 3B). Starting from *ca* 18 ka until *ca* 16.5 ka, sea level remained constant at about 115 to 120 mbpsl (Fig. 3B). At this time, reefs grew in the outer and mid terraces of the northern GBR (for example, Noggin Pass, Webster *et al.*, 2018) as well as at the margin of the narrow north-eastern GoP shelf (Droxler & Jorry, 2013; Harper, 2014). Differently, tops of carbonate atolls were still exposed (Jorry *et al.*, 2008). In southern GoP, sea-floor bathymetry of the outer shelf shows depth of about 115 to 120 mbpsl about 5 km inward of the shelf edge, which would indicate the location of the coastline from *ca* 18.0 to 16.5 ka (Fig. 3D). Hence, a narrow lagoon was present at that time.

Predominance of calcarinids among the benthic fauna suggests that the shelf-edge coralline reef was already active at that time. The presence of a nearby active reef is supported by increased carbonate MARs recorded in the upper slope (i.e. core MV24-13; Fig. 14B). However, the relative abundance of HMC suggests material derived mostly from disintegration of large benthic foraminifera (Dawson *et al.*, 2014) or/and red algae. Webster *et al.* (2018) showed that around 17 ka a second stage of reef growth, Reef 3b, took place in the outer and mid terrace of the northern GBR, replacing the post-LGM drowned Reef 3a that grew from *ca* 21 to 17 ka. In the southern GoP the situation seems different. The negligible values of aragonite MAR in cores MV26-74, MV24 06/07 and MD05-49 in the southern Ashmore Trough (Fig. 14B), points to lack of neritic carbonate sediment shed off the shelf and it suggests that, in the northernmost terminus of the GBR, there were no active reefs at this time. Lack of active reefs at the GBR northernmost terminus could reflect the different morphology of the GBR shelf in the southern GoP, where no mid/outer terrace is present and the shelf edge drops abruptly from 40 mbpsl down to 700 mbpsl oceanward (Hopley, 2006). Based on the above observations, it is interpreted that the northernmost GBR in the southern GoP was still subaerially exposed at *ca* 17 ka (Fig. 16A).

On the upper slope, downdip of core MV26-73, a large accumulation of siliciclastic mud in core MV24-13 is coeval with the increased terrigenous input recorded at the shelf edge (i.e. Unit B) at the beginning of the Mystery Interval (MI) (Fig. 14A). It is inferred that the siliciclastic fine fraction exited the shelf south of Portlock Reef, where no shelf-edge reef was present and it was redirected southward by shelf break currents associated with the counterclockwise gyre of the Coral Sea Current (CSC) (Fig. 16A). Very few studies have focused on the palaeo-CSC but one suggested its existence at least since the last deglaciation (Williams, 1984).

At the same time, low siliciclastic MARs in core MV24-17 suggest that this part of the slope was instead bypassed by sediment deposited down dip in the Pandora Trough (i.e. cores MV24-33, MV24-66 and MD05-40, Jorry *et al.*, 2008). Contemporaneous increase of terrigenous sediment flux recorded in the northern GBR seems to confirm the regional extent of such climate change (Webster *et al.*, 2018).

*16.5 to 15.0 ka (Unit C; Fig. 16B)*

During this time interval, sea level resumed rising rapidly and, by 15 ka, sea level was *ca* 100 mbpsl (Fig. 4B). Shelf bathymetry data show a 100 m contour at about 50 km from the shelf edge, which therefore would approximately correspond to the palaeo-coastline at *ca* 15 ka (Fig. 3C). Shelf edge with no barrier reef was at maximum water depth of about 30 m. The ITCZ was stationed south with associated higher precipitation (Ayliffe *et al.*, 2013; Zhang *et al.*, 2014).

On the upper slope, high siliciclastic accumulation rates up to 110 g cm<sup>-2</sup>\*kyr, recorded in core MV24-13, contrast with the reduced accumulation rates of the shelf edge (Fig. 14A). Siliciclastic sedimentation on the slope includes thin sandy turbidites pointing to gravity-driven sediment flows across the shelf (Fig. 14A). During this interval of sea-level rise and coastline backstepping (i.e. transgression), siliciclastic sediment was sourced either by riverine input associated with higher precipitation (Ayliffe *et al.*, 2013; Zhang *et al.*, 2014) or wave ravinement of coastal deposits (Catuneanu, 2006), or a combination of both.

Possible mechanisms for across-shelf sediment transport are current or wave-supported sediment gravity flows (Wright & Friedrichs, 2006; Macquaker *et al.*, 2010). Studies from the



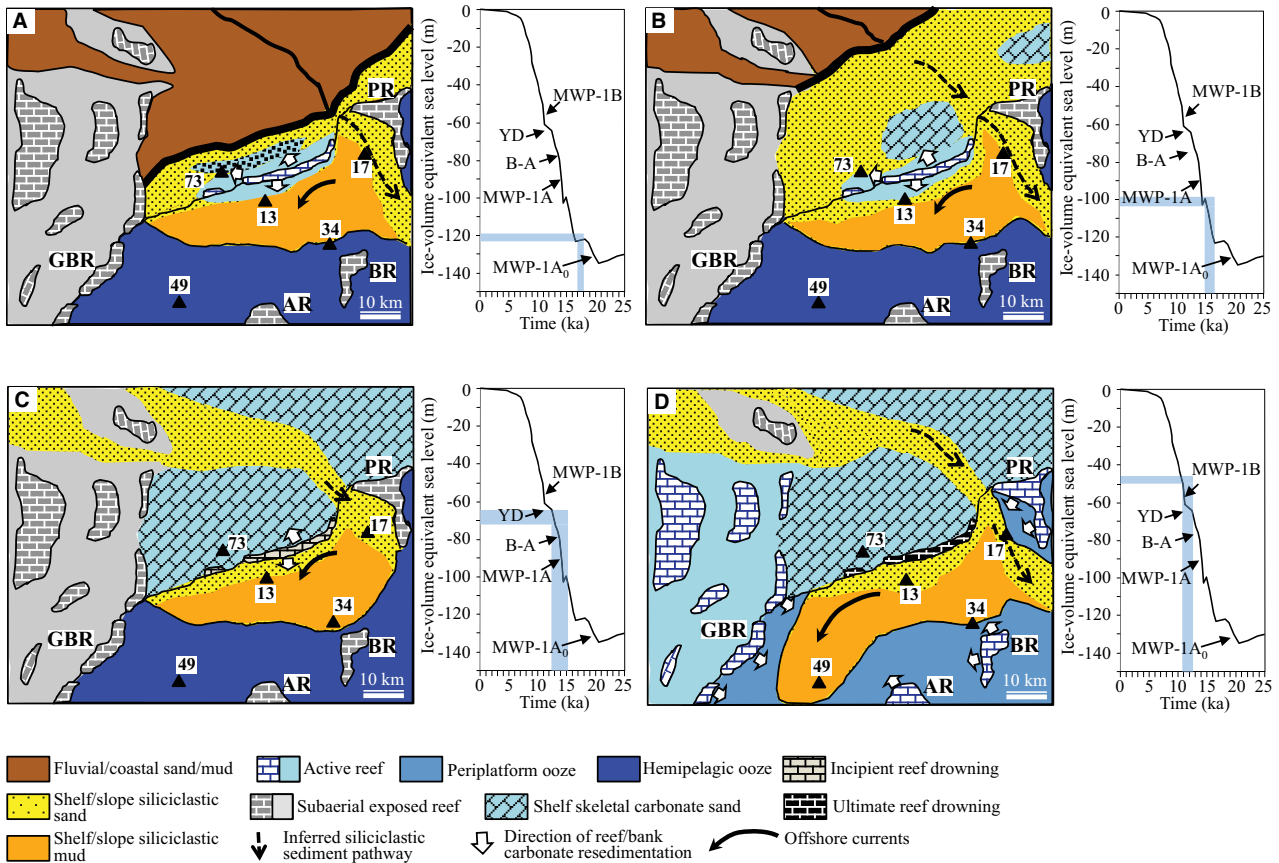


**Fig. 16.** Cartoons illustrating the reconstructed depositional history along northern Ashmore Trough shelf edge/slope during the last deglaciation (millennial scale). Time intervals correspond to the stratigraphic units A to E identified in core MV26-73 and are also marked on the last deglacial sea-level curve: (A) ca 17.0 to 16.5 ka, units A and B; (B) ca 16.5 to 15.0 ka, Unit C; (C) ca 15.0 to 12.5 ka, Unit D; (D) ca 12.5 to 11.0 ka, Unit E (AR = Ashmore Reef; BR = Boot Reef; GBR = Great Barrier Reef; PR = Portlock Reef; MWP = meltwater pulse; B-A = Bølling-Allerød; YD = Younger Dryas).

modern Amazon shelf show that a gravity flow deposited a 0.4 m thick mud layer at 65 m water depth about 100 km offshore of the delta complex. This mud layer was interpreted to be caused by a combination of tidal currents and high waves (Sternberg *et al.*, 1996; Wright & Friedrichs, 2006). Presently, on the GoP shelf, tidal currents are primarily cross-shore and are responsible for re-suspending unconsolidated sediments (Wolanski *et al.*, 1995; Ogston *et al.*, 2008). Modelling shows that strong tidal currents were present on the GoP shelf throughout the last glacial cycle and potentially could incise valleys (Harris *et al.*, 2005). Hence, it is likely that they were also capable of initiating downslope motion of unconsolidated sediments eventually evolving into across-shelf gravity flows. Incised valleys, either formed during

LGM sea-level lowstand or by tidal scarring during the subsequent sea-level rise and shelf flooding, could have acted as preferential conduits facilitating transport and delivery of sediment to the upper slope. High siliciclastic MARs in MV24-13 are paralleled by increased carbonate MARs (Fig. 14A) suggesting that gravity flows incorporated shelfal carbonates when moving downslope.

*15.0 to 12.5 ka (Unit D; Fig. 16C)*

This time interval is characterized by accelerated rates of sea-level rise during MWP-1A and, to a lesser extent, during the subsequent B-A (Fig. 4B; Deschamps *et al.*, 2012). The coastline further backstepped, the outer shelf became locus of carbonate sedimentation with reduced rates, and climate changed to relatively drier

conditions due to the northward shift of the ITCZ (Ayliffe *et al.*, 2013; Zhang *et al.*, 2014). The accelerated sea-level rise rates of MWP-1A and high rates of B–A, combined with siliciclastic influx, initiated the partial drowning of the shelf-edge barrier reef, at least in its southernmost segment. This event corresponds to the demise of Reef stage 3b of the GBR (Webster *et al.*, 2018). Terrigenous sediment influx on the southern GoP upper slope continued although with lower rates compared to the previous interval (Fig. 14A). During this interval, siliciclastic MARs up to  $52 \text{ g cm}^{-2} \text{ kyr}$  and including thin sandy turbidites are recorded in core MV24-17 (Fig. 14A). Such a record indicates that, at this location, the upper slope from an area of sediment bypass became the locus of sedimentation. This interpretation is consistent with the coeval lack of turbidites recorded down dip in the Ashmore Trough (Jorry *et al.*, 2008). Given the drier climate period (Ayliffe *et al.*, 2013; Zhang *et al.*, 2014), it is inferred that the source of terrigenous sediment derived mainly from erosion of coastal deposits associated with sea-level rise (Catuneanu, 2006). Sandy turbidites on the upper slope indicate that sediment gravity flows across the shelf continued during this time interval. Carbonate MARs co-increasing with siliciclastic MARs in core MV24-17 (Fig. 14A), suggest gravity flows with mixed siliciclastic and carbonate sediments.

#### 12.5 to 11.0 ka (Unit E; Fig. 16D)

This time interval includes lower rates of sea-level rise corresponding to the YD, in turn followed by accelerated rates of MWP-1B (Fig. 4B). Shelf bathymetry data and sea-level curve indicate that, by the end of this time interval, the shoreline had backstepped approximately 100 km from its original position at the shelf edge during LGM (Daniell, 2008). Climate during the YD returned to wetter conditions due to southward shift of the ITCZ (Ayliffe *et al.*, 2013; Zhang *et al.*, 2014). Condensed carbonate sedimentation took place on the outer shelf, whereas terrigenous sedimentation with accumulation rates up to  $56 \text{ g cm}^{-2} \text{ kyr}$  and thin fine sandy turbidites, continued on the upper slope (i.e. MV24-13 and MV24-17; Fig. 14A).

Tidal modelling of the GoP shelf indicates that during the last transgression tidal-bed stress on the middle shelf peaked at around 12 to 10 ka (Harris *et al.*, 2005). Tidal currents are inferred to have been the main mechanisms for initiating across-shelf gravity flows on the GoP shelf.

During the interval of MWP-1B, increased rates of sea-level rise caused the ultimate drowning of the southwestern GoP shelf-edge barrier reef, possibly in combination with augmented siliciclastic influx during the YD. The demise of stage Reef 4 in the GBR (Webster *et al.*, 2018), along with demises of shelf-edge barrier reefs in north-eastern GoP and offshore Texas (Harper, 2014; Khanna *et al.*, 2017) all occurred around MWP-1B, therefore suggesting a possible global drowning event.

Along Ashmore Trough slope, aragonite MARs started increasing during this interval (Fig. 14B), indicating re-flooding of the northernmost GBR and GoP atolls and re-initiation of neritic carbonate sedimentation ('re-flooding window' *sensu* Jorry *et al.*, 2010).

The northern Ashmore Trough slope recorded an unexpected pulse of siliciclastic sediment at ca 8.5 ka (Fig. 14A). This was a time of rapid rates of sea-level rise and it corresponds to the last of the meltwater pulses, MWP-1C. Such a siliciclastic pulse could reflect strengthening of the Australian–Indonesian summer monsoon and subsequent increased riverine discharge (Ayliffe *et al.*, 2013; Denniston *et al.*, 2013). A coeval siliciclastic pulse has been described on the slope of the northern GBR as well (Dunbar & Dickens, 2003; Francis *et al.*, 2007), supporting the regional extent of this event.

#### Comparison with other modern tropical and subtropical mixed systems

In addition to southern GoP, other major modern tropical and subtropical mixed siliciclastic–carbonate systems are the GBR, Belize barrier reef (BBR) and New Caledonia barrier reef (NCBR). The sedimentary record of these systems during the last sea-level cycle has been studied extensively (Ferro *et al.*, 1999; Dunbar *et al.*, 2000; Carson, 2007; Le Roy *et al.*, 2008, 2019; Bostock *et al.*, 2009; Gischler *et al.*, 2010; Harper *et al.*, 2015; Webster *et al.*, 2018). Hence, it is possible to make a comparison with the southern GoP system, highlighting similarities and differences in sedimentation patterns. Presuming that relative sea-level change was similar for the above mixed systems, all sites were far from major ice sheets and tectonic subsidence was negligible, such a comparison can reveal controls on deposition other than sea level.

During the penultimate interglacial sea-level high (MIS 5e), when sea level was up to 5 to 6 m higher than present level, production of

neritic carbonates and their export into adjacent slopes was predominant in southern Ashmore Trough, BBR and NCBR (Ferro *et al.*, 1999; Le Roy *et al.*, 2008; Jorry *et al.*, 2010). In contrast, in central GBR shedding of neritic carbonate did not take place due to temporary drowning of the platform caused by: (i) rapid rates of sea-level rise that culminated in MIS 5e sea-level maximum; and (ii) increased terrigenous input (Harper *et al.*, 2015).

In central GBR, carbonate sedimentation resumed during early sea-level fall MIS 5d to 5a resulting in accumulation of neritic carbonate mud on the slope (Harper *et al.*, 2015). In contrast, in Belize and New Caledonia, initial sea-level fall exposed the reef which no longer exported neritic sediment (Carson, 2007; Le Roy *et al.*, 2008; Droxler & Jorry, 2013). In Ashmore Trough, during MIS 5d to 5a, siliciclastic sedimentation became predominant on the slope with short-lived aragonite input corresponding to MIS 5c and MIS 5a sea-level rise. These pulses of neritic carbonate sedimentation on the slope indicate temporary re-flooding of nearby banks and reefs, and point to the role of magnitude of relative sea-level fluctuations in switching on and off the shallow-water carbonate factory. With continuing sea-level fall (MIS 4 and MIS 3), shelves became gradually more exposed, carbonate sedimentation waned, and rivers started incising the shelf plain and approaching the shelf margin. During this time, the sedimentary record on slopes shows some differences. In northern Ashmore Trough, siliciclastic sedimentation continued at sustained rates, whereas in southern Ashmore Trough and slopes off central GBR, BBR and NCBR, background pelagic sedimentation was predominant (Carson, 2007; Le Roy *et al.*, 2008; Droxler & Jorry, 2013; Harper *et al.*, 2015). Different shelf physiography may have played a role in the delivery of siliciclastic sediment to the slopes. In southern Ashmore Trough, central GBR, BBR and NCBR, a fairly continuous shelf-edge barrier reef became exposed during MIS 4 and MIS 3 sea-level fall, drastically reducing siliciclastic sediment delivery to the slope. Differently, in the northern Ashmore Trough, the lack of a similar positive relief on the shelf margin, allowed terrigenous sediment to reach the slope.

During the subsequent LGM, in spite of sea level falling *ca* 120 m below present level and exposing the shelf, all slopes were mainly loci of background pelagic sedimentation, with the exception of northern Ashmore Trough where

siliciclastic mud continued accumulating, although at reduced rates. Again, the physiography of the shelf was the main controlling factor for such a sedimentation pattern. In central and northern GBR, siliciclastic sediment was mainly sequestered on the exposed shelf characterized by rugged topography with emerged patch reefs and shelf-edge barrier reef (Dunbar *et al.*, 2000; Hinestrosa *et al.*, 2019). During LGM, carbonate sedimentation in central and northern GBR continued with scattered reefs along the outermost shelf (Webster *et al.*, 2018). Also in New Caledonia, siliciclastic sediment was sequestered on the exposed shelf due to a deep semi-enclosed inner shelf, a karstified outer shelf and a shelf-edge barrier reef (Le Roy *et al.*, 2019). In Belize, rivers did not reach the shelf edge and a southward drainage network on the exposed shelf likely routed siliciclastic sediment into the Gulf of Honduras (Gischler *et al.*, 2010). On the contrary, in northern Ashmore Trough, river deltas reached the shelf edge and siliciclastic sediment was delivered to deeper basins of the GoP (for example, Pandora Trough and Bligh Trough), whereas the slope became a bypass zone. Different sedimentation patterns persisted in northern Ashmore during the early sea-level rise of the last deglaciation. Here, carbonate sedimentation resumed during the first meltwater pulse (i.e. MWP-1A<sub>0</sub>) that re-flooded the outer shelf. Such a re-flooding likely triggered the growth of a shelf-edge reef on top of LGM fluvial/deltaic deposits as well as deposition of nearshore oolitic/skeletal sand. Subsequently, siliciclastic sand and mud sedimentation increased and peaked both on the shelf and slope during climate changes of the MI (*ca* 17.5 to 14.5 ka). In GBR, re-flooding of the shelf occurred asynchronously, based on shelf-edge physiography (Hinestrosa *et al.*, 2019). In southern GRB (for example, Capricorn Channel), where scattered or no barrier reef was present, re-flooding occurred as early as *ca* 18 ka (Hinestrosa *et al.*, 2019). In central and northern GBR, where terraces are present on the outer and mid shelf, re-flooding occurred gradually with reefs migrating landward in response to the stepwise sea-level rise of the last deglaciation (Webster *et al.*, 2018; Hinestrosa *et al.*, 2019). Similarly, on the slope, siliciclastic sediment input occurred asynchronously along the GBR in parallel with the gradual re-flooding of the shelf. Such a siliciclastic input is interpreted to be the result of erosion and resedimentation of LGM terrigenous material from rising sea level and storms, as

**Table 3.** Comparison tables for modern tropical and subtropical mixed siliclastic-carbonate systems. (A) Main sedimentation patterns and processes along outer shelf, shelf edge and slope during the last sea-level cycle and corresponding marine isotope stages (i.e. MIS 5e to MIS 1). Colour shading is used to emphasize similarities. Each depositional sub-environment is given a specific colour code: outer shelf = grey; shelf edge = green; slope = blue. Abbreviations are the following: NAT = northern Ashmore Trough; SAT = southern Ashmore Trough; GBR = Great Barrier Reef; NCBR = New Caledonia Barrier Reef; BBR = Belize Barrier Reef; NC = neritic carbonate; HO = hemipelagic ooze; PO = periplatform ooze; Sil = siliclastic; Exp = subaerial exposure; Drown = drowning; No sed = no sedimentation. Question marks in Ashmore Trough are inferred sedimentation patterns and processes due to lack of core data. (B) Geomorphic and climatic attributes that may have impacted sedimentation patterns and processes during the last sea-level cycle. No data are available on sediment yield for the south-west coast of New Caledonia. In this region, rivers are characterized by a torrential regime, with very low sediment supply in the absence of rainfall and short-lived very high sediment yield during cyclones (up to 0.02 Mt in a day, Quillon *et al.*, 2010). References for catchment area and river sediment yields are the following: NAT = Milliman (1995); SAT = Neil *et al.* (2002); GBR = Bainbridge *et al.* (2014); BBR = Burke and Sugg (2006).

		NAT			SAT			GBR			NCBR			BBR		
MIS	Sea level	Outer Shelf	Shelf edge	Slope	Outer Shelf	Shelf edge	Slope	Outer Shelf	Shelf edge	Slope	Outer Shelf	Shelf edge	Slope	Outer Shelf	Shelf edge	Slope
1	Late rise	No sed	Drown	PO/Sil	NC	Reefal	PO	NC	Reef	PO/Sil	NC	Reefal	PO/Sil	NC	Reefal	PO
Late 2	Early rise	Sil/NC	Reefal	Sil/PO	Exp	Exp	HO	Exp	Exp	HO/Sil	Exp	Exp	HO	Exp	Exp	HO
2	Min	Fluvial	Deltaic	Sil	Exp	Exp	HO	Exp	Exp	HO	Exp.	Exp	HO	Exp	Exp	HO
3-4	Late fall	Sil	Sil	Sil	Sil/NC	Exp	HO	Sil/NC	Exp	HO	Sil/NC	Exp	HO	Sil/NC	Exp	HO
5a-5d	Early fall	Sil/NC?	Sil/NC?	Sil/PO?	Sil/NC	Sil/NC	Sil/PO	NC	NC	PO	Sil/NC	Exp	HO	Sil/NC	Exp	HO
5e	Max	NC?	NC?	PO?	NC	NC	PO	Drown	Drown	HO	NC	NC	PO	NC	NC	PO
(A)																
		NAT			SAT			GBR			NCBR			BBR		
Present-day shelf width	120-150 km	Flat: fluvio-deltaic deposits	40-120 km	Rugged: patch reefs and inter-reef channels	50-100 km	Rugged: patch reefs and inter-reef channels	Up to 30 km	Rugged: patch reefs and inter-reef channels	Yes	Yes	Yes	Yes	Yes	Yes	Yes	Yes
Shelf physiography (pre-LGM)	No	Yes	Yes (few and small)	Up to 1000 m	From seasonally-dry tropical (south) to tropical humid (north)	Queensland east coast = 10-12 Mt	Tontouta River = n.a.	Dumbéa River = n.a.	Coulée River = n.a.	(rivers with torrential regime)	No	Yes, ITCZ southern boundary	Yes, ITCZ southern boundary	Yes, ITCZ southern boundary	Yes, ITCZ northern boundary	Yes, ITCZ northern boundary
Pre LGM shelf-edge barrier reef	Yes	Up to 2800 m	Tropical humid	GoP = 150-200 Mt	Fly River = ~0.7 Mt	No major river	Belize coast = ~4-6 Mt	Belize River = ~3 Mt								
Off-shelf atolls	Yes	Up to 200 m	Tropical humid	Yes	Yes	Yes	Yes	Yes	Yes	Yes	Yes	Yes	Yes	Yes	Yes	Yes
Hinterland elevation	Yes	Up to 200 m	Tropical humid	Yes	Yes	Yes	Yes	Yes	Yes	Yes	Yes	Yes	Yes	Yes	Yes	Yes
Hinterland climate	Yes	Up to 2800 m	Tropical humid	Yes	Yes	Yes	Yes	Yes	Yes	Yes	Yes	Yes	Yes	Yes	Yes	Yes
Catchment area and river sediment yields (Yearly)	Yes	Up to 2800 m	Tropical humid	Yes	Yes	Yes	Yes	Yes	Yes	Yes	Yes	Yes	Yes	Yes	Yes	Yes
Proximity to present-day ITCZ	Yes, ITCZ southern boundary	Yes, ITCZ southern boundary	Yes, ITCZ southern boundary	Yes, ITCZ southern boundary	Yes, ITCZ southern boundary	Yes, ITCZ southern boundary	Yes, ITCZ southern boundary	Yes, ITCZ southern boundary	Yes, ITCZ southern boundary	Yes, ITCZ southern boundary	Yes, ITCZ southern boundary	Yes, ITCZ southern boundary	Yes, ITCZ southern boundary	Yes, ITCZ southern boundary	Yes, ITCZ southern boundary	Yes, ITCZ southern boundary

well as increased precipitation and riverine discharge (Dunbar *et al.*, 2000; Dunbar & Dickens, 2003; Bostock *et al.*, 2009; Hinestroza *et al.*, 2019).

In Belize and New Caledonia, shelves were re-flooded later, after *ca* 12 ka, once sea level reached the top of exposed shelf-edge barrier reefs (Carson, 2007; Droxler & Jorry, 2013; Le Roy *et al.*, 2019). In all mixed systems, neritic carbonate sedimentation resumed or increased after the majority of bank and reef tops were re-flooded at *ca* 11.5 ka ('re-flooding window', Jorry *et al.*, 2010). On the slope of northern GBR and northern Ashmore Trough, siliciclastic sedimentation continued and peaked once again at *ca* 8.5 ka, possibly due to intensification of East Asian summer monsoon (Chen *et al.*, 2015). Interestingly, this renewed increase of siliciclastic sedimentation coincides with the Holocene 'thermal maximum', a period of increased precipitation and riverine discharge as recorded in the Northern Hemisphere (for example, Cariaco Basin; Haug *et al.*, 2001). In the NCBR slope, siliciclastic sedimentation during MIS 1 was related to erosion and off shelf transport of lagoonal sediment during storms (Le Roy *et al.*, 2019).

The above comparison allows drawing some conclusions on depositional controls, other than sea level, in mixed systems during the last glacial cycle (Table 3A and B). Whereas southern Ashmore Trough, GBR, NCBR and BBR share similar sedimentation patterns for most of the last sea-level cycle, northern Ashmore Trough shows some marked differences. During MIS 5e, shelf physiography in southern Ashmore Trough, GBR, NCBR and BBR was characterized by barrier reefs, patch reefs and inter-reef channels that became progressively exposed during the subsequent sea-level fall (MIS 5d to MIS 2). Differently, in northern Ashmore Trough a deltaic system prograded across the shelf from MIS 5d to MIS 2 and reached the present-day shelf edge during LGM. Moreover no shelf-edge barrier reef existed prior to LGM at this site. In northern Ashmore Trough such a physiography allowed siliciclastic sediment to persistently reach the slope from MIS 5d to MIS 2. On the contrary, in southern Ashmore Trough, GBR (central and northern), NCBR and BBR, siliciclastic sediment was mostly sequestered onto the shelf as the exposed shelf-edge barrier reef prevented sediment bypass into the slope.

Regionally, in areas proximal to the ITCZ southern boundary, climate played a role in the

delivery of siliciclastic sediment during the last deglaciation. On the slopes of Ashmore Trough and northern GBR, siliciclastic sedimentation during late MIS 2 and MIS 1 sea-level rise, was also associated with increased riverine discharge due to the southward shift of the ITCZ and intensification of summer monsoons.

Finally the southern GoP shelf-edge reef provides another case study on the edification of transgressive reefs and barrier reefs on a fluvio-deltaic substrate. Along with other case studies reported from Belize barrier reef (Ferro *et al.*, 1999; Droxler & Jorry, 2013), the Gulf of Mexico (Rezak & Bright, 1976; Belopolsky & Droxler, 1999), the north-east Brazilian outer shelf (Gomes *et al.*, 2020), the Calabrian continental shelf of Italy (Franchi *et al.*, 2018) and the Gulf of Elat/Aqaba in the Red Sea (Hartman *et al.*, 2015), all of these Quaternary case studies may constitute relevant analogues to interpret geometries and facies heterogeneities in the subsurface. Recently, it has been demonstrated that at least two Miocene palaeodeltas in the South China Sea provided favourable substratum of elevated sand bars for the emergence of transgressive carbonate build ups (Mathew *et al.*, 2020).

## CONCLUSIONS

This study reconstructed the sedimentary history along the shelf margin/slope of the Ashmore Trough (southern Gulf of Papua – GoP) mixed siliciclastic–carbonate system. The sedimentary record of several piston cores was analyzed at 100 kyr scale during the last sea-level cycle and millennial scale during the last deglaciation, a period of dramatic changes in rates of sea-level rise and climate. Sedimentary patterns were interpreted in the framework of independently reconstructed sea-level curves and climate history. The two different time-scales of investigation allowed determining multiple controls on spatial and temporal partitioning of siliciclastic and carbonate sediments.

During the last sea-level cycle, carbonate sedimentation in Ashmore Trough slopes was mainly controlled by magnitude of relative sea-level fluctuations. High accumulation rates of neritic carbonate mud on slopes occurred during the penultimate and current interglacial sea-level high (MIS 5e and MIS 1, respectively), when bank and reef tops were submerged. In addition, pulses of neritic carbonates occurred

during short-lived sea-level rise within early long-term sea-level fall (i.e. MIS 5c and MIS 5a), indicating that platform tops were temporarily re-flooded. Siliciclastic sedimentation patterns show a more complex interplay of sea-level fluctuations, shelf physiography, oceanic currents and sediment supply/delivery. During early sea-level fall (MIS 5d to 5a), erosion and reworking of terrigenous mud, previously stored on the inner shelf during MIS 5e, exited the narrow shelf and reached the southern Ashmore Trough slope due to southward oceanic currents. During late sea-level fall (MIS 4 and MIS 3), the main locus of siliciclastic sedimentation switched to northern Ashmore Slope. High mass accumulation rates (MARs) on the northern slope suggest that, during this interval, prograding river deltas reached the vicinity of the present-day shelf edge. At the same time, siliciclastic turbidites in Pandora Trough indicate that sediment bypass had started to take place on the northern Ashmore Trough slope. Slope sediment bypass peaked during the Last Glacial Maximum (LGM), when river deltas reached the present-day shelf edge and siliciclastic sediment was delivered to adjacent depocentres (for example, Pandora Trough and Bligh Trough).

At the millennial scale, climate was another control on sedimentation, in addition to sea level and shelf physiography. Coralgal reef and oolitic–skeletal sand (i.e. Unit A) resumed at the shelf edge following the first meltwater pulse (MWP-1A<sub>0</sub>) at *ca* 19 ka. Contemporaneously, the highest siliciclastic accumulation rates occurred both on the outer shelf (i.e. units B and C) and upper slope. These high rates resulted from increased precipitation and fluvial discharge, as well as near constant sea level, during a time of reorganization of global atmospheric and oceanic circulation patterns (i.e. ‘Mystery Interval’). The presence of sediment shelf-exit points with no barrier reef allowed shelf to slope sediment transfer. On the slope, sustained siliciclastic sedimentation continued during the late deglaciation and shortly increased again at *ca* 8.5 ka, possibly reflecting strengthening of the East Asian summer monsoon.

At the shelf edge, coralgal reefs drowned during meltwater pulse MWP-1B and the outer shelf became locus of condensed carbonate sedimentation (units D and E). On the slope periplatform ooze started to accumulate during late deglaciation, since *ca* 11.5 ka, once bank and reef tops (for example, Ashmore Reef and Great Barrier Reef northern terminus) were re-flooded following MWP-1B.

When comparing the main sedimentation patterns of the southern GoP shelf to slope mixed system with other modern tropical and subtropical mixed systems during the last sea-level cycle, the following conclusions on depositional controls can be drawn: (i) neritic carbonate and periplatform ooze sedimentation, at both the 100 kyr scale and millennial scale, was predominantly controlled by magnitude and rates of sea-level change; and (ii) siliciclastic sedimentation, at the 100 kyr scale, was primarily controlled by a combination of sea-level fluctuations and shelf physiography. At the millennial scale, in regions proximal to the ITCZ southern boundary (for example, southern GoP and northern GBR), siliciclastic input was also controlled by climate change during the unstable atmospheric and oceanic conditions of the last deglaciation.

## ACKNOWLEDGEMENTS

This research was supported by the National Science Foundation (OCE 0305688) to Droxler and Dickens, (OCE 0305373) to Bentley, and (OCE 0305250) to Peterson, and by the Swiss National Foundation (PBGE2-111250) to Jorry. We are grateful to the captain, officers, crew members, and scientific and technical shipboard parties of the PANASH cruise on the *R/V Melville* part of NSF MARGINS. Source-to-Sink initiative and the PECTEN cruise on the *R/V Marion Dufresne* part of IMAGES cruise. We would like to thank Editor Peir Pufahl, Associate Editor Jody Webster, and reviewers Gene Rankey and Angel Puga Bernabéu. Their comments and thorough reviews greatly improved the manuscript.

## DATA AVAILABILITY STATEMENT

The data that support the findings of this study are available from the corresponding author upon reasonable request.

## REFERENCES

- Abdul, N.A., Mortlock, R.A., Wright, J.D. and Fairbanks, R.G. (2016) Younger Dryas sea level and meltwater pulse 1B recorded in Barbados reef crest coral *Acropora palmata*. *Paleoceanography*, **31**, 330–344.
- Accordi, G. and Carbone, F. (2016) Evolution of the siliciclastic-carbonate shelf system of the northern Kenyan coastal belt in response to Late Pleistocene-Holocene relative sea level changes. *J. Afr. Earth Sci.*, **123**, 234–257.

- Andrews, J.C. and Clegg, S. (1989) Coral sea circulation and transport deduced from modal information models. *Deep-Sea Res., Part A*, **36**, 957–974.
- Aqrabi, A.A.N. and Sadooni, F.N. (1987) Recent ooids form Mesopotamian shallow shelf, NW Arabian Gulf. *J. Geol. Soc. Iraq*, **20**, 121–135.
- Ayliffe, L.K., Gagan, M.K., Zhao, J.X., Drysdale, R.N., Hellstrom, J.C., Hantoro, W.S., Griffiths, M.L., Scott-Gagan, H., Pierre, E.S., Cowley, J.A. and Suwargadi, B.W. (2013) Rapid interhemispheric climate links via the Australasian monsoon during the last deglaciation. *Nature Commun.*, **4**. <https://doi.org/10.1038/ncomms3908>
- Bainbridge, Z.T., Lewis, S.E., Smithers, S.G., Kuhnert, P.M., Henderson, B.L. and Brodie, J.E. (2014) Fine-suspended sediment and water budgets for a large, seasonally dry tropical catchment: Burdekin River catchment, Queensland, Australia. *Water Resour. Res.*, **50**, 9067–9087.
- Baldwin, S.L., Fitzgerald, P.G. and Webb, L.E. (2012) Tectonics of the New Guinea Region. *Ann. Rev. Earth Planet. Sci.*, **40**, 495–520.
- Bard, E., Hamelin, B., Arnold, M., Montaggioni, L., Cabiocch, G., Faure, G. and Rougerie, F. (1996) Deglacial sea-level record from Tahiti corals and the timing of global meltwater discharge. *Nature*, **382**, 241–244.
- Belopol'sky, A.V. and Droxler, A.W. (1999) Uppermost Pleistocene transgressive coralline reefs on the edge of the South Texas shelf: analogs for reefal reservoirs buried in siliciclastic shelf. In: *Advanced Reservoir Characterization for the 21st Century* (Ed. Hentz, T.F.). SEPM Gulf Coast Section, **19**, 41–50.
- Bird, P. (2003) An updated digital model of plate boundaries. *Geochem. Geophys. Geosys.*, **4**, 1–52.
- Blanchet, C.L., Thouveny, N. and de Garidel-Thoron, T. (2006) Evidence for multiple paleomagnetic intensity lows between 30 and 50 ka BP from a western Equatorial Pacific sedimentary sequence. *Quatern. Sci. Rev.*, **25**, 1039–1052.
- Blanchon, P., Jones, B. and Ford, D.C. (2002) Discovery of a submerged relic reef and shoreline off Grand Cayman: further support for an early Holocene jump in sea level. *Sed. Geol.*, **147**, 253–270.
- Blanchon, P. and Shaw, J. (1995) Reef drowning during the last deglaciation: evidence for catastrophic sea-level rise and ice-sheet collapse. *Geology*, **23**, 4–8.
- Bolton, B.R., Pile, J.L. and Kundapen, H. (2008) Texture, geochemistry, and mineralogy of sediments of the Fly River system. In: *The Fly River, Papua New Guinea: environmental studies in an impacted tropical river system* (Ed. Bolton, B.R.). *Dev. Earth Env. Sci.*, **9**, 51–112.
- Borer, J.M. and Harris, P.M. (1991) Lithofacies and cyclicity of the Yates Formation, Permian Basin; implications for reservoir heterogeneity. *AAPG Bull.*, **75**, 726–779.
- Bostock, H.C., Opdyke, B.N., Gagan, M.K. and Fifield, L.K. (2009) Late Quaternary siliciclastic/carbonate sedimentation model for the Capricorn Channel, southern Great Barrier Reef province, Australia. *Mar. Geol.*, **257**, 107–123.
- Breitzke, M. (2000) Acoustic and elastic characterization of marine sediments by analysis, modeling, and inversion of ultrasonic P wave transmission seismograms. *J. Geophys. Res.*, **105**, 21411–21430.
- Brodie, J.E. and Furnas, M. (1996) Cyclones, river flood plumes and natural water extremes in the central Great Barrier Reef. In: *Downstream effects of land use* (Eds Hunter, H.M., Eyles, A.G. and Rayment, G.E.), pp. 367–375. Department of Natural Resources, Brisbane.
- Burke, L. and Sugg, Z. (2006) Hydrologic modeling of watersheds discharging adjacent to the Mesoamerican Reef. WRI/ICRAN Report, 35 pp. <https://www.wri.org/publication/watershed-analysis-mesoamerican-reef>
- Carozzi, A.V. (1957) Contribution à l'étude des propriétés géométriques des oolithes - l'exemple du Grand Lac Salé, Utah, USA. *Bull. Inst. Nat. Genev.*, **58**, 3–32.
- Carson, B.E. (2007) Late Quaternary sediment accumulations and foraminiferal populations on the slopes of Gladded Basin (offshore Belize) and southern Ashmore Trough (Gulf of Papua) mixed siliciclastic-carbonate system. Rice University, Ph.D. thesis, 165 pp.
- Carson, B.E., Francis, J.M., Leckie, R.M., Droxler, A.W., Dickens, G.R., Jorry, S.J., Bentley, S.J., Peterson, L.C. and Opdyke, B.N. (2008) Benthic foraminiferal response to sea level change in the mixed siliciclastic-carbonate system of southern Ashmore Trough (Gulf of Papua). *J. Geophys. Res.*, **113**, F01S20. <https://doi.org/10.1029/2006JF000629>
- Catuneanu, O. (2006) *Principles of Sequence Stratigraphy*. Elsevier, Amsterdam. 375 pp.
- Chen, F., Xu, Q., Chen, J., Birks, H.J.B., Liu, J., Zhang, S., Jin, L., An, C., Telford, R.J., Cao, X., Wang, Z., Zhang, X., Selvaraj, K., Lu, H., Li, Y., Zheng, Z., Wang, H., Zhou, A., Dong, G., Zhang, J., Huang, X., Bloemendal, J. and Rao, Z. (2015) East Asian summer monsoon precipitation variability since the last deglaciation. *Nature*, **5**. <https://doi.org/10.1038/srep11186>
- Clark, P.U., McCabe, A.M., Mix, A.C. and Weaver, A.J. (2004) Rapid rise of sea level 19,000 years ago and its global implications. *Science*, **304**, 1141–1144.
- Clark, P.U., Shakun, J.D., Baker, P.A., Bartleind, P.J., Brewere, S., Brook, E., Carlson, A.E., Cheng, H., Kaufman, D.S., Liu, Z., Marchitto, T.M., Mix, A.C., Morrill, M., Otto-Bliesner, B.L., Pahnke, K., Russell, J.M., Whitlock, C., Adkins, J.F., Blois, J.L., Clark, J., Colman, S.M., Curry, W.B., Flower, B.P., He, F., Johnson, T.C., Stieglitz, J.L., Markgraf, V., McManus, J., Mitrovica, J.X., Moreno, P.I. and Williams, J.W. (2012) Global climate evolution during the last deglaciation. *Proc. Natl Acad. Sci. USA*, **109**, 1134–1142.
- Cloos, M., Sapiie, B., van Ufford, A.Q., Weiland, R.J., Warren, P.Q. and McMahon, T.P. (2005) Collisional delamination in New Guinea: The geotectonics of subducting slab breakoff. *GSA Spec. Paper*, **400**, 51 pp.
- D'Agostini, D.P., Bastos, A.C. and Dos Reis, A.T. (2015) The modern mixed carbonate-siliciclastic Abrolhos shelf: implications for a mixed depositional system. *J. Sed. Res.*, **85**. <https://doi.org/10.2110/jsr.2015.08>
- Daniell, J.J. (2008) Development of a bathymetric grid for the Gulf of Papua and adjacent areas: A note describing its development. *J. Geophys. Res.*, **113**, F01S15. <https://doi.org/10.1029/2006JF000673>
- Davies, P.J., Symonds, P.A., Feary, D.A. and Pigram, C.J. (1989) The evolution of the carbonate platforms of northeast Australia. In: *Controls on Carbonate Platform and Basin Development* (Eds. Crevello, P.D., Wilson, J.L., Sarg, J.F. and Read, J.F.) *SEPM Spec. Pub.*, **44**, 233–258.
- Dawson, J.L., Smithers, S.G. and Hua, Q. (2014) The importance of large benthic foraminifera to reef island sediment budget and dynamics at Raine Island, northern Great Barrier Reef. *Geomorphology*, **222**, 68–81.
- Denniston, R.F., Wyrwoll, K.H., Asmerom, Y., Polyak, V.J., Humphreys, W.F., Cugley, J., Woods, D., LaPointe, Z., Peota, J. and Greaves, E. (2013) North Atlantic forcing of millennial-scale Indo-Australian monsoon dynamics

- during the Last Glacial period. *Quatern. Sci. Rev.*, **72**, 159–168.
- Denton, G.H., Anderson, R.F., Toggweiler, J.R., Edwards, R.L., Schaefer, J.M. and Putnam, A.E.** (2010) The last glacial termination. *Science*, **328**, 1652–1656.
- Denton, G.H., Broecker, W.S. and Alley, R.B.** (2006) The mystery interval 17.5 to 14.5 kyrs ago. *PAGES News*, **14**, 14–16.
- Deschamps, P., Durand, N., Bard, E., Hamelin, B., Camoin, G., Thomas, A.L., Henderson, G.M., Okuno, J. and Yokoyama, Y.** (2012) Ice-sheet collapse and sea-level rise at the Bølling warming 14,600 years ago. *Nature*, **483**, 559–564.
- Dietrich, W.E., Day, G.M. and Parker, G.** (1999) The Fly River, Papua New Guinea: Inferences about river dynamics, floodplain sedimentation and fate of sediment. In: *Varieties of Fluvial Form* (Eds Miller, A.J. and Gupta, A.), pp. 345–376 John Wiley & Sons, Chichester.
- Draut, A.E., Raymo, M.E., McManus, J.F. and Oppo, D.W.** (2003) Climate stability during the Pliocene warm period. *Paleoceanography*, **18**. <https://doi.org/10.1029/2003PA000889>
- Droxler, A.W. and Jorjy, S.J.** (2013) Deglacial origin of barrier reefs along low latitude mixed siliciclastic and carbonate continental shelf edges. *Ann. Rev. Mar. Sci.*, **5**, 165–190.
- Droxler, A.W., Mallarino, G., Francis, J.M., Dickens, G.R., Beaufort, L., Bentley, S., Peterson, L. and Opdyke, B.** (2006) Early part of last deglaciation: A short interval favorable for the building of coralgal edifices on the edges of modern siliciclastic shelves (Gulf of Papua and Gulf of Mexico). AAPG Ann. Conv., Abstr. Prog., p. 37.
- Druffel, E.R.M. and Griffin, S.** (1999) Variability of surface ocean radiocarbon and stable isotopes in the southwestern Pacific. *J. Geophys. Res.*, **104**, 23607–23613.
- Dunbar, G.B., Dickens, G.R. and Carter, R.M.** (2000) Sediment flux across the Great Barrier Reef shelf to the Queensland Trough over last 300 ky. *Sed. Geol.*, **133**, 49–92.
- Dunbar, G.B. and Dickens, G.R.** (2003) Massive siliciclastic discharge to slopes of the Great Barrier Reef Platform during sea-level transgression: constraints from sediment cores between 15°S and 16°S latitude and possible explanations. *Sed. Geol.*, **162**, 141–158.
- Dykoski, C.A., Edwards, R.L., Cheng, H., Yuan, D., Cai, Y., Zhang, M., Lin, Y., Jiaming Qing, J., An, Z. and Justin Revenaugh, J.** (2005) A high-resolution, absolute-dated Holocene and deglacial Asian monsoon record from Dongge Cave, China. *Earth Planet. Sci. Lett.*, **233**, 71–86.
- Esker, D., Eberli, G.P. and McNeill, D.F.** (1998) The structural and sedimentological controls on the reoccupation of Quaternary incised valleys, Belize Southern Lagoon. *AAPG Bull.*, **82**, 2075–2109.
- Fairbanks, R.G., Mortlock, R.A., Chiu, T., Cao, L., Kaplan, A., Guilderson, T.P., Fairbanks, T.W., Bloom, A.L., Grootes, P.M. and Nadeau, M.** (2005) Radiocarbon calibration curve spanning 0 to 50,000 years BP based on paired  $^{230}\text{Th}/^{234}\text{U}/^{238}\text{U}$  and  $^{14}\text{C}$  dates on pristine corals. *Quatern. Sci. Rev.*, **24**, 1781–1796.
- Ferro, C.E., Droxler, A.W., Anderson, J.B. and Mucciarone, D.** (1999) Late Quaternary shift of mixed siliciclastic-carbonate environments induced by glacial eustatic sea-level fluctuations in Belize. In: *Advances in Carbonate Sequence Stratigraphy: Application to Reservoirs, Outcrops and Models* (Eds Harris, P.M., Saller, A.H. and Simo, J.A.), *SEPM Spec. Publ.*, **63**, 385–411.
- Flügel, E.** (1982) *Microfacies Analysis of Limestones*. Springer-Verlag, New York, NY, 633 pp.
- Franchi, F., Bergamasco, A., Da Lio, C., Donnici, S., Mazzoli, C., Montagna, P., Taviani, M., Tosi, L. and Zecchin, M.** (2018) Petrographic and geochemical characterization of the early formative stages of Northern Adriatic shelf rocky buildups. *Mar. Petrol. Geol.*, **91**, 321–337.
- Francis, J.M., Daniell, J.J., Droxler, A.W., Dickens, G.R., Bentley, S.J., Peterson, L.C., Opdyke, B.N. and Beaufort, L.** (2008) Deep water geomorphology of the mixed siliciclastic-carbonate system, Gulf of Papua. *J. Geophys. Res.*, **113**, F01S16. <https://doi.org/10.1029/2007JF000851>
- Francis, J.M., Dunbar, G.B., Dickens, G.R., Sutherland, I.A. and Droxler, A.W.** (2007) Siliciclastic sediment across the north Queensland margin, (Australia): a Holocene perspective on reciprocal versus coeval deposition in tropical mixed siliciclastic-carbonate systems. *J. Sed. Res.*, **77**, 572–586.
- de Garidel-Thoron, T., Beaufort, L., Bassinot, F. and Henry, P.** (2004) Evidence for large methane releases to the atmosphere from deep-sea gas-hydrate dissociation during the last glacial episode. *Proc. Natl Acad. Sci. USA*, **101**, 9187–9192.
- Gischler, E., Ginsburg, R.N., Herrle, J.O. and Prasad, S.** (2010) Mixed carbonates and siliciclastics in the Quaternary of southern Belize: Pleistocene turning points in reef development controlled by sea-level change. *Sedimentology*, **57**, 1049–1068.
- Gomes, M.P., Vital, H. and Droxler, A.W.** (2020) Terraces, reefs, and valleys along the Brazil northeast outer shelf: deglacial sea-level archives? *Geo-Mar. Lett.*, **40**, 699–711.
- Handford, C.R. and Loucks, R.G.** (1993) Carbonate depositional sequences and systems tracts - responses of carbonate platforms to relative sea-level changes. In: *Carbonate Sequence Stratigraphy: Recent Developments and Applications* (Eds Loucks, R.G. and Sarg, J.F.) *AAPG Mem.*, **57**, 3–41.
- Harper, B.B.** (2014) Late Quaternary mixed carbonate-siliciclastic sediment slope accumulation: unexpected responses of Australia and Papua New Guinea reefs to glacio-eustatic sea level fluctuations. Ph.D. thesis, Rice University, 219 pp.
- Harper, B.B., Puga-Bernabéu, Á., Droxler, A.W., Webster, J.M., Gischler, E., Tiwari, M., Lado-Insua, T., Thomas, A.L., Morgan, S., Jovane, L. and Röhl, U.** (2015) Mixed carbonate-siliciclastic sedimentation along the Great Barrier Reef upper slope: a challenge to the reciprocal sedimentation model. *J. Sed. Res.*, **85**, 1019–1036.
- Harris, P.T., Baker, E.K., Cole, A.R. and Short, S.A.** (1993) Preliminary study of sedimentation in the tidally dominated Fly River Delta, Gulf of Papua. *Cont. Shelf Res.*, **13**, 441–472.
- Harris, P.T., Davies, P.J. and Marshall, J.F.** (1990) Late Quaternary sedimentation on the Great Barrier Reef continental shelf and slope east of Townsville, Australia. *Mar. Geol.*, **94**, 55–77.
- Harris, P.T., Heap, A., Passlow, V., Hughes, M., Daniell, J.J., Hemer, M. and Anderson, O.** (2005) Tidally incised valleys on tropical carbonate shelves: An example from the northern Great Barrier Reef, Australia. *Mar. Geol.*, **220**, 181–204.
- Harris, P.T., Pattiaratchi, C.B., Keene, J.B., Dalrymple, R.W., Gardner, J.V. and Baker, E.K.** (1996) Late Quaternary deltaic and carbonate sedimentation in the Gulf of Papua



- foreland basin: Response to sea-level change. *J. Sed. Res.*, **66**, 801–819.
- Hartman, G., Niemi, T.M., Ben-Avraham, B., Tibor, G., Al-Zoubi, A., Sade, R.A., Hall, J.K., Akawi, E., Abueladas, A., Al-Ruzouq, R. and Makovsky, Y. (2015) Distinct relict fringing reefs in the northern shelf of the Gulf of Elat/Aqaba: Markers of Quaternary eustatic and climatic episodes. *Sedimentology*, **62**, 516–540.
- Haug, G.H., Hughen, K.A., Sigman, D.M., Peterson, L.C. and Röhl, U. (2001) Southward migration of the intertropical convergence zone through the Holocene. *Science*, **293**, 1304–1308.
- Hinestrosa, G., Webster, J.M. and Beaman, R.J. (2016) Postglacial sediment deposition along a mixed carbonate-siliciclastic margin: New constraints from the drowned shelf edge reefs of the Great Barrier Reef, Australia. *Palaeogeogr. Palaeoclimatol. Palaeoecol.*, **446**, 168–185.
- Hinestrosa, G., Webster, J.M. and Beaman, R.J. (2019) Spatio-temporal patterns in the postglacial flooding of the Great Barrier Reef shelf, Australia. *Cont. Shelf Res.*, **173**, 13–26.
- Hohenegger, J., Yordanova, E., Nakano, Y. and Tatzreiter, F. (1999) Habitats of larger foraminifera on the upper reef slope of Sesoko Island, Okinawa, Japan. *Mar. Micropaleont.*, **36**, 109–168.
- Hopley, D. (2006) Coral reef growth on the shelf margin of the Great Barrier Reef with special reference to the Pompey Complex. *J. Coastal Res.*, **22**, 150–174.
- Howell, A.L., Bentley, S.J., Xu, K., Ferrell, R.E., Muhammad, Z. and Septama, E. (2014) Fine sediment mineralogy as a tracer of latest Quaternary sediment delivery to a dynamic continental margin: Pandora Trough, Gulf of Papua, Papua New Guinea. *Mar. Geol.*, **357**, 108–122.
- Ishiwa, T., Yokoyama, Y., Reuning, L., McHugh, C.M., De Vleeschouwer, D., Stephen, J. and Gallagher, S.J. (2019) Australian Summer Monsoon variability in the past 14,000 years revealed by IODP Expedition 356 sediments. *Prog. E. Pla. Sci.*, **6**. <https://doi.org/10.1186/s40645-019-0262-5>
- James, N.P. and Choquette, P.W. (1990) Limestones - the sea floor diagenetic environment. In: *Diagenesis* (Eds McIlreath, I.A. and Morrow, D.W.) *Geoscience Canadian Reprint Series*, **4**, 13–34.
- Jorry, S.J., Droxler, A.W., Mallarino, G., Dickens, G.R., Bentley, S.J., Beaufort, L., Peterson, L.C. and Opdyke, B.N. (2008) Bundled turbidite deposition in the central Pandora Trough (Gulf of Papua) since Last Glacial Maximum: Linking sediment nature and accumulation to sea level fluctuations at millennial timescale. *J. Geophys. Res.*, **113**, F01S19. <https://doi.org/10.1029/2006JF000649>
- Jorry, S.J., Droxler, A.W. and Francis, J.M. (2010) Deepwater carbonate deposition in response to re-flooding of carbonate bank and atoll-tops at glacial terminations. *Quat. Sci. Rev.*, **29**, 2010–2026.
- Kerans, C. and Tinker, S. (1999) Extrinsic stratigraphic controls on development of the Capitan reef complex. In: *Geological Framework of the Capitan Reef* (Eds Saller, A.H., Harris, P.M., Kirkland, B.L. and Mazzullo, S.J.), *SEPM Spec. Publ.*, **65**, 15–36.
- Khanna, P., Droxler, A.W., Nittrouer, J.A., Tunnell Jr, J.W. and Shirley, T.C. (2017) Coral reef morphology records punctuated sea-level rise during the last deglaciation. *Nature*, **8**. <https://doi.org/10.1038/s41467-017-00966-x>
- Kuhnt, W., Holbourn, A., Xu, J., Opdyke, B., De Deckker, P., Röhl, U. and Mudelsee, M. (2015) Southern Hemisphere control on Australian monsoon variability during the late deglaciation and Holocene. *Nature*, **6**, 5916. <https://doi.org/10.1038/ncomms6916>
- Lambeck, K. and Chappell, J. (2001) Sea level change through the last glacial cycle. *Science*, **292**, 679–686.
- Lambeck, K., Esat, T.M. and Potter, E.K. (2002) Links between climate and sea levels for the past three million years. *Nature*, **419**, 199–206.
- Lambeck, K., Rouby, H., Purcell, A., Sun, Y. and Sambridge, M. (2014) Sea level and global ice volumes from the Last Glacial Maximum to the Holocene. *Proc. Natl Acad. Sci. USA*, **111**, 15296–15303.
- Land, L.S., Behrens, E.W. and Frishman, S.A. (1979) The ooids of Baffin Bay, Texas. *J. Sed. Petrol.*, **49**, 1269–1277.
- Le Roy, P., Cabioch, G., Monod, B., Lagabrielle, Y., Pelletier, B. and Flamand, B. (2008) Late Quaternary history of the Noumea lagoon (New Caledonia, Southwestern Pacific) as depicted by seismic stratigraphy and multibeam bathymetry: a modern model of tropical rimmed shelf. *Palaeogeogr. Palaeoclimatol. Palaeoecol.*, **270**, 29–45.
- Le Roy, P., Jorry, S.J., Jouet, G., Ehrhold, A., Michel, M., Gautier, V. and Guérin, C. (2019) Late Pleistocene evolution of the mixed siliciclastic and carbonate southwestern New Caledonia continental shelf/lagoon. *Palaeogeogr. Palaeoclimatol. Palaeoecol.*, **514**, 502–521.
- Leduc, G., Thouveny, N., Bourles, D.L., Blanchet, C.L. and Carcaillet, J.T. (2006) Authigenic  $^{10}\text{Be}/^{9}\text{Be}$  signature of the Laschamp excursion: A tool for global synchronisation of paleoclimatic archives. *Earth Planet. Sci. Lett.*, **245**, 19–28.
- Lisiecki, L.E. and Raymo, M.E. (2005) A Pliocene-Pleistocene stack of 57 globally distributed benthic  $\delta^{18}\text{O}$  records. *Paleoceanography*, **20**, PA1003. <https://doi.org/10.1029/2004PA001071>
- Liu, P.J. and Milliman, J.D. (2004) Reconsidering melt-water pulses 1A and 1B: Global Impacts of rapid sea-level rise. *J. Ocean U. China*, **3**, 183–190.
- Macquaker, J.H.S., Bentley, S.J. and Bohacs, K.M. (2010) Wave-enhanced sediment-gravity flows and mud dispersal across continental shelves: Reappraising sediment transport processes operating in ancient mudstone successions. *Geology*, **38**, 947–950.
- Marshall, J.F. and Davis, P.J. (1975) High-magnesium calcite ooids from the Great Barrier Reef. *J. Sed. Petrol.*, **45**, 285–291.
- Mathew, M., Makhankova, A., Menier, D., Sautter, B., Betzler, C. and Pierson, B. (2020) The emergence of Miocene reefs in South China Sea and its resilient adaptability under varying eustatic, climatic and oceanographic conditions. *Sci. Rep.*, **10**. <https://doi.org/10.1038/s41598-020-64119-9>
- Maxwell, W.G.H. and Swinchatt, J.P. (1970) Great Barrier Reef: Regional variation in a terrigenous carbonate province. *Geol. Soc. Am. Bull.*, **81**, 691–724.
- McGee, D., Donohoe, A., Marshall, J. and Ferreira, D. (2014) Changes in ITCZ location and cross-equatorial heat transport at the Last Glacial Maximum, Heinrich Stadial 1, and the mid-Holocene. *Earth Planet. Sci. Lett.*, **390**, 69–79.
- McManus, J.F., Oppo, D.W. and Cullen, J.L. (1999) A 0.5-million-year record of millennial-scale climate variability in the North Atlantic. *Science*, **283**, 971–974.
- Miller, K.G., Browning, J.V., Schmelz, W.J., Kopp, R.E., Mountain, G.S. and Wright, J.D. (2020) Cenozoic sea-level and cryospheric evolution from deep-sea geochemical and continental margin records. *Sci. Adv.*, **6**, eaaz1346. <https://doi.org/10.1126/sciadv.aaz1346>

- Milliman, J.D.** (1995) Sediment discharge to the ocean from small mountainous rivers: The New Guinea example. *Geo-Mar. Lett.*, **15**, 127–133.
- Mitrovica, J.X. and Milne, G.A.** (2002) On the origin of late Holocene sea-level highstands within equatorial ocean basins. *Quat. Sci. Rev.*, **21**, 2179–2190.
- Müller, G. and Gastner, M.** (1971) The “Karbonat-Bombe”, a simple device for the determination of the carbonate content in sediments, soils and other materials. *N. Jahrb. Mineral.*, **10**, 466–469.
- Muhammad, Z., Bentley, S.J., Febo, L.A., Droxler, A.W., Dickens, G.R., Peterson, L.C. and Opdyke, B.N.** (2008) Excess  $^{210}\text{Pb}$  inventories and fluxes along the continental slope and basins of the Gulf of Papua. *J. Geophys. Res.*, **113**, 1–14.
- Muller, J., Kylander, M., Wu, R.A.J., Weiss, D., Martinez-Cortizas, A., LeGrande, A.N., Jennerjahn, T., Behling, H., Anderson, W.T. and Jacobson, G.** (2008) Possible evidence for wet Heinrich phases in tropical NE Australia: The Lynch’s Crater deposit. *Quat. Sci. Rev.*, **27**, 468–475.
- Nakada, M. and Lambeck, K.** (1987) Glacial rebound and relative sea-level variations: A new appraisal. *Geophys. J. R. Astron. Soc.*, **90**, 171–224.
- Neil, D.T., Orpin, A.R., Ridd, P.V. and Bofu, Y.** (2002) Sediment yield and impacts from river catchments to the Great Barrier Reef lagoon. *Aust. J. Mar. Freshw. Res.*, **53**, 733–752.
- Ogston, A.S., Sternberg, R.W., Nittrouer, C.A., Martin, D.P., Goni, M.A. and Crockett, J.S.** (2008) Sediment delivery from the Fly River tidally dominated delta to the nearshore marine environment and the impact of El Niño. *J. Geophys. Res.*, **113**, F01S11. <https://doi.org/10.1029/2006JF000669>
- Opdyke, B.N. and Wilkinson, B.H.** (1990) Paleolatitude distribution of Phanerozoic marine ooids and cements. *Palaogeogr. Palaeoclimatol. Palaeoecol.*, **7–8**, 135–148.
- Ouillon, S., Douillet, P., Lefebvre, J.P., Le Gendre, R., Jouan, A., Bonneton, P., Fernandez, J.M., Chevillon, C., Magand, O., Lefèvre, J., Le Hir, P., Laganier, R., Dumas, F., Marchesiello, P., Bel Madani, A., Andréfouët, S., Panché, J.Y. and Fichez, R.** (2010) Circulation and suspended sediment transport in a coral reef lagoon: The south-west lagoon of New Caledonia. *Mar. Pollut. Bull.*, **61**, 269–296.
- Peltier, W.R. and Andrews, J.T.** (1976) Glacial-isostatic adjustment-I. The forward problem. *Geophys. J. R. Astron. Soc.*, **46**, 605–646.
- Pigram, C.J., Davies, P.J., Feary, D.A. and Symonds, P.A.** (1989) Tectonic controls on carbonate platform evolution in southern Papua New Guinea: Passive margin to foreland basin. *Geology*, **17**, 199–202.
- Pirmez, C., Bradford, P.E., Mallarino, G., O’Hayer, W.W., Droxler, A.W. and Winkler, C.D.** (2012) Chronostratigraphy of the Brazos-Trinity depositional system, western Gulf of Mexico: Implications for deep-water depositional models. In: *Application of the principles of seismic geomorphology to continental-slope and base-of-slope systems: case studies from seafloor and near-seafloor analogues* (Eds Prather, B.E., Deptuck, M.E., Mohrig, D., Van Hoorn, B. and Wynn, R.B.), *SEPM Spec. Publ.*, **99**, 111–143.
- Railsback, L.B., Gibbard, P.L., Head, M.J., Voarinstoa, N.R.G. and Toucanne, S.** (2015) An optimized scheme of lettered marine isotope substages for the last 1.0 million years, and the climatostratigraphic nature of isotope stages and substages. *Quatern. Sci. Rev.*, **111**, 94–106.
- Rankey, E.C. and Reeder, S.L.** (2009) Holocene ooids of Aitutaki Atoll, Cook Islands, South Pacific. *Geology*, **37**, 971–974.
- Rasser, M. and Piller, W.E.** (1997) Depth distribution of calcareous encrusting associations in the northern Red Sea (Safaga, Egypt) and their geological implications. Proc. 8th Int. Coral Reef Symp., 743–748.
- Reeves, J.M., Barrows, T.T., Cohen, T.J., Kiem, A.S., Bostock, H.C., Fitzsimmons, K.E., Jansen, J.D., Kempf, J., Krause, C., Petherick, L., Phipps, S.J. and OZ-INTIMATE Members** (2013) Climate variability over the last 35,000 years recorded in marine and terrestrial archives in the Australian region: an OZ-INTIMATE compilation. *Quatern. Sci. Rev.*, **74**, 21–34.
- Renema, W.** (2006) Large benthic foraminifera from the deep photic zone of a mixed siliciclastic-carbonate shelf off East Kalimantan, Indonesia. *Mar. Micropaleont.*, **58**, 73–82.
- Renema, W.** (2010) Is increased calcarinid (foraminifera) abundance indicating a larger role for *macroalgae* in Indonesian Plio-Pleistocene coral reefs? *Coral Reefs*, **29**, 165–173.
- Rezak, R. and Bright, T.J.** (1976) Coral reefs and banks of Texas outer continental shelf. *AAPG Bull.*, **60**, 713–714.
- Riegl, B., Poiriez, A., Janson, X. and Bergman, K.L.** (2010) The Gulf: Facies belts, physical, chemical, and biological parameters of sedimentation on a carbonate ramp. In: *Carbonate Depositional Systems: Assessing Dimensions and Controlling Parameters*. (Eds Westphal, H., Riegl, B. and Eberli, G.P.), pp. 145–214. Springer Science, New York, NY.
- Rohling, E.J., Grant, K., Bolshaw, M., Roberts, A.P., Siddall, M., Hemleben, C. and Kucera, M.** (2009) Antarctic temperature and global sea level closely coupled over the past five glacial cycles. *Nature Geosci.*, **2**(7), 500–504.
- Ryan-Mishkin, K., Walsh, J.P., Corbett, D.R., Dail, M.B. and Nittrouer, J.A.** (2009) Modern sedimentation in a mixed siliciclastic-carbonate coral reef environment, La Parguera, Puerto Rico. *Caribb. J. Sci.*, **45**, 151–167.
- Schlager, W., Reijmer, J.J.G. and Droxler, A.W.** (1994) Highstand shedding of carbonate platforms. *J. Sed. Res.*, **64**, 270–281.
- Septama, E., Bentley, S.J. and Droxler, A.W.** (2016) Conduits, timing and processes of sediment delivery across a highrelief continental margin: Continental shelf to basin in Late Quaternary, Gulf of Papua. *Mar. Petrol. Geol.*, **72**, 447–462.
- Septama, E. and Bentley, S.J.** (2017) Source-to-sink sediment delivery in the Gulf of Papua from scanning electron microscopy and mineral liberation analysis-aided provenance analysis of deep-sea turbidite sands. *AAPG Bull.*, **6**, 907–936.
- Shew, R.D.** (1991) Upward-shoaling sequence of mixed siliciclastics and carbonates from the Jurassic Smackover Formation of central Mississippi. In: *Mixed Carbonate Siliciclastic Sequences* (Eds Lomando, A.J. and Harris, P.M.), *SEPM Core Workshop*, **15**, 135–167. SEPM, Tulsa, OK.
- Shiau, L.J., Chen, M.T., Clemens, S.C., Huh, C.A., Yamamoto, M. and Yokoyama, Y.** (2011) Warm pool hydrological and terrestrial variability near southern Papua New Guinea over the past 50k. *Geoph. Res. Lett.*, **38**, L00F01. <https://doi.org/10.1029/2010GL045309>
- Silver, B.A. and Todd, R.G.** (1969) Permian cyclic strata, Northern Midland and Delaware Basins, West Texas and Southeastern Mexico. *AAPG Bull.*, **53**, 2223–2251.
- Simone, L.** (1981) Ooids: a review. *Earth Planet. Sci. Rev.*, **16**, 319–355.

- Sirocko, F., Garbe-Schönberg, D., McIntyre, A. and Molfino, B. (1996) Teleconnections between the subtropical monsoons and high-latitude climates during the last deglaciation. *Science*, **272**, 526–529.
- Slingerland, R., Driscoll, N.W., Milliman, J.D., Miller, S.R. and Johnstone, E.A. (2008a) Anatomy and growth of a Holocene clinothem in the Gulf of Papua. *J. Geophys. Res.*, **113**, F01S13. <https://doi.org/10.1029/2006JF000628>
- Slingerland, R., Selover, R.W., Ogston, A.S., Keen, T.R., Driscoll, N.W. and Milliman, J.D. (2008b) Building the Holocene clinothem in the Gulf of Papua: An ocean circulation study. *J. Geophys. Res.*, **113**, F01S14. <https://doi.org/10.1029/2006JF000680>
- Slowey, N.C., Neumann, A.C. and Baldwin, K.C. (1989) Seismic expression of Quaternary climatic cycles in the peri-platform carbonate ooze of the northern Bahamas. *Geol. Soc. Am. Bull.*, **101**, 1563–1573.
- Sternberg, R.W., Cacchione, D.A., Paulson, B., Kineke, G.C. and Drake, D.E. (1996) Observations of sediment transport on the Amazon subaqueous delta. *Cont. Shelf Res.*, **16**, 697–715.
- Stuiver, M., Reimer, P.J., Bard, E., Beck, J.W., Burr, G.S., Hughen, K.A., Kromer, B., McCormac, G., van der Plicht, J. and Spurk, M. (1998) INTCAL98 radiocarbon age calibration 24,000–0 cal BP. *Radiocarbon*, **40**, 1041–1083.
- Tachikawa, K., Vidal, L., Sonzogni, C. and Bard, E. (2009) Glacial/interglacial sea surface temperature changes in the southwest Pacific Ocean over the past 360 ka. *Quatern. Sci. Rev.*, **28**, 1160–1170.
- Tcherepanov, E.N., Droxler, A.W., Lapointe, P., Dickens, G.R., Bentley, S.J., Beaufort, L., Peterson, L.C., Daniell, J.J. and Opdyke, B.N. (2008) Neogene evolution of the mixed carbonate-siliciclastic system in the Gulf of Papua, Papua New Guinea. *J. Geophys. Res.*, **113**, F01S21. <https://doi.org/10.1029/2006JF000684>
- Tcherepanov, E.N., Droxler, A.W., Lapointe, P., Mohn, K. and Larsen, O.A. (2010) Siliciclastic influx and burial of the Cenozoic carbonate system in the Gulf of Papua. *Mar. Pet. Geol.*, **27**, 533–554.
- Testa, V. and Bosence, D.W.J. (1999) Physical and biological controls on the formation of carbonate and siliciclastic bedforms on the north-east Brazilian shelf. *Sedimentology*, **46**, 279–301.
- Thompson, P.R., Bé, A.W.H., Duplessy, J.C. and Shackleton, N.J. (1979) Disappearance of pink-pigmented *Globigerinoides ruber* at 120,000 yr BP in the Indian and Pacific Oceans. *Nature*, **280**, 554–558.
- Thompson, R. and Oldfield, F. (1986) *Environmental magnetism*. Springer, Dordrecht, 227 pp.
- Turney, C.S.M., Haberle, S., Fink, D., Kershaw, A.P., Barbetti, M., Barrows, T.T., Black, M., Cohen, T.J., Corrège, T., Hesse, P.P., Hua, Q., Johnston, R., Morgan, V., Moss, P., Nanson, G., van Ommen, T., Rule, S., Williams, N.J., Zhao, J.X., D'Costa, D., Feng, Y.X., Gagan, M., Mooney, S. and Xia, Q. (2006) Integration of ice-core, marine and terrestrial records for the Australian Last Glacial Maximum and Termination: a contribution from the OZ INTIMATE group. *J. Quat. Sci.*, **21**, 751–761.
- van Ufford, A.Q. and Cloos, M. (2005) Cenozoic tectonics of New Guinea. *AAPG Bull.*, **89**, 119–140.
- Veron, J.E.N. (1978) Deltaic and dissected reefs of the far northern region. *Phil. Trans. Roy. Soc. London B.*, **284**, 23–37.
- Walsh, J.P. and Nittrouer, C.A. (2003) Contrasting styles of off-shelf sediment accumulation in New Guinea. *Mar. Geol.*, **196**, 105–125.
- Walsh, J.P., Nittrouer, C.A., Palinkas, C.M., Ogston, A.S., Sternberg, R.W. and Brunskill, G.J. (2004) Clinofold mechanics in the Gulf of Papua, New Guinea. *Cont. Shelf Res.*, **24**, 2487–2510.
- Weber, M.E., Niessen, F., Kuhn, G. and Wiedicke, M. (1997) Calibration and application of marine sedimentary physical properties using a multisensory core logger. *Mar. Geol.*, **136**, 151–172.
- Webster, J.M., Beaman, R.J., Puga-Bernabéu, A., Ludman, D., Renema, W., Wust, R.A.J., George, N.P.J., Reimer, P.J., Jacobsen, G.E. and Moss, P. (2012) Late Pleistocene history of turbidite sedimentation in a submarine canyon off the northern Great Barrier Reef, Australia. *Palaeogeogr. Palaeoclimatol. Palaeoecol.*, **331–332**, 75–89.
- Webster, J.M., Braga, J.C., Humblet, M., Potts, D.C., Iryu, Y., Yokoyama, Y., Fujita, K., Bourillot, R., Esat, T.E., Fallon, S., Thompson, W.G., Thomas, A.L., Kan, H., McGregor, H.V., Hinestroza, G., Obrochta, S.P. and Lougheed, B.C. (2018) Response of the Great Barrier Reef to sea-level and environmental changes over the past 30,000 years. *Nature Geosci.*, **11**(6), 426–432.
- Wei, E.A., Driscoll, N.W. and Slingerland, R.L. (2019) Oceanographic currents, differential subsidence, and physiography control three-dimensional clinothem growth in the Gulf of Papua, Papua New Guinea. *Mar. Geol.*, **407**, 164–180.
- Wei, E.A. and Driscoll, N.W. (2020) Clay mineralogy of Gulf of Papua Shelf and Pandora Trough deposits constrains sediment routing during the last sea-level cycle. *Sedimentology*, **67**, 2502–2528.
- Williams, M.A.J. (1984) Palaeoclimates and Palaeoenvironments: Quaternary environments. In: *Phanerozoic Earth History of Australia*. (Ed. Veevers, J.J.), pp. 42–47. Clarendon Press, Oxford.
- Wilson, J.L. (1967) Cyclic and reciprocal sedimentation in Virgilian strata of southern New Mexico. *GSA Bull.*, **78**, 805–818.
- Wolanski, E. and Alongi, D.M. (1995) A hypothesis for the formation of a mud bank in the Gulf of Papua. *Geo-Mar. Lett.*, **15**, 166–171.
- Wolanski, E., Norro, A. and King, B. (1995) Water circulation in the Gulf of Papua. *Cont. Shelf Res.*, **15**, 185–212.
- Wright, L.D. and Friedrichs, C.T. (2006) Gravity-driven sediment transport on continental shelves: A status report. *Cont. Shelf Res.*, **26**, 2092–2107.
- Yamano, H., Miyajima, T. and Koike, I. (2000) Importance of foraminifera for the formation and maintenance of a coral sand cay: Green Island, Australia. *Coral Reefs*, **19**, 51–58.
- Yokoyama, Y., Purcell, A., Marshall, J.F. and Lambeck, K. (2006) Sea-level during the early deglaciation period in the Great Barrier Reef. *Australia. Global Planet. Change*, **53**, 147–153.
- Zeller, M., Verwer, K., Eberli, G.P., Massafiero, J.L., Schwarz, E. and Spalletti, L. (2015) Depositional controls on mixed carbonate-siliciclastic cycles and sequences on gently inclined shelf profiles. *Sedimentology*, **62**, 2009–2037.
- Zhang, W., Wu, J., Wang, Y., Wang, Y., Cheng, H., Konga, X. and Fucai Duan, F. (2014) A detailed East Asian monsoon history surrounding the 'Mystery Interval' derived from three Chinese speleothem records. *Quatern. Res.*, **82**, 154–163.

Manuscript received 18 December 2019; revision accepted 4 March 2021